From Department of Biosciences and Nutrition

Karolinska Institutet, Stockholm, Sweden

BIOMIMETIC SPIDER SILK AND BIOACTIVE HYDROGELS FORMED BY ENGINEERED RECOMBINANT SPIDER SILK PROTEINS

Tina Arndt

Stockholm 2022

Published by Karolinska Institutet.
Printed by Universitetsservice US-AB, 2022

ISBN 978-91-8016-831-1
Cover illustration: Spider silk protein hydrogels stained with Thioflavin T and imaged with brightfield microscopy (left) and fluorescence microscopy (right).

BIOMIMETIC SPIDER SILK AND BIOACTIVE HYDROGELS FORMED BY ENGINEERED RECOMBINANT SPIDER SILK PROTEINS

THESIS FOR DOCTORAL DEGREE (Ph.D.)

By

Tina Arndt

The thesis will be defended in public at Erna Möller Salen, Neo, Karolinska Institutet Flemingsberg, 9th of December 2022 at 10 am.

Principal Supervisor:
Professor Anna Rising
Karolinska Institutet
Department of Biosciences and Nutrition

Co-supervisor(s):
Professor Jan Johansson
Karolinska Institutet
Department of Biosciences and Nutrition

Opponent:
Professor Keiji Numata
Kyoto University
Department of Material Chemistry
And
RIKEN
Biomacromolecules Research Team

Examination Board:
Professor Per Hammarström
Linköping University
Department of Physics, Chemistry and Biology

Docent Ana Teixeira
Karolinska Institutet
Department of Medical Biochemistry

Professor Lena Mäler
Stockholm University
Department of Biochemistry and Biophysics

To my family ❤️

ABSTRACT

Spider silk is a unique material and its properties have fascinated material scientists, biologists and physicians for decades. Spider silk display one of the highest toughness found among fibers in nature, is used by spiders for web-spinning, prey-wrapping and cocoon building, while scientists have explored its biomaterials properties for multiple purposes. Spider silk appears to be generally well tolerated when implanted and is biodegrade but it comes with a limited availability and variable quality.

Artificial silk production by recombinant expression of spider silk proteins (spidroins) in heterologous hosts is a promising path to overcome drawbacks associated with natural silk. To recapitulate the elaborate structure of natural silk one must understand the nature of silk formation and mimic this process closely. Previously, an artificial spidroin, NT2RepCT, was developed that can be spun into fibers with impressive mechanical properties in a biomimetic setup. However, NT2RepCT fibers cannot match the properties of natural silk fibers which may be due to incomplete biomimicry of the spidroin, and/or spinning procedure. In **paper I**, we analyzed to what extent the spidroin solution (dope), from which the silk fiber are spun, recapitulates important features of natural dope and found that it has shear-thinning and viscoelastic behavior and undergoes pH-induced phase-separation and structural changes similar to native dope, but lacks the high viscosity typically seen for natural spinning dope.

In **Paper II**, we took advantage of insights in the constraints that spidroins have evolved under and used rational protein engineering of the repeat region of NT2RepCT. More specifically, we increased the hydrophobicity of the β-sheet forming poly-Ala regions since hydrophobic amino acid residues side chains are generally more prone to form β-sheets and steric zippers. Such proteins are unlikely to be secreted since the translocon would inserts proteins with hydrophobic sections in the endoplasmic reticulum membrane. Since the NT2RepCT proteins accumulate intracellularly during expression in prokaryotic hosts, we are not confined by these restrictions. When spun into fibers in a biomimetic spinning device, the toughness of fibers spun from several of the engineered proteins improved significantly compared to fibers spun from NT2RepCT. Importantly, one of the fibers had an unprecedented toughness for an as-spun artificial silk fiber. Furthermore, expression of the engineered spidroin in a bioreactor resulted in protein yields that make large-scale production economically feasible.

Paper III explores the surprising finding that the hyper-soluble and stable spidroin N-terminal domain (NT) forms hydrogels when incubated at 37°C, and that gel formation is associated with a conversion of NT into amyloid-like fibrils. The high structural flexibility of NT combined with the presence of amyloidogenic sequences in its α-helices are factors that are important for formation of the gel. Furthermore, by fusing NT to target proteins, we present a novel immobilization platform in which NT is used both as an expression tag for high yield production of soluble fusion proteins and as a fibrillar scaffold in the gel. As hydrogel formation occurred rapidly and under benign conditions also for NT2RepCT, **Paper IV** focuses on the potential application of NT2RepCT hydrogels as a drug release device and for cell encapsulation. Successful encapsulation and release of active green fluorescent protein suggest that the hydrogels could be suitable candidates for use as drug release devices. An encapsulated cell line released the bioactive molecule progranulin for 31 days to a similar extent as cells cultured under standard conditions. Human mesenchymal stem cells encapsulated in the hydrogels showed high survival but limited proliferation, likely due

to restricted space in the dense fibrillar network that is characteristic of the gels. This thesis describes major steps forward in the development of novel spidroin-based materials.

LIST OF SCIENTIFIC PAPERS

This thesis is based on the following papers, which are referred to by Roman numerals in the text:

I. **Native-like flow properties of an artificial spider silk dope.**
Arndt, T., Laity, P. R., Johansson, J., Holland, C., Rising, A.
ACS Biomaterials Science & Engineering, *(2021); 7*(2), 462-471.

II. **Engineered Spider Silk Proteins for Biomimetic Spinning of Fibers with Toughness Equal to Dragline Silks.**
Arndt, T., Greco, G., Schmuck, B., Bunz, J., Shilkova, O., Francis, J., Pugno, N. M., Jaudzems, K., Barth, A., Johansson, J., Rising, A.
Advanced Functional Materials, *(2022);* 2200986.

III. **Spidroin N-terminal domain forms amyloid-like fibril based hydrogels and provides a protein immobilization platform.**
Arndt, T., Jaudzems, K., Shilkova, O., Francis, J., Johansson, M., Laity, P. R., Sahin, C., Chatterjee, U., Kronqvist, N., Barajas-Ledesma, E., Kumar, R., Chen, G., Strömberg, R., Abelein, A., Langton, M., Landreh, M., Barth, A., Holland, C., Johansson, J., Rising, A.
Nature communications, *(2022); 13*(1), 1-14

IV. **Tuneable recombinant spider silk protein hydrogels for drug release and 3D cell culture.**
Arndt, T.*, Chatterjee, U.*, Shilkova, O., Francis, J., Lundkvist, J., Johansson, D., Schmuck, B. , Ekblad Nordberg, Å., Altskär, A., Lorén, N., Li, Y., Wahlberg L. U., Langton M., Johansson, J., Götherström, C., Rising, A.
*These authors contributed equally to this work.
Manuscript.

Papers not inculded in this thesis:

Properties of biomimetic artificial spider silk fibers tuned by postspin bath incubation.
Greco, G., Francis, J., **Arndt, T**., Schmuck, B., G. Bäcklund, F., Barth, A., ... & Rising, A.
Molecules, (2020); 25(14), 3248.

Artificial spider silk supports and guides neurite extension in vitro.
Hansson, M. L., Chatterjee, U., Francis, J., **Arndt, T.**, Broman, C., Johansson, J., Sköld, M. K., Rising, A.
The FASEB Journal, *(2021);* 35(11), e21896.

Tyrosine residues mediate supercontraction in biomimetic spider silk.
Greco, G., **Arndt, T**., Schmuck, B., Francis, J., Bäcklund, F. G., Shilkova, O., Barth, A., Gonska, N., Seisenbaeva, G., Kessler, V., Johansson, J., Pugno, N. M., Rising, A.
Communications Materials, *(2021);* 2(1), 1-10

CONTENTS

LIST OF ABBREVIATIONS

A. diadematus	*Araneus diadematus*
A_{15}-A_{14}	Also NT2RepCT; mini-spidroin with NT, two repeats and CT
AcNi	Acetonitrile
AdCT	CT from *A. diadematus* fibroin 3
APS	Ammonium persulfate
ARPE-19	Spontaneously arising retinal pigment epithelia
ATP	Adenosine triphosphate
BHK	Baby hamster kidney
BMP-2	Bone morphogenetic protein 2
CD	Circular dichroism
CT	C-terminal domain of spidroins
DMEM	Dulbecco's Modified Eagle's Medium
DMSO	Dimethyl sulfoxide
E. australis	*Euprosthenops australis*
EaCT	CT from *E. australis* MaSp1 (recombinant)
eADF4(Ω16)	Uncharged variant of eADF4(C16)
eADF4(κ16)	Positively charged variant of eADF4(C16)
eADF4(C16)	Engineered recombinant spidroin with 16 repeats from *Araneus diadematus* fibroin 4 (MaSp2)
ECM	Extracellular matrix
ELISA	Enzyme-linked immunosorbent assay
EMA	European Medicines Agency
ER	Endoplasmic reticulum
EtOH	Ethanol
FDA	The Food and Drug Administration
FGF-18	Fibroblast growth factor 18
FID	Free-induction decay
FlSp	Flagelliform spidroin
FRAP	Fluorescence recovery after photobleaching
FTIR	Fourier-transform infrared
Gdm-SCN	Guanidine thiocyanate
GFP	Green fluorescent protein
H(f)MSC	Human fetal mesenchymal stem cells

HFIP	Hexafluoroisopropanol
hPBMCs	Human peripheral blood mononuclear cells
HSQC	Hetero single quantum coherence
IMAC	Immobilized metal affinity chromatography
IPA	Isopropanol
IPTG	Isopropyl beta-D-1thiogalactopytanoside
ISO	International Organization for Standardization
KPi	Potassium phosphate
LLPS	Liquid-liquid phase separation
MAC-T	Bovine Mammary Alveolar Cell Line
MaSp	Major ampullate spidroin
MaSpIC	Four repeats from MaSp1 with CT from *T. clavipes* (recombinant)
MetOH	Methanol
MiSp	Minor ampullate spidroin
mRNA	Messenger ribonucleic acid
n.s.	Not stated
NaAc	Sodium acetate
NcCT	MaSp1 CT from *T. clavipes* (recombinant)
NMR	Nuclear magnetic resonance
NP	Nanoparticle
NT	N-terminal domain of spidroins
NT-L6	NT with six Met to Leu mutations
NT*	Charge reversed double mutant of NT
NT2RepCT	Chimeric mini-spidroin with NT, two repeats and CT (recombinant)
NT^{A72R}	Ala to Arg mutant at position 72 in NT
O.N.	Overnight
PBS	Phosphate-buffered saline
PDB	Protein data base
PEG	Polyethylene glycol
PNP	Purine nucleoside phosphorylase
PPII	Polyproline type II helix
PTM	Post-translational modifications
RF	Radiofrequency

RGD	Peptide of Arg Gly and Asp
SEM	Scanning electron microscopy
SP	Signal peptide
SRP	Signal recognition particle
T. clavipes	*Trichonephila clavipes* (former *Nephila clavipes*)
TEM	Transmission electron microscopy
ThT	Thioflavin T
tRNA	Transfer ribonucleic acid
YM	Young's modulus

1 LITERATURE REVIEW

1.1 BIOLOGICAL MATERIALS, BIOMIMETIC MATERIALS, BIOINSPIRED MATERIALS AND BIOMATERIALS

These terms will be discussed throughout the thesis and while they appear alike, they describe different concepts which warrant clarification.

- Biological materials: Materials produced by living organisms
- Biomimetic materials: Materials that are engineered to imitate biological materials by directly applying their principles to solve technological problems
- Bioinspired materials: Materials that are engineered by learning from biological materials, capturing the essential principles, and applying those in a conceptual way to solve technological problems
- Biomaterials: Materials that interact with biological systems for medical applications as a preventive, diagnostic, therapeutic or prosthetic tool

Today's living organisms have evolved over billions of years and are well adapted to their niches (Ohtomo *et al.*, 2014). This has led to the evolution of biological materials such as various types of fibers which serve an array of different purposes. As these materials are often optimized for their intended purpose, recyclable and produced in environmentally friendly processes, researchers and engineers alike are trying to mimic biological materials to solve technological problems.

To produce biomimetic materials, knowledge of the natural material is needed, including its synthesis, assembly, structure, properties and function, which is then directly applied to solve technological problems (Cranford *et al.,* 2014). However, a material that is biomimetic in all aspects is not always required or technologically possible to produce .

For the development of bioinspired materials, researchers learn from nature, capture the essential principles, and apply those in a conceptual way (Cranford *et al.,* 2014). The synthesis and assembly methods may be adapted to comply with available production methods and/or the properties and functions may be fine-tuned to be suitable for the intended application. For example, the development of superhydrophobic surfaces is based on the surface structure of lotus leaves (Erbil *et al.*, 2003) but is not, for example, mimicking the composition of the leaf.

It can be argued that for a true biomimetic material, the natural material must be fully understood and replicated (including components, their synthesis, assembly, structure and properties) which is often not achievable (nor necessary) and hence, most biomimetic materials should in fact be termed bioinspired. However, a looser definition of the term biomimetic is usually used. In fact, the line between both terms can be blurry and they are often even used interchangeably (Naik and Singamaneni, 2017).

Biomaterials are materials that interact with biological systems for medical applications as a preventive, diagnostic, therapeutic or prosthetic tool (Tiwari *et al.*, 2014). In therapeutics, biomaterials may support regeneration of the structure and/or function of tissues or organs, (Parida et al., 2012). Examples used in the clinics are sutures, wound dressings, prostheses

for joint replacement, bone plates, catheters, pacemakers, and stents (Pignatello, 2013). Biomaterials ought to be well tolerated by the biological system during interaction.

In tissue engineering, biomaterials serve as a scaffold often attempting to mimic the extracellular matrix (ECM). Cell adhesion, proliferation and differentiation should be promoted by biomaterials intended for tissue engineering. Generally, cells are affected by the composition of the biomaterial and its physical properties such as dimensions, surface structures and mechanical properties, thus these need to be considered when designing a biomaterial (Rice *et al.*, 2013). Biomaterials can be of natural or synthetic origin, each with their own advantages and disadvantages (Samavedi *et al.*, 2014; Ullah and Chen, 2020). While natural biomaterials are often bioactive and biodegradable, they display high batch-to-batch variation and poor mechanical stability (Ullah and Chen, 2020). Synthetic biomaterials are chemically defined and can have tunable mechanical properties but frequently lack bioactivity and biodegradability (Samavedi *et al.*, 2014).

1.2 SPIDER SILK AS A BIOMATERIAL

Spider silk fibers are a promising biomaterial due to their outstanding toughness, biodegradability and they are well tolerated when implanted (Allmeling et al., 2008; Blackledge & Hayashi, 2006; Gosline et al., 1999; Kornfeld et al., 2016; Thurber et al., 2015). Spider silk fibers have been explored as suture material (Hennecke *et al.*, 2013), wound dressing (Liebsch *et al.*, 2018) and as scaffolds to support peripheral nerve regeneration (Allmeling *et al.*, 2008; Kornfeld *et al.*, 2016, 2021; Radtke *et al.*, 2011; Resch *et al.*, 2018) as well as cartilage regeneration (Gellynck *et al.*, 2005). Radtke and colleagues have developed a promising nerve conduit composed of a decellularized vein filled with aligned spider silk fibers. This nerve conduit promotes axonal regeneration in peripheral nerve defects with a gap size of 6 cm *in vivo* (Kornfeld *et al.*, 2021; Radtke *et al.*, 2011). This is impressive as current US Federal Drug Administration (FDA) approved products can bridge nerve gap sizes of only up to 3 cm (Kehoe *et al.*, 2012).

1.2.1 Immunogenicity of spider silk

In the literature, spider silk is often referred to as non-immunogenic (Borkner *et al.*, 2014; Harvey *et al.*, 2020; Herold *et al.*, 2020; Schacht *et al.*, 2015; Sonnleitner *et al.*, 2021) or even “invisible to the human immune system” (Babb *et al.*, 2017). However, any foreign material implanted in the human body causes an immunogenic reaction (Boehler *et al.*, 2011; Franz *et al.*, 2011). While there are studies supporting tolerance of spider silk *in vitro* and *in vivo* (Allmeling, 2006; Allmeling *et al.*, 2008) other reports show that spider silk fibers cause a light immune response when implanted (Gellynck *et al.*, 2008; Kornfeld *et al.*, 2021; Schäfer-Nolte *et al.*, 2014; Vollrath *et al.*, 2002). This is not necessarily negative as a physiological immune response is an important process for wound healing and tissue repair (Laurent *et al.*, 2017). A local immune response promotes the desired tissue regeneration as well as degradation of the biomaterial that the new tissue replaces (Boehler *et al.*, 2011; Franz *et al.*, 2011). In line with this, the European Society of Biomaterials defined biocompatibility as “the ability of a material to perform with an appropriate host response in a specific application” (Williams and European society for biomaterials, 1986). This implies that an immune response-provoking biomaterial is considered biocompatible if, for example

the responds aids in tissue repair and degradation of the biomaterial and does not cause any other adverse effects to the host.

Recently however, fibrin-spider silk scaffolds implanted into spinal cord lesions of rats were found to cause a foreign body reaction (Koop *et al.*, 2022). Perhaps spider silk fibers are not suitable for implantation in the central nervous system, but they remain a promising biomaterial due to their mechanical, degradation and immunogenic properties in other tissues (Allmeling *et al.*, 2008; Gosline *et al.*, 1999; Kornfeld *et al.*, 2016; Thurber *et al.*, 2015).

1.2.2 Challenges with industrial production of spider silk

Industrial level production of spider silk fibers, which would be needed if they were to make their way into the clinics, cannot be realized mainly due to the spiders' cannibalistic behavior which limits the availability of the fibers and leads to high production costs. Furthermore, composition and properties of spider silk fibers can vary (Blackledge *et al.*, 2005; Blamires *et al.*, 2017, 2022; Greco *et al.*, 2022; Lacava *et al.*, 2018; Madsen *et al.*, 1999). Large variations in mechanical properties of the same silk type from different spiders of the same species and even from the same individual are commonly observed and are probably caused by environmental factors such as temperature, humidity and reeling speed (Madsen *et al.*, 1999; Vollrath *et al.*, 2001). This is especially problematic from a regulatory perspective. The International Organization for Standardization (ISO) requires precise chemical characterization (ISO 10993-18:2020) and biological evaluation (ISO 10993-:2018) of medical devices and even stricter regulations apply when the biomaterial is derived from animals (ISO 22442-1:2022). These are hard to meet considering the variability of composition and mechanical properties in natural spider silk. Reproducibility issues may also prevent natural spider silk fibers to meet the standards of good manufacturing practice.

To solve these issues, the development of methods to produce recombinant silk proteins for making spider silk mimics have been an active area of research in the past decades (Koeppel and Holland, 2017). Recombinant proteins are considered synthetic from a regulatory perspective and their composition is defined. However, as described under section 1.9.1, production of spider silk proteins (spidroins) in heterologous hosts is problematic for several reasons associated with the biochemical properties of the spidroins and our limited understanding of native silk production and spinning. Even though significant progress has been made in understanding fiber assembly and spinning conditions in the past decades, we still cannot produce replicas of this material at large scales (Koeppel and Holland, 2017).

1.3 SPIDER SILK TYPES AND THEIR FUNCTION

Spiders produce up to seven different silks from dedicated glands, including major ampullate, minor ampullate, flagelliform, pyriform, aggregate, aciniform and tubiliform silk (Figure 1), (Peakall, 1969). Each type of silk fiber has unique mechanical properties and is used for distinct purposes in a spiders' life (Blackledge and Hayashi, 2006). Major ampullate silk serves as a lifeline, is used to build the radii and the frame of the web (marked in red in Figure 1) and is the strongest silk with a tensile strength exceeding 3 GPa in *Clubiona vigil* (Arakawa *et al.*, 2022). The minor ampullate silk serves as an auxiliary spiral used to stabilize the web (green in Figure 1). It is not as strong as major ampullate silk, but it is slightly more

extensible (Blackledge and Hayashi, 2006). Flagelliform silk is used for the capture spiral (blue in Figure 1) and sticky aggregate silk droplets are present on the flagelliform silk which aid in prey capture (turquoise in Figure 1). Pyriform silk is composed of fibers and a glue-like substance, and it is used for attachment of silks to surfaces or to each other (yellow in Figure 1), (Wirth *et al.*, 2019). Aciniform silk is used for prey wrapping and for the inner lining of the egg sac (pink in Figure 1), (Blackledge and Hayashi, 2006; Hayashi *et al.*, 2004). Tubuliform (or cylindriform) silk forms the outer layer of the egg sack (grey in Figure 1).

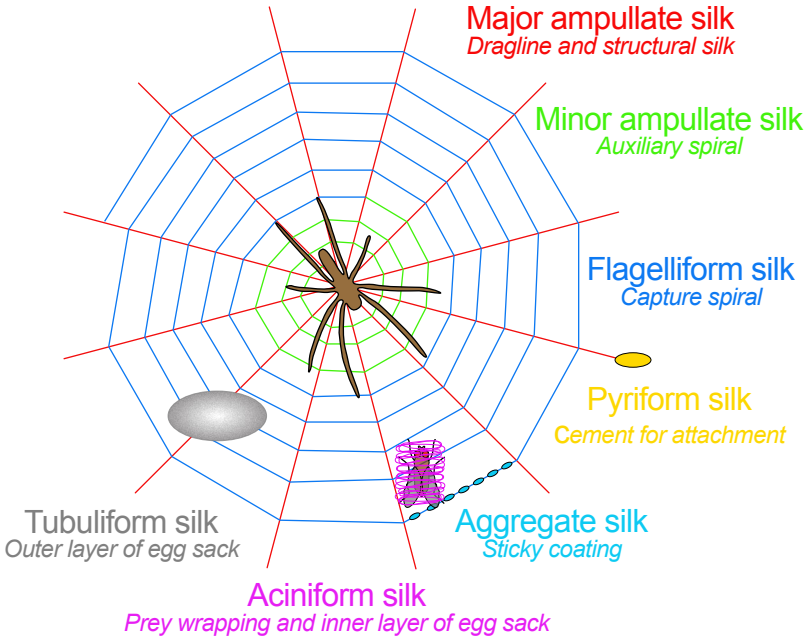

Figure 1: Different silk types and their applications. Depicted is a female orb-weaving spider and the seven silk types it can produce from specialized glands.

1.4 SPIDROINS

11,155 putative spidroin genes have been described by transcriptomics of over thousand spider species (Arakawa *et al.*, 2022). These encode spidroins that in general are composed of an N-terminal domain (NT), (Rising *et al.*, 2006), a repetitive region (Ayoub *et al.*, 2007) and a C-terminal domain (CT), (Hagn *et al.*, 2010; Sponner *et al.*, 2004), (Figure 2 A). NT and CT are responsible for controlling spidroin storage and fiber assembly. The repetitive region consists of sequence motifs that are characteristic for the different spidroin types.

In major ampullate glands, at least three types of spidroins are dominating the expression profile; major ampullate spidroin 1 (MaSp1), MaSp2 and MaSp3 (Arakawa *et al.*, 2022; Babb *et al.*, 2017, 2022; Chaw *et al.*, 2015; Collin *et al.*, 2018; Kono *et al.*, 2019; Larracas *et al.*, 2016; A Sponner *et al.*, 2005). Generally, the repetitive regions of the MaSps are composed of up to 100 alternating tandem repeats of poly-Ala and Gly-rich motifs. These two motifs are the most prevalent ones, but it should be noted that there are many different motifs found in the spidroin repeat region (Babb *et al.*, 2022, 2017), for example 157 different repeat motifs in MaSp (including poly-Ala and Gly-rich motifs of different lengths) were identified in the genome of *Trichonephila clavipes* (Babb *et al.*, 2017). While poly-Ala regions can be up to 15 amino acid residues long, other motifs are between 4 and 41 amino acid residues in length (Arakawa *et al.*, 2022; Babb *et al.*, 2022).

In addition to MaSps, proteomics studies have revealed that major ampullate silk fibers also contain other silk typical spidroins such as aciniform spidroins (Chaw *et al.*, 2015; Larracas *et al.*, 2016) and besides the classical spidroins, non-canonical silk constituents and over 100 non-spidroin proteins were identified (Han et al., 2013; Kono et al., 2019, 2021; Larracas et al., 2016; Sanggaard et al., 2014).

The repeat motifs adopt different secondary structures in the fiber which convey the mechanical properties of the different silks (Hayashi *et al.*, 1999). In the major ampullate silk fiber, poly-Ala motifs form antiparallel β-sheets while the Gly-rich region forms β-turns and 3_1-helices (Figure 2 B), (Ayoub *et al.*, 2007; Dicko, Knight, *et al.*, 2004; Hayashi *et al.*, 1999; Hijirida *et al.*, 1996; Holland *et al.*, 2008; Jenkins *et al.*, 2013; Lefèvre *et al.*, 2011; Parkhe *et al.*, 1997; van Beek *et al.*, 2002).

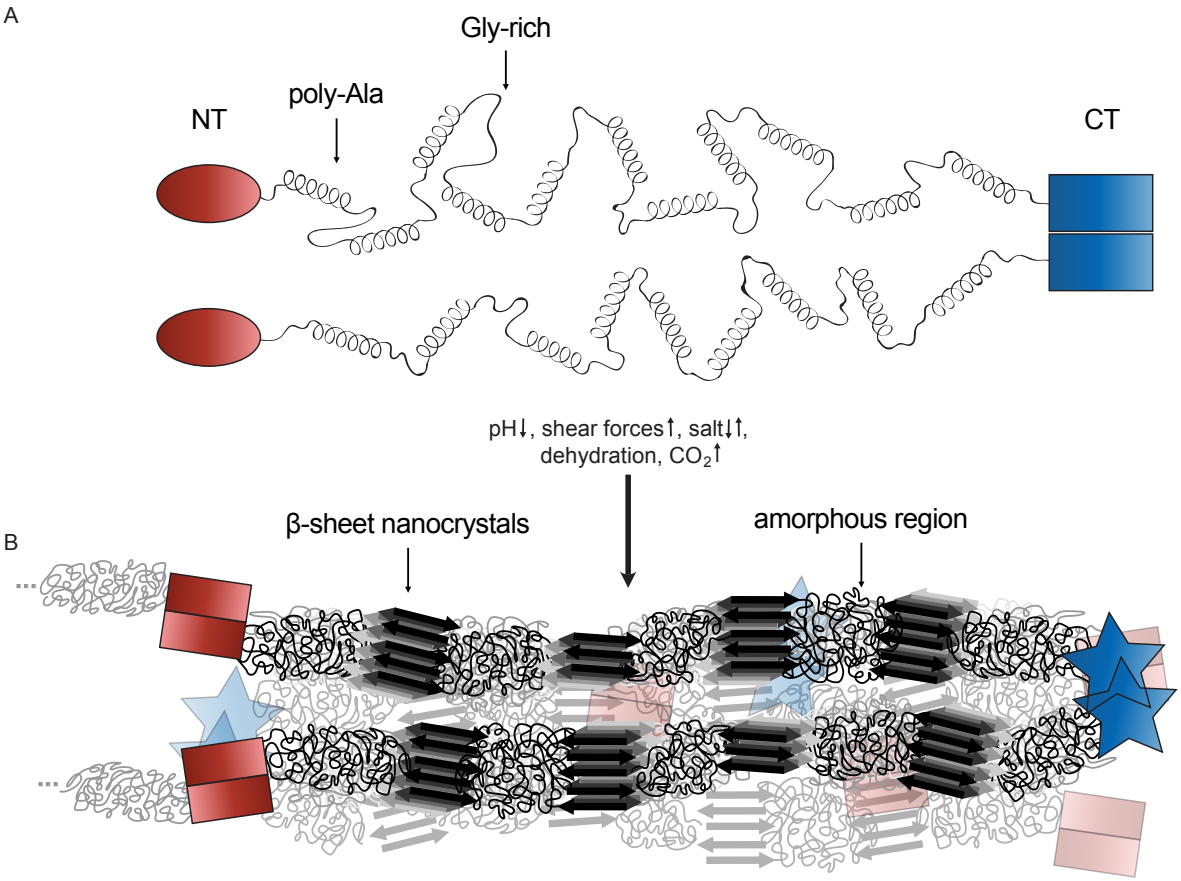

Figure 2: Schematic illustration of a typical spidroin and their secondary structures in the dope and in the fiber. A) The non-repetitive NT (red symbols) and CT (blue symbols) are flanking the large repetitive region (black). The repetitive region in MaSps is composed of alternating poly-Ala and Gly-rich regions. In the dope, the poly-Alas are mainly in an α-helical conformation and the Gly-rich regions are in a random coil conformation. B) The lock and trigger mechanisms states that NT undergoes structural changes (illustrated oval in A to rectangle shapes in B) to form antiparallel dimers at low pH to lock the spidroins together while CT acts as a trigger (blue rectangles before in A and stars after structural changes in B) for the repetitive region to convert into β-sheets.

Minor ampullate spidroins contain similar motifs as MaSps but the poly-Ala blocks are shorter which could be one explanation for the lower tensile strength of minor ampullate silk compared to major ampullate silk fibers (Chen *et al.*, 2012; Colgin and Lewis, 1998; Guinea *et al.*, 2012; Hayashi *et al.*, 1999). Aciniform spidroins contain lower percentage of β-sheets than major ampullate, minor ampullate and tubulin silk as well as 3_1-helices, α-helices and β-turns (Hayashi *et al.*, 2004; Lefèvre *et al.*, 2011; Rousseau *et al.*, 2009). Flagelliform silk

mainly contains β-turns, 3_1-helices and potentially β-sheet and the high content of β-turns and 3_1-helices explain its outstanding extensibility (Ohgo *et al.*, 2006; Zhou *et al.*, 2001). Tubuliform silk, similar to aciniform silk, contains β-sheets, 3_1-helices, α-helices, and β-turns but tubuliform has a higher percentage of β-sheets (35-37% vs 30%), (Lefèvre *et al.*, 2011; Rousseau *et al.*, 2009; Tian and Lewis, 2005).

Table 1: Motifs and secondary structure content of different silks.

Spidroin type	Motif	Secondary structure in the fiber	References
Major ampullate	MaSp1: Poly-Ala, poly-GlyAla Gly-rich (GGX) MaSp2: Poly-Ala, GPGXX MaSp3: Poly-Ala, GPG, GGR	β-sheet (35-40%), 3_1-helices, β-turns	(Dicko, Knight, *et al.*, 2004; Gray *et al.*, 2016; Holland *et al.*, 2008; Jenkins *et al.*, 2013; Kono *et al.*, 2019; Lefèvre *et al.*, 2007; van Beek *et al.*, 2002)
Minor ampullate	Poly-Ala, poly-GlyAla G-rich (GGX)	β-sheet (35-37%) 3_1-helices	(Lefèvre *et al.*, 2011; Rousseau *et al.*, 2009)
Aciniform	Poly-S unspecific motifs	β-sheet (30%), 3_1-helices, α-helices and β-turns	(Hayashi *et al.*, 2004; Lefèvre *et al.*, 2011; Rousseau *et al.*, 2009)
Flagelliform	GGX GPGXX Spacer	3_1-helices β-turns β-sheet (potentially)	(Ohgo *et al.*, 2006; Zhou *et al.*, 2001)
Tubuliform	(S)n, (T)n, and (SX)n unspecific motifs	β-sheet (35-37%), 3_1-helices, α-helices, and β-turns	(Lefèvre *et al.*, 2011; Rousseau *et al.*, 2009; Tian and Lewis, 2005)

1.5 THE MAJOR AMPULLATE GLAND

The major ampullate gland and its silk are the most widely studied, for example (Agnarsson *et al.*, 2010; Andersson *et al.*, 2013; Arakawa *et al.*, 2022; Blackledge and Hayashi, 2006; Casem *et al.*, 2002; Hijirida *et al.*, 1996; Lawrence *et al.*, 2004; Riekel *et al.*, 2017) and the main focus of this thesis is on this silk.

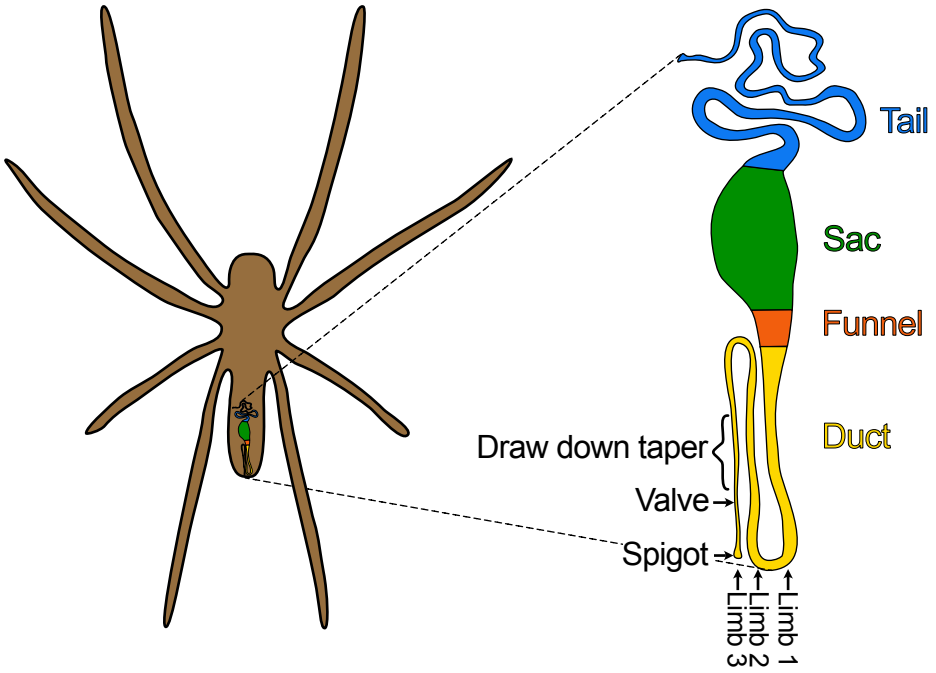

Figure 3: Schematic of a major ampullate silk gland in the opisthosoma (abdomen) of a spider. The major ampullate gland consists of a tail, a sac, a funnel and a duct. Spidroins are mainly secreted in the tail of the gland and stored as a concentrated protein solution in the sac. The duct is composed of three limbs where the third limb contains the draw down taper, the valve and the spigot. Upon spinning, chemical and mechanical cues lead to a phase and structure transition of the spidroins in the duct.

The major ampullate gland consist of a tail, a sac and a duct (Figure 3). MaSps are secreted into the lumen of the gland from specialized epithelial cells mainly in the tail but also in the sac of the gland (Bell and Peakall, 1969; Chaw *et al.*, 2015; Larracas *et al.*, 2016; A Sponner *et al.*, 2005). The epithelial cells in the tail have a large endoplasmic reticulum (ER), specific tRNAs and secretory vesicles to enable a high level of spidroin production (Candelas and Cintron, 1981; Casem *et al.*, 2002; Knight and Vollrath, 2001). The spidroins are stored as a solution (dope) in the sac of the gland. Upon spinning, the spidroins align and assemble when they travel through the funnel, a tapered duct, the spigot and the spinneret where the fiber is pulled out (Figure 3), (Bell and Peakall, 1969; Casem *et al.*, 2002). The duct is structured into three limbs to form an S shape (Andersson *et al.*, 2013; Lefèvre *et al.*, 2008; Vollrath and Knight, 1999). The diameter decreases in the duct lumen from around 100 μm to below 10 μm (Davies *et al.*, 2013; Knight and Vollrath, 1999). In the third limb, the diameter decreases more rapidly in the draw down taper compared to the first and second limb (Knight and Vollrath, 1999). The valve is located between the draw down taper and the spigot and is a muscle that has been suggested to have a clamping function (Vollrath and Knight, 1999; Wilson, 1969). Fiber formation likely occurs in the third limb of the duct (Knight *et al.*, 2000) in response to a number of external cues.

The physicochemical changes in the silk gland include a decrease in pH, changes in ion concentrations, increased carbon dioxide pressure and increasing shear forces (Figure 4), (Andersson *et al.*, 2014; Breslauer *et al.*, 2009; Casem *et al.*, 2002; Dicko, Vollrath, *et al.*, 2004; Knight *et al.*, 2000; Knight and Vollrath, 2001; Vollrath and Knight, 1999).

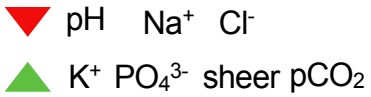

Figure 4: Summary of environmental changes in the spider silk gland. While the pH, and concentrations of Na^+ and Cl^- decrease in the duct, the concentrations of K^+ and $PO4^{3-}$, as well as sheer forces and CO_2 pressure, increase.

The epithelial cells in the distal part of the sac and in the duct contain carbonic anhydrase that interconverts carbon dioxide and water with carbonic acid which releases a proton under formation of bicarbonate (Andersson *et al.*, 2014). This causes the pH to progressively decrease from 7.6 in the tail to 5.7 half-way through the duct. Possibly, the action of ATP driven proton pumps, are also involved in regulating the pH (Vollrath *et al.*, 1998). Along the gland there is an increase in carbon dioxide pressure, from 4 torr in the tail to 139 torr in the distal part of the sac (Andersson *et al.*, 2014).

In the sac, high concentrations of the chaotropic ions Na^+ and Cl^- are found (192 and 164 mM, respectively), (Andersson *et al.*, 2014) which could prevent aggregation and oligomerization of the spidroins by shielding electrostatic interactions (Eisoldt *et al.*, 2010; Leclerc *et al.*, 2013; Oktaviani *et al.*, 2019). In the duct, Na^+ and Cl^- concentrations decrease and PO_4^{3-} and SO_4^{2-} concentrations increase (Knight and Vollrath, 2001) which could lead to a salting-out effect of the spidroins (Leclerc *et al.*, 2013; Oktaviani *et al.*, 2019). Finally, microvilli containing cells were found in the distal part of the duct which are hypothesized to absorb water from the dope (Casem *et al.*, 2002).

1.6 BIOPROCESSING OF SPIDROINS

1.6.1 The secretion of spidroins

Being secretory proteins, spidroins carry a signal peptide (SP) that is recognized by the signal recognition particle (SRP) which directs the ribosome complex including the mRNA, SP and SRP to target the SRP-receptor at the ER membrane (Figure 5), (Blobel, 1980; Blobel and Dobberstein, 1975; von Heijne, 1990). There, the nascent polypeptide chain passes the ER membrane through the translocon (Figure 5 A), (Blobel, 1980; Johnson & van Waes, 1999; White & von Heijne, 2005). The translocon determines the destination of polypeptide chains according to the biological hydrophobicity scale. Hydrophilic segments will translocate through the membrane into the lumen of the ER, while hydrophobic segments are instead inserted into the ER membrane and proteins that carry such segment(s) are thus not secreted (Figure 5 B), (Hessa *et al.*, 2005, 2007). After signal peptide cleavage and when translation is completed, proteins destined for secretion are sent through the Golgi apparatus and the trans-Golgi network where they are packed into secretory vesicles (Figure 5 A), (Griffiths and Simons, 1986; Kienzle and von Blume, 2014; von Heijne, 1990). The vesicles are then delivered to the plasma membrane where the protein contents leave the cell through exocytosis (Burgess and Kelly, 1987; Viotti, 2016).

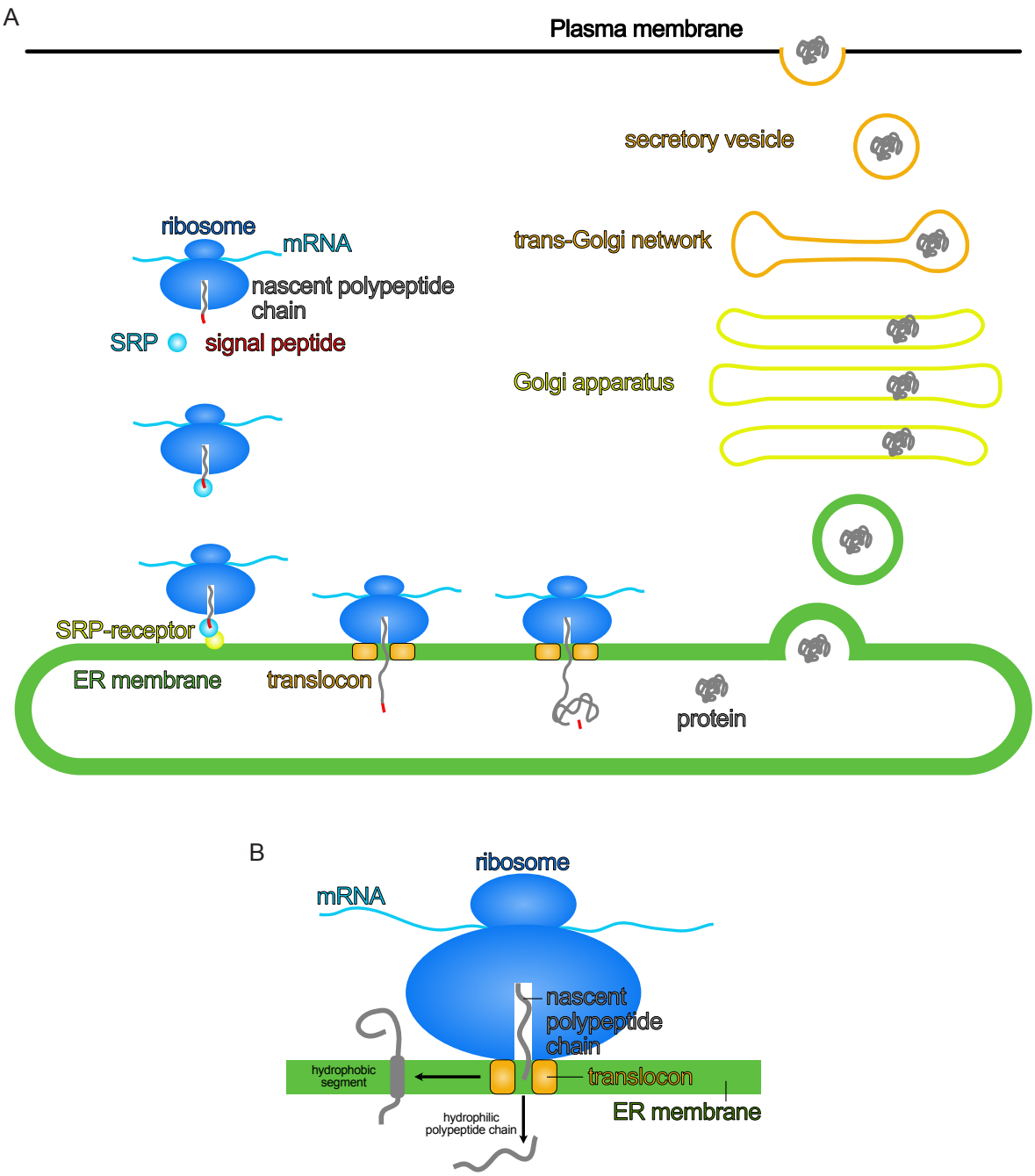

Figure 5: Schematic presentation of biosynthesis of secretory and membrane proteins. A) The SRP binds the SP of the nascent polypeptide chain at the ribosome and targets the complex to its receptor at the ER membrane. Secretory polypeptides pass through the translocon while membrane-resident proteins are inserted in the ER membrane according to the biological hydrophobicity scale (Hessa *et al.*, 2005). Secretory proteins are folded and packed in vesicles that pass the Golgi apparatus, the trans-Golgi network, and eventually fuse with the plasma membrane. Adapted with permission from (Viotti, 2016). B) Zoom in on the ribosome-translocon complex at the ER membrane. The nascent polypeptide chain passes the translocon which mediates passage through the ER membrane of hydrophilic peptide segments or insertion into the ER membrane of hydrophobic segments. Adapted with permission from (White and von Heijne, 2005).

Post-translational modifications (PTM) take place in the ER and/or in the Golgi apparatus. It has been suggested that spidroins get glycosylated and phosphorylated in *Trichonephila* spiders (dos Santos-Pinto *et al.*, 2016, 2015, 2014, 2019; Sponner *et al.*, 2007). Dityrosin and hydroxyprolines have also been identified in MaSp (Craig *et al.*, 2019; dos Santos-Pinto *et al.*, 2014, 2016, 2018). Even though PTM can have profound effects on the structure and function of proteins (Müller, 2018), the presence and effects of PTM on spidroins have not been extensively studied.

1.6.2 Spidroin storage

After secretion, spidroins in the dope are stored at neutral pH in the sac of the gland (Figure 3), (Andersson *et al.*, 2014; Chen *et al.*, 2002; Dicko, Vollrath, *et al.*, 2004; Hijirida *et al.*, 1996). The dope is a highly concentrated solution, 25-30% (w/v) as determined by weighing after drying (Chen *et al.*, 2002; Holland *et al.*, 2006) or around 50% (w/v) as determined by solution nuclear magnetic resonance (NMR) spectroscopy of ^{13}C labeled dope (Hijirida *et al.*, 1996). NMR spectroscopy studies on dope showed that the soluble proteins are in random coil conformations (Hijirida *et al.*, 1996; Hronska *et al.*, 2004; Xu *et al.*, 2014). Small angle scattering, wide angle X-ray scattering, circular dichroism (CD) and Raman spectroscopy revealed presence of α-helices, β-turns and polyproline type II helices (PPII), (Greving *et al.*, 2020; Hijirida *et al.*, 1996; Lefèvre *et al.*, 2007, 2008; Lin *et al.*, 2017). Which parts of the spidroins contribute to these secondary structures is not entirely clear from the literature. Hijirida observed Ala to be in flexible helix conformations (Hijirida *et al.*, 1996) while Lefevre and colleagues saw poly-Ala in PPII conformation by using vibrational CD spectroscopy and in random coil and α-helix conformations by using Raman spectromicroscopy (Lefèvre *et al.*, 2008, 2007).

Studies of a recombinant miniature spidroin with a repetitive region from MaSp1 (and terminal domains from MaSp and MiSp) in solution showed that the Gly-rich regions adopt a random coil conformation and that the poly-Ala regions forms α-helices (Otikovs *et al.*, 2017), (Figure 2 A). In another study of recombinant MaSp1 without the terminal domains, the Gly-rich regions show PPII conformation (Oktaviani *et al.*, 2018) which may seem counterintuitive considering that MaSp1 does not contain Pro residues in the repetitive region. However, structures that resemble PPIIs have been identified in peptides that lack proline residues, for example in GGXGG peptides (where X is any of the 20 natural amino acids except Gly) (Rucker and Creamer, 2002; Shi *et al.*, 2005, 2002). Interestingly, a model peptide consisting of seven Ala residues was found to be in PPII conformation (Shi *et al.*, 2002).

The inconsistencies in the literature describing the conformation of both native spidroins in the dope and recombinant spidroins may be due to the use of different methods, different interpretations or inconsistencies in the nomenclature of secondary structures. For instance, NMR spectroscopy has longer time scales and dynamic averaging of flexible secondary structures might be interpreted as random coil structures. In CD spectroscopy, that has shorter time scales than NMR spectroscopy, spectra of PPII are sometimes interpreted as random coils (Adzhubei *et al.*, 2013). Sometimes, PPII is also referred to as poly-Gly type II helix, although they are not the same (Warkentin *et al.*, 2017), or, as discussed below possibly also as 3_1-helix which complicate interpretations further. To clarify, PPII is an extended, left-handed helix that, in its ideal form, has three residues per turn (Figure 6), torsion angles ϕ= -75° and ψ = +145° and in CD spectroscopy shows a minima around 200 nm and a positive peak around 220 nm (Adzhubei *et al.*, 2013; Lopes *et al.*, 2014).

If the poly-Ala regions of spidroins in the dope are in PPII, it might play an important role during silk formation as PPII is an extended structure with similar phi and psi angles as β-strands (Lefèvre *et al.*, 2007), (Figure 6). Similarly, it has been suggested that PPII in the Gly-rich regions pre-aligns the soluble spidroins in a prefibrillar state in protein bundles and that some PPII may be retained in the fiber (Lefèvre *et al.*, 2007; Oktaviani *et al.*, 2018).

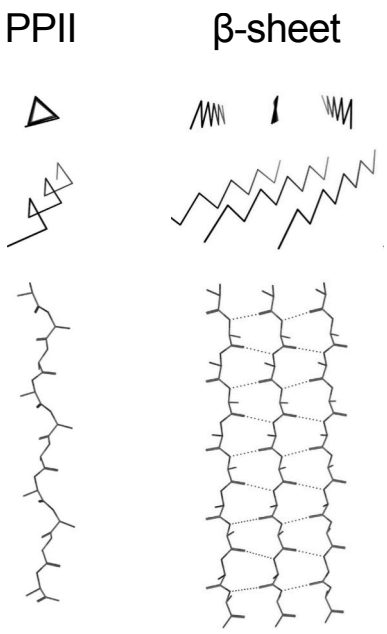

Figure 6: Schematics of ideal structures of PPII and β-sheets. Top, diagonal and side view. Modified with permission from (Adzhubei *et al.*, 2013).

The physico-mechanical properties of spider silk dope have been characterized using rheology (Chen *et al.*, 2002; Holland *et al.*, 2006; Kojić *et al.*, 2006). Spider silk dope exhibits remarkable rheological properties that are fundamental for silk fiber spinning, namely viscoelastic properties with high viscosity but shear-thinning behavior, a cross-over of the viscous and elastic moduli at increasing angular frequencies, and strain-induced phase separation (Chen *et al.*, 2002; Holland *et al.*, 2006; Kojić *et al.*, 2006). Spider silk dope has a viscosity of 3.5 – 4 kPa·s which is mediated by the high concentration and the spidroins high molecular weight (Holland *et al.*, 2006; Kojić *et al.*, 2006), as a comparison water has a viscosity of 1 mPa·s. Extruding a highly viscous fluid through a narrow duct is energetically demanding, but shear causes the viscosity of the dope to decrease at least 10-fold, likely by aligning the molecules (Holland *et al.*, 2006; Kojić *et al.*, 2006). Thus, the shear-thinning properties of the dope allows the spider to spin its silk using minimal amounts of energy (Holland *et al.*, 2006; Kojić *et al.*, 2006). Exceeding a critical shear stress contributes to solidification of the silk dope into fibers (Chen *et al.*, 2002; Giesa *et al.*, 2016; Holland *et al.*, 2006). Oscillatory measurements show that at low angular frequencies, spider silk dope responds like a liquid as the viscous modulus dominates above the elastic modulus. At frequencies above 2 rad/s, the elastic modulus is higher than the viscous modulus indicating that the dope behaves like a solid. This behavior is typical for a concentrated polymer solution with a high molecular weight (Holland *et al.*, 2006). The rheological properties of native dope are not only important for the spinning process but also influence the properties of spun fibers (Boulet-Audet *et al.*, 2016; Holland *et al.*, 2007).

As mentioned above, the spidroins are stored at very high concentrations (25-50% w/v), and it is not fully understood how the large spidroins avoid premature aggregation. There are three main hypotheses regarding how the spidroins are stored at a mesoscale: as micelles, as a liquid crystalline feedstock or as liquid-liquid phase separated (LLPS) droplets.

According to the micelle theory, the spidroins organize with the highly soluble terminal domains oriented outward shielding the aggregation prone repetitive region in the core (Hagn *et al.*, 2010; Lin *et al.*, 2017; Parent *et al.*, 2018). The micelles are hypothesized to

elongate and fuse due to shear and a decreased pH in the duct (Eisoldt *et al.*, 2012; Hagn *et al.*, 2010; Parent *et al.*, 2018). Cryo-TEM and NMR diffusion experiments of diluted dope suggested the presence of larger assemblies of micelles with around 300 nm in diameter (Parent *et al.*, 2018). Micelle formation has also been observed for a recombinant mini-spidroin containing both terminal domains (Andersson *et al.*, 2017).

The second hypothesis suggests that the dope forms a liquid crystalline feedstock (Kerkam *et al.*, 1991; Knight and Vollrath, 1999; Vollrath and Knight, 1999), which infers that the proteins act as a liquid that enables them to move through the narrow duct, and at the same time, the dope has the molecular characteristics of a crystal (Knight and Vollrath, 1999). While Knight and Vollrath observed liquid crystals of 2.2 μm in diameter (Knight and Vollrath, 1999), studies using small angle X-ray scattering, atomic force microscopy and scanning electron microscopy have identified heterogenous liquid crystalline granules with around 1 μm in diameter in the storage sac (Lin *et al.*, 2017) but how the spidroins are ordered in those is not clear.

Lastly, LLPS has been observed for recombinant spidroins as well as for native dope in response to incubation in potassium phosphate (> 300 mM) and other kosmotropic anions forming 1-10 μm diameter large droplets (Exler *et al.*, 2007; Malay *et al.*, 2020; Mohammadi *et al.*, 2019; Slotta *et al.*, 2008). The repetitive region and CT were shown to be the main drivers of this phenomenon, although LLPS can also occur without CT (Exler *et al.*, 2007; Malay *et al.*, 2020). The recombinant spidroins are in an oligomeric state but it is not clear if they are in a β-sheet conformation (Exler *et al.*, 2007; Mohammadi *et al.*, 2019; Slotta *et al.*, 2008) or in their native state (Malay *et al.*, 2020). Interestingly, acidification of phase separated spidroins containing both terminal domains triggered the formation of nanofibrils, and fibers could be pulled from the liquid surface indicating that the LLPS state might be of importance during silk formation (Malay *et al.*, 2020). Even though studies of LLPS have only been conducted on spidroins based on MaSp2, native dope has also been shown to undergo LLPS in response to incubation in potassium phosphate at pH 8, while the formation of a fibrillar network was observed when the pH was lowered to pH 4.5 (Malay *et al.*, 2020).

The three theories do not necessarily contradict each other but the precise storage mode of the aggregation prone spidroins still remains to be described. A difficulty in such studies is that available methods often require sample preparation procedures, for instance drying, dilution, fixation in formaldehyde, freezing or exposure to vacuum, that are likely to induce artefacts.

1.6.3 Spidroin polymerization

The environmental changes in the silk gland that were described above cause the soluble spidroins to convert from an overall helical and disordered conformation in the storage sac into a solid fiber rich in β-sheets (Hijirida *et al.*, 1996; Hronska *et al.*, 2004; Lefèvre *et al.*, 2007). The main structural transition might take place in the draw down taper as Congo red, an amyloid fibril staining dye, stained the content of the lumen from the draw down taper onwards (Knight *et al.*, 2000). Furthermore, cryo-SEM showed that the dope pulls away from cuticle intima in the draw down taper indicating that this is the location where the dope is converted into the fiber (Vollrath and Knight, 1999). In line with this, Raman spectroscopy of dried gland content at various positions along the duct showed that in the first and second limb of the duct, the spidroins maintain unordered structures while β-sheets start to form between the second and the third limb. Most β-sheets seem to form between the draw down

taper and the valve while alignment of the chains occurred closer to the valve, hence β-sheet formation and alignment may occur sequentially (Lefèvre et al., 2008).

Structural transitions of the spidroins are proposed to take place via a “lock and trigger” mechanism (Andersson *et al.*, 2014; Rising and Johansson, 2015), (Figure 2). The lock and trigger mechanism states that NT is monomeric at neutral pH but locks the spidroins together in a network by dimerizing at a low pH while CT unfolds and adopts a β-sheet conformation which probably triggers the repetitive region to convert into β-sheets, much like the seeding phenomenon observed in the formation of amyloid fibrils (Figure 2). This mechanism is described in detail below.

1.6.4 Structure and function of the terminal domains

1.6.4.1 The N-terminal domain

The 130-residue long, structurally conserved NT domain consist of five α-helices. The N-terminal pole is positively charged while the C-terminal pole has an overall negative charge (Figure 7 A), (Askarieh *et al.*, 2010; Garb *et al.*, 2010; Hagn *et al.*, 2011; Jaudzems *et al.*, 2012; Kronqvist *et al.*, 2014; Rising *et al.*, 2006). In isolation, NT is monomeric and highly soluble at neutral pH (Askarieh *et al.*, 2010; Hedhammar *et al.*, 2008; Kronqvist *et al.*, 2014) as it can be concentrated to 200 mg/ml at 4°C without precipitation and at lower concentrations it is stable at room temperature for weeks (Hedhammar *et al.*, 2008).

In MaSp NT of *Euprosthenops australis*, charged residues (Asp40, Arg60 and Lys65) mediate electrostatic interactions between subunits (Kronqvist *et al.*, 2014). Around pH 6.5, which is found in the beginning of the duct, protonation of Glu79 and 119 occurs and the buried Trp10 residue that is located between helix 1 and 3 rearranges to allow helix 3 to relocate leading to the formation of a loose, antiparallel dimer (Kronqvist *et al.*, 2014). At pH 5.7, as measured half-way through the duct, Glu84 becomes protonated leading to the formation of a stable dimer (Figure 7 B), (Andersson *et al.*, 2014; Kronqvist *et al.*, 2014; Wallace and Shen, 2012). In the dimer, Asp40 and Lys65 form a conserved salt bridge (Kronqvist *et al.*, 2014). Importantly, the formation of the dimer makes the protein significantly more stable as studied by thermal and chemical denaturation assays (Andersson *et al.*, 2014; Kronqvist *et al.*, 2014). Due to its pH-sensitivity, NT has a dual function during fiber formation; (i) it mediates solubility to the spidroins during storage in the sac and (ii) interconnects the spidroins in a continuous network during silk formation (Figure 2), (Andersson *et al.*, 2014; Askarieh *et al.*, 2010; Kronqvist *et al.*, 2014; Landreh *et al.*, 2010; Rising *et al.*, 2006).

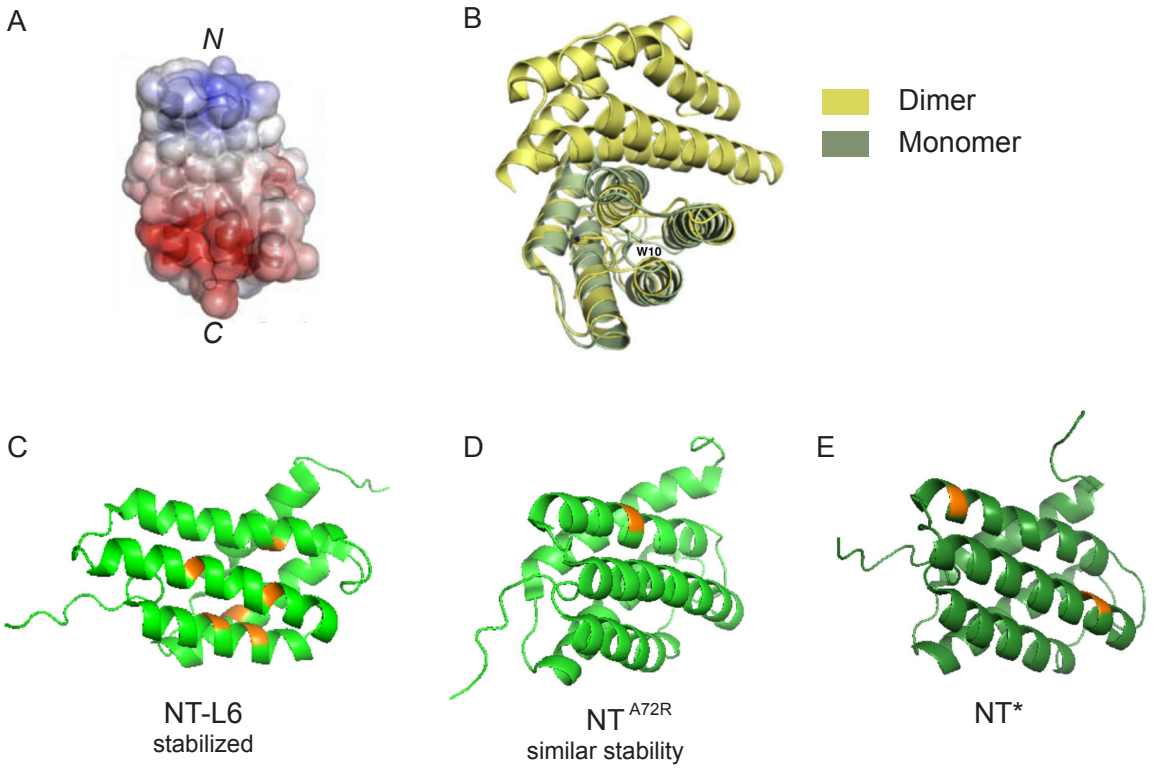

Figure 7: Structures of NTs. A) Dipolar charge distribution on NT with a positively charged N-terminal pole (blue) and a negatively charged C-terminal pole (red). Reprinted with permission from (Askarieh *et al.*, 2010). B) Structural changes in monomeric NT (pale green) compared to the dimer (pale yellow). Monomeric NT structure was determined by NMR spectroscopy (PDB ID: 2LPJ) and dimeric NT with X-ray crystallography (PDB ID: 3LR2). Reproduced with permission from (Jaudzems *et al.*, 2012). C) Structure of NT-L6. Mutations are indicated in orange (PDB ID: 6QJY), (Heiby *et al.*, 2019). D) Solution NMR structure of NT^{A72R} . Mutations are indicated in orange (PDB ID: 2LPI), (Jaudzems *et al.*, 2012). E) Mutations in NT* are indicated in orange in the NT wildtype structure determined by solution NMR spectroscopy (PDB ID: 2LPJ).

NT has an unusually high Met content which fluidizes its fold. Substitutions of six Met residues located in the hydrophobic core of NT to Leu (NT-L6; Figure 7 C) results in no evident structural changes, but the NT-L6 mutant monomer is stabilized and dimerization at low pH is impaired (Heiby *et al.*, 2019). Met side chains are highly flexible as the thioether bond can rotate easily. It is suggested that this flexibility gives NT the structural plasticity that is required for structural rearrangements during dimerization (Heiby *et al.*, 2019).

In the study of the dimerization mechanisms, many mutant variants of NT have been generated, e.g. NT^{A72R} and NT*, both of which are constitutive monomers. In NT^{A72R} an Ala residue, located in the dimer interface and in contact with the corresponding residue of the other subunit, is substituted with an Arg (Figure 7 D) which makes that NT mutant monomeric also at lower pH, probably as a result of steric hindrance (Jaudzems *et al.*, 2012). The other mutant, NT*, is a charge-reversed double mutant in which electrostatic interactions between the monomers are prevented (Figure 7 E), (Kronqvist *et al.*, 2017). More specifically, Asp40 was replaced by Lys and Lys65 was replaced by Asp as to decrease the dipole charge distribution. Interestingly, NT* is highly soluble and stable in its monomeric form, properties that have enabled the development of this mutant as an effective solubility- and expression-enhancing fusion partner for heterologous protein expression (Abdelkader and Otting, 2021; Abelein *et al.*, 2020; Kronqvist *et al.*, 2017; Sarr *et al.*, 2018). Even though dimerisation is inhibited in both these mutants, they differ in their stability; NT^{A72R} shows a lower thermal stability (similar to monomeric NT at pH 8) also at low pH than NT* which is considerably more stable across a pH range of 5-8 (has the same stability as the dimer form of NT also at high pH), (Jaudzems *et al.*, 2012; Kronqvist *et al.*, 2014).

As apparent, NT has been studied extensively in the past in terms of structure, function, and stability. Wildtype NT and several of its mutants have been characterized under different conditions such as low pH, high salt and even in the crowded environment of bacterial cells. The α-helical secondary structure content of the monomer, the dimer and the mutants remain constant under all these conditions (Bauer and Scheibel, 2017b; Hedhammar *et al.*, 2008; Heiby *et al.*, 2019; Jaudzems *et al.*, 2012; Kaldmäe *et al.*, 2020; Kronqvist *et al.*, 2014; Sarr *et al.*, 2022). Even though amyloidogenic regions are predicted in the primary structure of NT, amyloid formation by NT has never been observed prior to this thesis work (Kaldmäe *et al.*, 2020; Kronqvist *et al.*, 2014).

1.6.4.2 The C-terminal domain

The spidroin CT consists of 5 helices and forms a constitutive parallel dimer (Figure 8). The monomer subunit in most of the CTs characterized to date is stabilized by two intramolecular salt bridges that connect helix 1 and 2 with helix 4 (Collin *et al.*, 2018; Gao *et al.*, 2013; Strickland *et al.*, 2018). Notably, the salt bridge between helix 2 and 4 is evolutionary strictly conserved (Andersson *et al.*, 2014; Gao *et al.*, 2013; Hagn *et al.*, 2010).

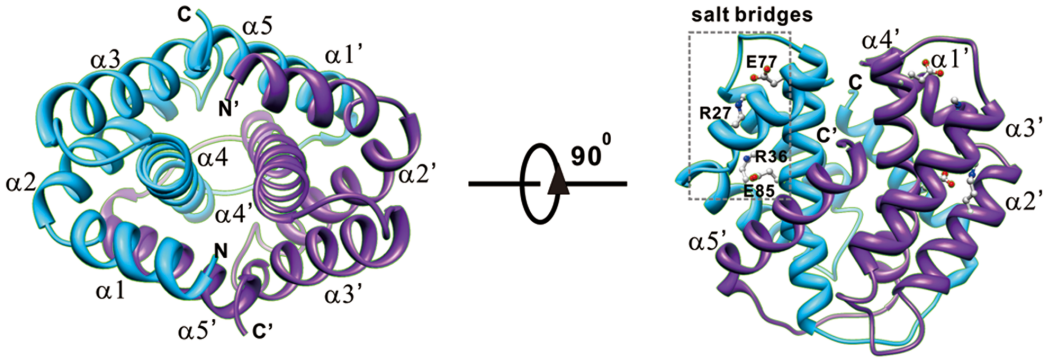

Figure 8: Structure of the minor ampullate (MiSp) CT dimer at neutral pH. Each subunit in the CT dimer consists of 5 helices that are stabilized by two intramolecular salt bridges and dimer is held together mainly by hydrophobic interactions. Reprinted with permission from (Gao *et al.*, 2013).

The dimers are held together by hydrophobic interactions (between helix 1 and 5', helix 5 and 1', and helix 4 and 4'), (Gao *et al.*, 2013; Alexander Sponner *et al.*, 2005). Additionally, a disulfide bridge connects the monomers in MaSp CTs, but its presence is not crucial for fiber formation *in vitro* (Hedhammar *et al.*, 2008; Ittah *et al.*, 2007). The CT dimer from the minor ampullate spidroin (MiSp) lacks this disulfide bridge. The surface of the domain is a polar and overall negatively charged while hydrophobic residues are buried in the core (Gao *et al.*, 2013). CT is soluble during storage conditions while it is prone to form β-sheets when destabilized by low pH, shear forces, high salt and possibly also CO_2 (Andersson *et al.*, 2014; Gao *et al.*, 2013; Hagn *et al.*, 2010). In line with this, the MiSp CT has three predicted amyloidogenic regions as predicted with the Waltz algorithm (Figure 9), (Maurer-Stroh *et al.*, 2010).

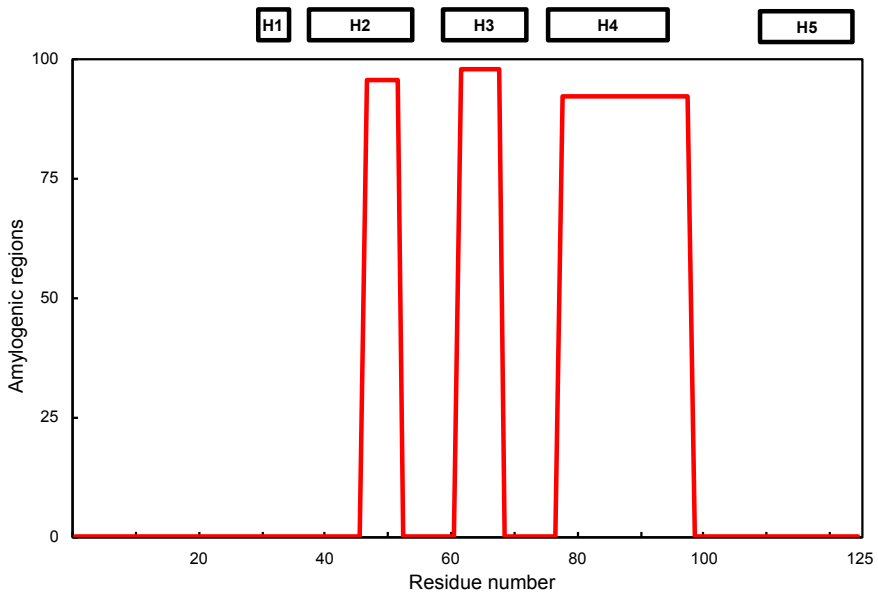

Figure 9: Predicted amyloidogenic regions in MiSp CT from *A. ventricosus*. Three amyloidogenic regions are predicted in MiSp CT in helix 2, 3 and 4. Predicted with the Waltz algorithm (Maurer-Stroh *et al.*, 2010)

CT is likely crucial for silk formation. For example, solutions made from recombinant spidroins that lack CT show no shear-thinning behavior (Rammensee *et al.*, 2008; Vezy *et al.*, 2009) and the proteins are more prone to unspecific aggregation, while fibers made from proteins containing CT have a more well-defined fiber structure (Hagn *et al.*, 2010; Hedhammar *et al.*, 2008; Malay *et al.*, 2020). Thus, CT may promote protein alignment. Below pH 6.8, recombinant MiSp CT in isolation gradually unfolds to eventually form β-sheet fibrils at pH 5.5 and below (Andersson *et al.*, 2014). Protonation of negatively charged residues on the surface of CT decreases the solubility leading to unfolding of the hydrophobic core (Hagn *et al.*, 2010; Alexander Sponner *et al.*, 2005). Helix 2, 3 and 5 of MiSp CT show increased structural flexibility in hydrogen-deuterium exchange mass spectrometry experiments at pH 5.5 (Andersson *et al.*, 2014). The conserved Glu residue in helix 4 is predicted to have a pKa $\geq$ 6 which means it can be protonated along the duct which would disrupt the salt bridge between helix 2 and 4 (Andersson *et al.*, 2014) and contribute to the unfolding of CT. In support of this, mutations of that Glu residue designed to disrupt the salt bridge significantly destabilize CT (Andersson *et al.*, 2014; Gao *et al.*, 2013; Hagn *et al.*, 2010). However, some MaSp CTs do not show this pH dependency (Bauer and Scheibel, 2017a; Hedhammar *et al.*, 2008).

In addition to the pH-induced structural changes, shear forces lead to unfolding and aggregation of the CT (Gao *et al.*, 2013; Hagn *et al.*, 2010). Generally, spidroins are sensitive to shear forces and can form fibers in a process known as flow-induced self-assembly (Chen *et al.*, 2002; Holland *et al.*, 2006). Due to the high flow rate of the dope in the spinning duct as well as the decreased diameter of the duct lumen (Davies *et al.*, 2013; Knight and Vollrath, 1999), considerable shear stress is acting on the spidroins. As shear rates exceeds 2 – 5 s^{-1}, the dope solidifies (Holland *et al.*, 2006). It is hypothesized that the shear aligns and extends the proteins (Hagn *et al.*, 2010; Holland *et al.*, 2006) but it is not known if only CT or also the repetitive region is sensitive to shear forces.

CO_2 is yet another cue that is suggested to aid in the unfolding of CT. A CO_2 analogue (CS_2) has been shown to interact with partially buried hydrophobic residues in helices 2, 3 and 4 which could facilitate the unfolding of CT. Thus, it is possible that CO_2 acts in a similar way which would explain the function of the increased pCO_2 that has been observed along the

gland (Andersson *et al.*, 2014). However, detailed information regarding CT's structural transition from overall α-helical to β-sheet conformation is still lacking.

Interestingly, the fibrils formed by recombinant CT at low pH harbor several hallmarks of amyloid-like fibrils: they bind Thioflavin T (ThT), stain with Congo red, show green birefringence under polarized light, and the fibrils are morphologically similar to amyloid fibrils as observed by electron microscopy (Andersson *et al.*, 2014). Based on this, it has been proposed that the β-sheets formed by CT act as nuclei for the conversion of the repetitive region from α-helix and random coil conformations into β-sheet rich structures (Andersson *et al.*, 2014; Gao *et al.*, 2013; Hagn *et al.*, 2010; Alexander Sponner *et al.*, 2005). Hence, this mechanism resembles the seeding mechanism of amyloid formation, in which natively folded and soluble proteins convert into β-sheet fibrils, and the kinetics of the process can be greatly accelerated by the addition of preformed fibrils (seeds), (Lomakin *et al.*, 1996).

1.6.5 Structure of the spidroin repetitive region in the silk fiber

The currently available models for the molecular structure of the major ampullate fiber is based on the repetitive region only, omitting the terminal domains. In the major ampullate silk fiber, the Gly-rich regions form amorphous structures that contain β-turns, 3_1 helices and possibly 3_{10}-helices which contribute to the extensibility of the fiber (Gray *et al.*, 2016; Holland *et al.*, 2008; Jenkins *et al.*, 2010, 2013; van Beek *et al.*, 2002; Xu *et al.*, 2015). While β-turns and 3_{10}-helices are common secondary structures, the 3_1-helix is less common. The 3_1-helix was first mentioned by Ramachandran and Gould in 1967 in relation to the conformation of collagen (Ramachandran and Gould, 1967). Collagen is now known to form a triple helix with each helix being a PPII (Fraser *et al.*, 1979; Shoulders and Raines, 2009). More than 15 years after Ramachandran's description of the 3_1-helix, Saito and colleagues claimed to observe chemical shifts by NMR spectroscopy that correspond to 3_1-helices in collagen and silk fibroin (Saitô, Tabeta, Asakura, *et al.*, 1984; Saitô, Tabeta, Shoji, *et al.*, 1984) with reference to Ramachandran and Gould. Kümmerlen et al., showed similar chemical shifts for spider silk fibers and Hijirida et al., in spider silk dope in both in 1996 (Hijirida *et al.*, 1996; Kümmerlen *et al.*, 1996) and numerous studies have found 3_1-helices since then (see Table 1), (Jenkins *et al.*, 2013; Lefèvre *et al.*, 2011; Rousseau *et al.*, 2009; van Beek *et al.*, 2002). However, from the literature it is not clear what structure a 3_1-helix corresponds to and, if it is present in the silk fiber, it is not known what part of the spidroins adopts this structure. Most likely, it refers to PPII in the Gly-rich regions (Perea *et al.*, 2013). Even though the Gly rich region is thought to confer the extensibility to the silk fibers, the presence of the GYGQGG has been suggested to increase both tensile strength and extensibility (Arakawa *et al.*, 2022).

The poly-Ala region confers the strength to the fiber by forming β-sheets that are stacked to form crystals (Figure 2 and Figure 10), (Hayashi *et al.*, 1999; Holland *et al.*, 2008; Nova *et al.*, 2010; Sampath *et al.*, 2012). Molecular dynamics suggests that up to 8 strands make up a sheet and that 2-4 sheets compose a crystal (Keten and Buehler, 2010). Crystals size has been estimated to be 2-4 nm in length, 3.1-3.4 nm in width and 1-2 nm in height by computational methods (Bratzel and Buehler, 2012; Keten and Buehler, 2010), while X-ray diffraction studies show that crystal are 2.1-2.7, 2.7-4.0, and 6.4-9.2 nm in size (Du *et al.*, 2006; Sampath *et al.*, 2012). In the β-strands, the orientations of the side chains are alternating sides relative to the backbone and in that way, the sidechains of two strands can

tightly interdigitate in a structure that resembles a zipper. Tight interactions are promoted by high complementarity, hydrophobic and van der Waals interactions (Hayashi et al., 1999). This is similar to the packing of β-strands in steric zippers that are found in amyloid fibrils (Figure 10), (Keten *et al.*, 2010; Nelson *et al.*, 2005; Nova *et al.*, 2010; Sawaya *et al.*, 2007).

Ala has a very low propensity to form β-strands (Johansson *et al.*, 2010) and thus could be considered suboptimal for forming β-sheets in the silk. Hydrophobic amino acid residues generally have a higher propensity to form β-sheets (Johansson *et al.*, 2010) and intriguingly, Ala is the most hydrophobic amino acid that still favors secretion and not insertion in the ER membrane by the translocon (Hessa *et al.*, 2005, 2007). Thus, the poly-Ala sequences are a compromise to comply with opposite constraints; ensuring secretion and preventing precocious aggregation in the gland while still forming β-sheet in the silk fiber (Johansson and Rising, 2021).

In some species, Thr, Gly, Pro, Gln, Ser and Val residues can be found in the poly-Ala segments of MaSps but their effect on the structure, if any, has not been determined (Ayoub *et al.*, 2007; Babb *et al.*, 2022, 2017; Garb *et al.*, 2019; Kono, Ohtoshi, *et al.*, 2021; Lane *et al.*, 2013).

Although poly-Ala is believed to confer the strength and the Gly-rich regions to contribute to the extensibility of the fiber, evidence is emerging that suggest that it might not be that simple (Arakawa *et al.*, 2022; Craig *et al.*, 2020) and the exact structure-function relationship remains to be established. In line with this, in a meta-analysis, comparing alternative residues and the mechanical properties of major ampullate silk fibers, an increased Gly content was found to positively correlate with tensile strength (Craig *et al.*, 2020).

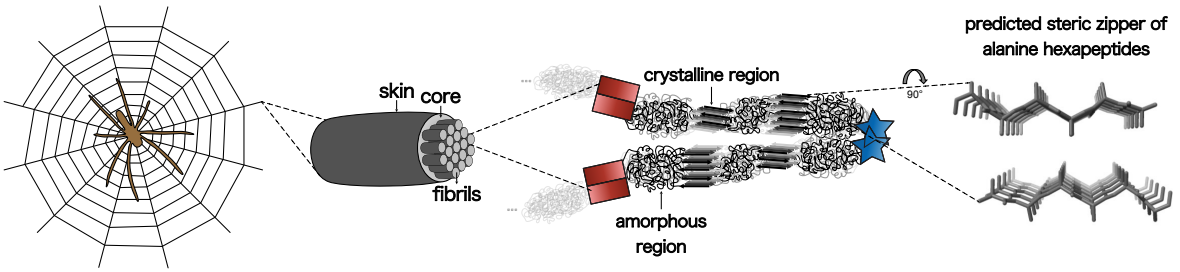

Figure 10: Proposed molecular structure of spider silk fibers. Silk fibers have a skin-core architecture with fibrils in the core. Nanocrystals within the fibrils are composed of stacked β-sheets that are proposed to form steric zippers.

1.7 MAJOR AMPULLATE SILK FIBERS AND THEIR MECHANICAL PROPERTIES

Major ampullate silk fibers have a diameter of 0.3 to 8 μm (Arakawa *et al.*, 2022; Blackledge *et al.*, 2005), are composed of bundles of microfibrils and show a two-to-five-layer architecture (Figure 10), (Andersson *et al.*, 2013; Augsten *et al.*, 2000; dos Santos-Pinto *et al.*, 2015; Frische *et al.*, 1998; Li *et al.*, 1994; Sogawa *et al.*, 2020; A Sponner *et al.*, 2005; Sponner *et al.*, 2007; Vollrath *et al.*, 1997). The difference in the number of identified layers may be due to that harsh and diverse experimental conditions were used which may have introduced artifacts. However, most studies suggest the presence of an inner core that contains the spidroins and an outer skin layer that contains glycoproteins, carbohydrates and lipids. The skin layer has been proposed to protect the fiber for example against proteolysis whereas the core is responsible for the mechanical properties (Yazawa *et al.*, 2018).

The mechanical properties of silk fibers are commonly displayed in stress-strain curves (Figure 11). Initially, the stress-strain curve of a major ampullate silk fiber shows elastic deformation of the silk fiber which is reversible and attributed to stretching of the amorphous region (Keten *et al.*, 2010; Nova *et al.*, 2010). After the yield point, irreversible plastic deformation occurs due to breaking of hydrogen bonds in the amorphous region and eventually the force is transferred onto the β-sheet crystals. Fiber fracture is temporarily hindered by a stick and slip mechanism of the β-strands in the crystals, but increasing pulling forces will ultimately result in breaking of the fiber when the crystals fail (Cranford *et al.*, 2012; Keten *et al.*, 2010; Nova *et al.*, 2010).

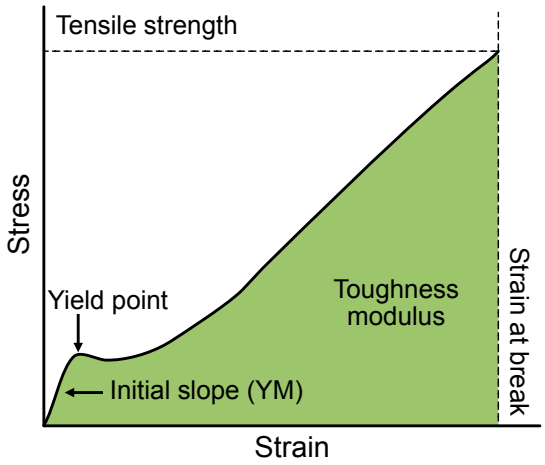

Figure 11: Typical stress-strain curve of spider silk fibers showing key mechanical properties. Fibers show an initial elastic phase, the slope of which is the stiffness of the fiber (Young's modulus, YM). After the yield point, plastic deformation occurs until the breaking point of the fiber. The stress and strain at fiber failure give the tensile strength and extensibility of the fiber, respectively. The toughness is given by the area under the curve.

The strength of the fiber is defined as the force required to break the fiber divided by the area of the initial cross-section of the fiber. The strain is a measure of the maximum extensibility of the fiber, while the Young's modulus (or stiffness) is given by the slope in the elastic phase of the stress-strain curve. The toughness modulus of a fiber is the energy required to break it and is calculated by integrating the stress-strain curve.

1.8 SIMILARITIES AND DIFFERENCES TO AMYLOID FIBRILS

The structure of the spidroins in the fiber is suggested to have some resemblance to that of amyloid fibrils (Andersson *et al.*, 2014; Kenney *et al.*, 2002; Knight and Vollrath, 1999; Slotta *et al.*, 2007; Vollrath and Knight, 2001). Amyloid fibrils are often but not exclusively related to diseases such as Alzheimer's and Parkinson's disease and self-assemble *in vivo* (Sipe *et al.*, 2016). The amyloid fibrils are composed of cross β-sheets in which the β-strands run perpendicular to the fibril axis (Eanes and Glenner, 1968; Jahn *et al.*, 2010) , while the β-strands in the silk fiber are oriented parallel to the fiber axis (Jenkins *et al.*, 2013; Kümmerlen *et al.*, 1996; Parkhe *et al.*, 1997; Simmons *et al.*, 1996; van Beek *et al.*, 2002; Xu *et al.*, 2015). Amyloid fibrils are 5-11 nm in diameter and several microns in length which is significantly smaller than silk fibers (Lopes *et al.*, 2014; Petkova *et al.*, 2002; Sunde and Blake, 1997). Both disease related amyloids and silk fibers originate from soluble precursors and the structural transition occurs under physiological conditions (Eanes and Glenner, 1968; Eisenberg and Jucker, 2012). However, amyloid precursor proteins generally have a

function prior to amyloid formation (Müller *et al.*, 2017). Interestingly, the β-sheet content in a silk-derived peptides was similar to the one in amyloid-β, however, silk was not cytotoxic to neurons in an *in vitro* model while amyloid-β showed cytotoxicity and it was suggested that the surface charge impacts cytotoxicity (Numata and Kaplan, 2011).

1.9 RECOMBINANT SPIDER SILK PRODUCTION

Recombinant production of spidroins in heterologous hosts has been intensely studied in recent years. Various expression systems have been used, ranging from *Escherichia coli* (Prince *et al.*, 1995; Xia *et al.*, 2010), yeast (Jansson *et al.*, 2016) and mammalian cells (Lazaris *et al.*, 2002) to more exotic approaches such as tobacco leaves (Heppner *et al.*, 2016), silkworms (Teulé *et al.*, 2012; Zhang *et al.*, 2019), goat milk (Copeland *et al.*, 2015; Lazaris *et al.*, 2002) and soon potentially even sheep wool (Li *et al.*, 2020). A summary of literature regarding artificial spider silk production is given in Table 2.

1.9.1 Challenges with recombinant spider silk production

Major obstacles in the production of recombinant spidroins are the large and repetitive genes which are often unstable in heterologous hosts and the high demand for Gly and Ala during translation which often results in low expression levels (Koeppel and Holland, 2017). Low protein yield is a problem many protocols struggle with especially since the production of a highly concentrated spinning solution requires large amounts of proteins (Lazaris *et al.*, 2002; Lin *et al.*, 2016; Stark *et al.*, 2007; Zhou *et al.*, 2018).

Another hurdle to overcome is to maintain solubility of the spidroins during recombinant expression as aggregates need to be resolubilized which requires the use of harsh solvents. Solubility is also an issue during protein purification and the following concentration process to produce the spinning dope. Often, recombinant spidroins cannot be concentrated to the high concentrations required for spinning without the use of harsh chemicals (Table 2), (Koeppel and Holland, 2017).

Another challenge recombinant fibers are facing is to match the mechanical properties of natural silk. While recombinant approaches often reach similar toughness values as natural silk, the extendibility is larger and the tensile strength is lower (Cheng *et al.*, 2022; Heidebrecht *et al.*, 2015; Thamm and Scheibel, 2017).

1.9.2 Strategies to overcome the challenges

In a study by Cao et al, an *E. coli* strain that was metabolically engineered to increase the Gly- and Ala-tRNA pool and cultured in media supplemented with Gly and Ala, could express a 110 kDa large spidroin based on MaSp2 (Cao *et al.*, 2017). Even though the protein was relatively large, it stayed soluble and the yield after purification was relatively high (150 mg per liter culture), (Cao *et al.*, 2017). However, no fibers were spun from this protein.

Along the same lines, Xia *et al.* produced spidroins with metabolically engineered *E. coli* with an impressive molecular weight of 285 kDa and yield after purification of 1.2 gram per liter culture in a fermenter. Fibers spun from those spidroins reached a tensile strength of 508 MPa (Xia *et al.*, 2010). In another approach, split-inteins were used to produce even larger

proteins (556 kDa) with even better tensile strength (1031 MPa), (Bowen *et al.*, 2018). However, both approaches faced solubility issues.

To overcome solubility issues, methods often rely on the use of hexafluoroisopropanol (HFIP), urea or guanidine thiocyante (Gdm-SCN) to create spinning dopes (see Table 2), which are subsequently spun into fibers using extrusion in isopropanol (IPA), ethanol or methanol coagulation baths for instance in (Asakura *et al.*, 2022; Heidebrecht *et al.*, 2015; Saric *et al.*, 2021; Teulé *et al.*, 2007; Thamm and Scheibel, 2017; Xia *et al.*, 2010; Zhu, Sun, *et al.*, 2020). Other strategies to improve solubility include the production of mini-spidroins that have a shorter repetitive region than natural spidroins, incorporation of terminal domains and production of chimeric spidroins, i.e. combining domains from different spiders and/or different silks with high solubility. These strategies are discussed in more detail in section 1.9.3.

The production of chimeric proteins is also widely used to improve the mechanical properties (Andersson *et al.*, 2017; Finnigan *et al.*, 2020; Lin *et al.*, 2016; Teulé *et al.*, 2007; Xu *et al.*, 2020; Zhou *et al.*, 2018; Zhu, Rising, *et al.*, 2020; Zhu, Sun, *et al.*, 2020). The toughest as-spun (i.e. without stretching after spinning) artificial spider silk fiber reported to date was produced by Zhu et al (Zhu, Sun, *et al.*, 2020) from a chimeric spidroin containing four pyriform repeats and both terminal domains (from MaSp1 and MiSp, respectively). Recombinant spidroins were dissolved in HFIP and fibers spun in a methanol coagulation bath reached a toughness modulus of 94 MJ/m^3 which is still considerably lower than the toughness of natural silk (136 MJ/m^3), (Blackledge and Hayashi, 2006).

Grip *et al.* employed another elegant strategy by substituting two Ala residues with Cys and saw an increase in tensile strength and stiffness of the fibers likely due to the formation of disulfide bonds (Grip *et al.*, 2009).

Other approaches to improve the mechanical properties of artificial silk fibers include crosslinking or incorporation of inorganic molecules (Cheng *et al.*, 2022; Grip *et al.*, 2009; Zhu, Sun, *et al.*, 2020). Remarkably, by incorporating titanium dioxide and crosslinking fibers with formaldehyde, Zhu and colleagues were able to increase the toughness modulus of their fibers from 94 MJ/m^3 to remarkable 249 MJ/m^3 (Zhu, Sun, *et al.*, 2020). However, the strength was with 167 MPa markedly lower than that of natural spider silk (1217 MPa), Blackledge and Hayashi, 2006).

As the mechanical properties of as-spun fibers do not yet match their natural counterpart, fibers are commonly post-drawn in IPA, ethanol and methanol to enhance their mechanical properties, for example in (Albertson *et al.*, 2014; Bowen *et al.*, 2018; Copeland *et al.*, 2015; Gnesa *et al.*, 2012; Saric *et al.*, 2021; Thamm and Scheibel, 2017). Some of the post-drawn fibers reach impressive mechanical properties with a fiber toughness approaching (Bowen *et al.*, 2018; Copeland *et al.*, 2015; Lazaris *et al.*, 2002; Saric *et al.*, 2021) or even matching natural silk (Heidebrecht *et al.*, 2015; Saric *et al.*, 2021; Thamm and Scheibel, 2017). Recently, it has even been possible to mimic the strength of natural silk (around 1 GPa), (Bowen *et al.*, 2018).

1.9.3 The biomimetic approach

One possible caveat with approaches relying on solubilized proteins, alcohol coagulation baths and the use of crosslinking agents is that the process is fundamentally different from natural silk formation, and it does not resemble the natural spinning process. For example,

the alcohol rapidly removes the hydration shell of the protein which leads to denaturation and aggregation of the proteins in a process that is very distant from the elaborate structural changes seen during natural fiber formation (Rising, 2014). It may very well be that the mechanical properties of natural spider silk fibers can only be reproduced in the lab by mimicking the natural cues and the resulting structural changes (Malay *et al.*, 2022). Current approaches including HFIP and methanol are also problematic from a safety, biocompatibility and environmental perspective and thus should be avoided (Edlund *et al.*, 2018).

As an alternative, a chimeric mini-spidroin termed NT2RepCT has been developed that can be spun in a biomimetic way without the use of hazardous chemicals (Andersson *et al.*, 2017; Finnigan *et al.*, 2020; Gonska *et al.*, 2020; Schmuck *et al.*, 2021). The repeat region of the mini-spidroin contains two poly-Ala and three Gly-rich regions based on *E. australis* MaSp1 and has a low molecular weight compared to the native major ampullate spidroins. A longer repeat region could increase the mechanical properties of artificial fibers since the repetitive region confers the mechanical properties to the silk and more repeats will likely result in increased intermolecular interaction. However, a positive correlation between the molecular weight and mechanical properties of artificial silk fibers has only been found in studies using denaturing conditions (Jin *et al.*, 2022; Xia *et al.*, 2010; Zhu, Rising, *et al.*, 2020) and it is not clear if the same holds true for a biomimetic spinning approach.

The terminal domains are crucial for fiber assembly and solubility of the protein, and they should thus be included in recombinant proteins intended for biomimetic spinning (Eisoldt *et al.*, 2012; Ittah *et al.*, 2006; Malay *et al.*, 2020; Saric *et al.*, 2021). NT2RepCT contains both terminal domains (NT from *E. australis* MaSp1 and CT from *A. ventricosus* MiSp) and can be produced under conditions that are compatible with a native protein fold. Expression in *E. coli* in a bioreactor yielded 14.5 mg/l of purified protein (Schmuck *et al.*, 2021), and NT2RepCT can be concentrated to >50% in an aqueous buffer at pH 8 and spun into fibers by extrusion into a sodium acetate buffer at pH 5 (Andersson *et al.*, 2017). The assembly of NT2RepCT is pH dependent and recapitulates important molecular mechanisms associated with native silk spinning (Otikovs *et al.*, 2017). To clarify, silk production of NT2RepCT is biomimetic in the sense that the protein is purified under non-denaturing conditions, and the spinning process aims to mimic the natural spinning process (i.e. all-aqueous solvents, shear forces and lowered pH). However, the salt concentrations and the gradual decrease in pH were not mimicked yet. This was attempted by Saric *et al.,* Gonska *et al.,* and Peng *et al.*

Saric and colleagues observed that dialyzing artificial spinning dope against phosphate buffer prior to spinning increased the fibers strength (reaching 834 MPa after post-spin stretching) and extensibility (32%), possibly by initiating self-assembly of the proteins (Saric *et al.*, 2021). Peng and colleagues developed a microfluidic chip that mimics the shear stress acting on the spidroins in the duct. By pumping an artificial spinning dope through the chip that mimics the shape of the duct, they were able to spin fibers with a strength of 286 MPa after post-spin stretching (Peng *et al.*, 2016). Gonska *et al.* used the straining flow spinning method in which the pH is decreased more gradually (Gonska *et al.*, 2020). However, only the strain of the fibers improved while the strength decreased significantly compared to the fibers spun in Andersson *et al.,* 2017. Even though the methods use alcohol for post-spin stretching or acetonitrile in the spinning bath which makes them incompatible with a biomimetic approach, mimicking the change in ions and shear stress are promising approaches to further increase the degree of biomimicry.

The NT2RepCT fibers have impressive mechanical properties for an as-spun fiber and is outcompeting most non-biomimetic fibers that are produced by using HFIP and other alcohol spinning baths (Table 2). Hence, the protein NT2RepCT and the fibers spun from it are interesting for further characterization and development to enable large scale production of materials that match native spider silk fibers.

While much focus has been put on the properties of the spun artificial silk fibers, the dope prepared from recombinant spidroins has gotten little attention. To the best of my knowledge, only two papers have included rheological characterization of recombinant spidroin solutions (Finnigan *et al.*, 2020; Rammensee *et al.*, 2008). Rammensee *et al.* prepared colloidal suspensions from recombinant spidroins based on two MaSp sequences from the *Araneus diadematus* lacking the terminal domains and subjected them to shear. One of them showed Newtonian behavior, the other one showed shear-induced aggregation at very high shear rates, and both showed very low viscosity of around 0.002 Pa·s (Rammensee *et al.*, 2008). Finnigan and colleagues developed a mini-spidroin composed of both terminal domains, three poly-Ala repeats and four Gly-rich repeats which they subjected to shear. Similarly to native dope, the artificial dope was shear-thinning but unlike native dope, it had a significantly lower viscosity of 9 Pa·s (Finnigan *et al.*, 2020). Thus, both studies struggled to mimic the key rheological properties of native dope (Chen *et al.*, 2002; Holland *et al.*, 2006; Kojić *et al.*, 2006). Oscillatory measurements were not conducted in either of the studies. The rheological properties of silkworm dope, which has very similar rheological properties to spider silk dope, influence the fiber properties, and thus a truly biomimetic production method of spider silk fibers should include the rheological behavior of the dope (Boulet-Audet *et al.*, 2016; Holland *et al.*, 2007, 2006; Park and Um, 2018).

Table 2: Production and mechanical properties of recombinant silk fibers based on MaSp sequences and chimeras with MaSps (including the terminal domains) and natural silk. Only studies showing mechanical properties are shown. If several fibers were produced in a study, the one with the highest stress or toughness is shown in the table. Values were rounded to integers if appropriate. YM: Young's modulus, MAC-T: Bovine Mammary Alveolar Cell Line, BHK: Baby hamster kidney fibroblasts, PBS: phosphate-buffered saline, HFIP: Hexafluoroisopropanol, Gdm-SCN: guanidine thiocyante, MetOH: methanole, EtOH: ethanol, IPA: isopropanole, NaAc: sodium acetate, AcNi: acetonitrile, PEG: polyethylene glycol, KPi: potassium phosphate CuS: Copper sulfide, NP: nano particles, (-) not performed/not applicable, n.s.: not stated, * produced in a fermenter, § incorporation titanium oxide and crosslinking with formaldehyde, ‡ protein was purchased from Spiber Inc., # estimated values from stress-strain curves. Note, Grip et al., 2009 states that comparisons with the literature should be made with caution as diameter might be underestimated, and fibers always broke at grips during tensile tests.

								Mechanical properties (as-spun)						Mechanical properties after post-spinstretching				
Reference	NT	CT	Size (kDa, monomer)	Host	Yield after purification (mg/l)	Protein concentration (%)	Solvent	Spinning bath	Strength (MPa)	Strain at break (%)	Toughness modulus (MJ/m3)	Diameter (µm)	YM (GPa)	Medium for stretching	Draw ratio	Strength (MPa)	Strain at break (%)	Toughness modulus (MJ/m3)	Diameter (µm)	YM (GPa)
Lazaris, 2002	–	+	60	MAC-T and BHK	20 –50	>23	PBS	MetOH, water	–	–	–	–	–	75%MetOH	5	270	43	101	20	13.2
Teule, 2007	–	–	62	E. coli	n.s.	2.5–3.0	HFIP	90%IPA	50±19	15.8±6.1	11±10	16±6	1.1 ±1.0	–	–	–	–	–	–	–
Stark, 2007	–	+	24	E. coli	40	0.06–0.2	Tris-HCl pH 8	tilting in tubes	–	–	–	–	–	air	2	200	800%		80	
Grip, 2009	–	+	24	E. coli	n.s.	n.s.	Tris-HClpH 8	20 mM Tris-HCl, pH 8	–	–	–	–	–	air	"gently until straight"	110±30	1.2±0.3	n.s	40 –90	12±4
Xia,2010	–	–	285	E. coli*	1200	2	urea, HFIP	90%MetOH	–	–	–	–	–	90%MetOH	5	508±108	15±5	82	n.s.	21±4
An, 2011	–	–	70	E. coli*	n.s.	3	HFIP	100%IPA	36±8	3.1±1.8	0.9±0.6	41±4	2.8±0.5	75%IPA	3	133±49	23±19	24±19	17±5	5.7±2.4
Teule, 2012	–	–	58	E. coli	n.s.	2.6–2.7	HFIP	90%IPA	28±25	1.7±0.6	0.3±0.4	68±25	1.1±1.3	90%IPA	2–2.5	128±23	52±24	55±24	28±6	4.4±1.0
An, 2012	–	–	66/48	E. coli*	120	3	HFIP	100%IPA	23±11	1.2±0.4	0.2±0.1	58±5	2.3±0.7	75%IPA	3	38±20	54±68	17±20	29±5	3.4±1.1
An, 2012	–	–	66/48	E.coli*	120	3	HFIP	100%IPA	13±6	0.9±0.4	0.07±0.07	58±5	1.6±0.4	75%IPA	3	60±19	5±9	2.5±5.4	29±5	4.3±0.9
Albertson, 2014	–	–	87	E. coli*	n.s.	45-60	HFIP	100%IPA	14±7	1.2±0.5	0.10±0.13	62±3	1.9±1.9	85%IPA	4	39±7	181±103	59±37	36±6	1.6±0.4
Heidebrecht, 2015	–	+	60	E. coli	n.s.	1.0–1.7	Gdm-SCN	90%IPA	54±16	7±2	2±0.8	39±6	2±0.9	90%IPA	6	383±118	95±24	172±52	26±6	3±2
Heidebrecht, 2015	+	+	134	E. coli	n.s.	1.0–1.7	Gdm-SCN	90%IPA	13 ±2	6±1	0.3±0.1	155±8	0.5±0.1	90%IPA	6	370±59	110±25	189±33	27±10	4±1
Copeland, 2015	–	+	65	Transgenic goats (milk)	n.s.	2.5	HFIP +formic acid	100%IPA	33±7	1.1±0.3	0.18±0.07	61±2	3	80%MeOH	1.5 and 2.0	222±11	56±7	103±14	29±1	n.s.
Jones, 2015	–	–	50–75	Transgenic goats (milk)	n.s.	1.2	H_2O	100%IPA	–	–	–	–	–	80% and 20% IPA	2–2.5	192±52	28±26	34±34	n.s.	8.3
Peng, 2016	–	–	47	E. coli	n.s.	21	water, NaCl	100%EtOH	–	–	–	–	–	70% EtOH	3	286±137	18±13	38±29	14	8.4±4.3
Lin, 2016	–	+	64	E. coli	25	0.04	K_3PO_4	Air (hand drawn)	–	–	–	–	–	75%IPA	n.s.	21±1	28±17	5±3	3±0.3	0.8±0.05
Lyda, 2017	+	+	~60	Leishmania tarentolae	n.s.	12.5–25.0	urea, Tris-HCl, NaH_2PO_4, NaCl, pH 5	air and 0.5% gellan gum solution	67±21	2±7	8.07±0.55	20 –150	1.2±0.9	–	–	–	–	–	–	–
Andersson, 2017	+	+	33	E. coli	125	50	Tris-HCl pH 8	500 mM NaAc, 200 mM NaCl pH 5	162±8	37±5	45±7	12±2	6±0.8	–	–	–	–	–	–	–

Thamm, 2017	+	+	43	E. coli*	300 –400	15	Gdm-SCN	IPA	31±7	4±1	0.9±0.2	77±7	0.9±0.1	IPA	4	282±66	102±24	144±44	49±7	1.5±0.3
Bowen, 2018	–	–	556	E. coli*	n.s.	17	urea, HFIP	95% MetOH	–	–	–	–	–	75% MetOH	6	1031±111	18±6	114±51	6±1	13.7±3
Zhou, 2018	+	+	104	E. coli	35	4	urea, Triton X–100	Air (hand drawn)	245±34	280±11	51±20	1.5±0.4	6.7±1.8	–	–	–	–	–	–	–
Xu, 2020	+	+	43	E. coli	71	0.08–0.1	Tris–HCl	Air (hand drawn)	149±65	18±8	21±13	2.2±1.2	7.3±3.6	–	–	–	–	–	–	–
Zhang, 2020	+	+	40–50	E. coli	n.s.	10–30	urea	200 mM NaCl and 400 mM CH_3COONa, pH 6	53±2	97±2	3.6±0.1	92±5	1.7±0.3	–	–	–	–	–	–	–
Zhu, Rising, 2020	+	+	92	E. coli	n.s.	8–10	HFIP	100% MetOH	119±4	70±7	63±5	7.4±0.1	3.9±0.3	–	–	–	–	–	–	–
Zhu, Sun, 2020	+	+	93	E. coli	n.s.	6–7	HFIP	100% MetOH	48±5	30±17	94±9	9±1	3.1±0.2	–	–	–	–	–	–	–
Zhu, Sun, 2020 §	+	+	93	E. coli	n.s.	6–7	HFIP	100% MetOH	167±14	197±20	249 ±22	8.9±0.8	6.3±0.7	–	–	–	–	–	–	–
Gonska, 2020	+	+	33	E. coli	n.s.	40	Tris–HCl pH 8	500 mM NaAc, 200 mM NaCl, 10% AcNi, 30% PEG	8±2	90±80	6±6	38±6	0.3±0.05	n.s.	n.s.	29±5	20±0	4±1	27±4	0.5±0.07
Greco et al., 2020	+	+	33	E. coli	n.s.	30	Tris–HCl pH 8	500 mM NaAc, 200 mM NaCl pH 5	80±64	37±56	40 ±70	15±7	2.4 ±1.7	–	–	–	–	–	–	–
Finnigan, 2020	+	+	35	E. coli	420	30	Tris–HCl pH 8	50 mM NaAc, 500 mM KPi pH 5	40±14	3±1.5	3.9±3.4	28±7	1.8±0.7	–	–	–	–	–	–	–
Kvick, 2021	–	+	23	E. coli	n.s.	0.1	Tris–HCl pH 8	Liquid–air interface	60	1	n.s.	40–75	2 –8	–	–	–	–	–	–	–
Hu, 2021	+	+	~65	E. coli*	1200	20	phosphate, urea, NaCl	90% EtOH, 17.5 mM AcOH pH 5	n.s.	n.s.	n.s.	n.s.	n.s.	80% EtOH	5	289±21	47±4	101±13	34±0.7	3.8±0.3
Kono 2021	+	+	50/26	E. coli*	n.s.	22	DMSO, LiCl	MetOH/DMSO	~100#	~28#	~25#	n.s.	n.s.	–	–	–	–	–	–	–
Asakura, 2022	–	–	210	n.s.‡	n.s.	22	formic acid	MetOH	–	–	–	–	–	air (1.5x) and water (3.0x)	4.5	286±13	31±4	n.s.	35.3	n.s.
Jin, 2022	–	–	169	Corynebacterium glutamicum*	68	40	water	90% EtOH	–	–	–	–	–	80% EtOH	4	~170	59±11	~75	n.s.	~4.5
Cheng, 2022	+	+	~65	E. coli*	n.s.	19	phosphate, urea, NaCl pH 7.4	90% EtOH, 17.5 mM AcOH pH 5	–	–	–	–	–	with CuS–EtOH NP	n.s.	218±10	94±9	160±21	n.s.	4.9±0.2
Saric, 2021	+	+	~60	E. coli	n.s.	15	Gdm-SCN	0.5–1 M KPi, pH 6	–	–	–	–	–	80% IPA	4	834±34	32±1	143±6	27±1	5±0.4
Paper II	+	+	33	E. coli*	9000	30	Tris–HCl pH 8	750 mM NaAc, 200 mM NaCl pH 5	132±32	160±37	146±42	4.1±0.78	3.5±0.9	–	–	–	–	–	–	–
Native silk (Blackledge, 2006)	+	+	250 –300	–	–	30-50	–	–	1217±56	23±7	136±7	1 –6	8.0±0.8	–	–	–	–	–	–	–

1.10 RECOMBINANT SPIDROINS FOR BIOMEDICAL APPLICATIONS

Materials made from recombinant spidroins are promising for biomedical applications as they (i) can be produced at a consistent quality (ii) are defined and of non-animal origin (iii) can be processed into several different morphologies and (iv) can be functionalized through genetic engineering (Aigner *et al.*, 2018).

1.10.1 Immune response to recombinant spidroins

Few studies have analyzed the immune response to recombinant spidroins. One reason to this could be that that most methods use *E. coli* to produce spidroins, which means that the target proteins likely will be contaminated with endotoxins. Endotoxins from gram-negative bacteria can cause serious health issues in humans ranging from inflammation, fever to death (Cookson *et al.*, 1997; Wolff, 1973). Unfortunately, endotoxins are inherently challenging to remove (Mamat *et al.*, 2015). Thus, it is difficult to differentiate if an acute immunological response is due to endotoxin contaminants or a response to the spidroins. Indeed, in an *in vitro* study, soluble proteins purified from *E. coli* at 1 mg/ml caused cytotoxicity and macrophage activation in fibroblasts (Dams-Kozlowska *et al.*, 2013). In another *in vitro* study, human peripheral blood mononuclear cells (hPBMCs) were cultured on a scaffold of recombinant spidroins and hyaluronic acid. hPBMCs showed T cell, B cell and natural killer cell activation likely caused by the endotoxins from *E. coli* (Lin *et al.*, 2021). However, in both studies endotoxin removal was not performed.

Protocols to remove contaminating endotoxins have been developed, although these are tedious and not suitable for large-scale production. However, in support of the importance of removing endotoxin, implantation of fibers made from spidroins that had undergone endotoxin removal procedures evoked a low immunogenic response (Fredriksson *et al.*, 2009). Deptuch and colleagues published two *in vivo* studies on their endotoxin purified spheres composed of recombinant spidroins based on MaSp1 from *Trichonephila clavipes* (Deptuch *et al.*, 2021, 2022). No toxicity was detected when the spheres were administered intravenously or implanted subcutaneously in mice (Deptuch *et al.*, 2021, 2022). However, the latter procedure caused an immune response including increased level of B lymphocytes and the formation of anti-silk antibodies suggesting that this reaction is caused by the spidroin spheres (Deptuch *et al.*, 2022).

1.10.2 Versatile morphologies and applications of recombinant spidroins

In addition to using recombinant silk proteins to make fibers for the production of nerve conduits (An *et al.*, 2015; Bini *et al.*, 2006; Hansson *et al.*, 2021), they can also be processed into various 2D and 3D morphologies such as films, foams, meshes, spheres and hydrogels for example in (Åstrand *et al.*, 2020; Esser *et al.*, 2021; Florczak *et al.*, 2017; Kozlowska *et al.*, 2017; Numata *et al.*, 2012; Schacht *et al.*, 2016; Schacht and Scheibel, 2011; Stern-Tal *et al.*, 2021; Widhe *et al.*, 2016, 2010, 2013). Potential applications of those include scaffolds for tissue engineering (Gomes *et al.*, 2011; Johansson *et al.*, 2019; Schacht *et al.*, 2016; Widhe *et al.*, 2010; Zhu *et al.*, 2015), carriers for drug delivery (Hermanson *et al.*, 2007; Lammel *et al.*, 2008; Numata and Kaplan, 2010; Price *et al.*, 2014) or as implant coatings (Borkner *et al.*, 2014; Huang *et al.*, 2020; Nilebäck *et al.*, 2017; Zeplin *et al.*, 2014). A complete survey of the topic is beyond the scope of this thesis, however, it should be highlighted that the approach of producing spidroins recombinantly comes with the

possibility to change the protein sequence relatively easily, e.g. to add functional motifs to the proteins (Åstrand *et al.*, 2020; Bini *et al.*, 2006; Chouhan *et al.*, 2018; Harvey *et al.*, 2020; Johansson *et al.*, 2020; Kozlowska *et al.*, 2017; Lang *et al.*, 2022; Mulinti *et al.*, 2022; Widhe *et al.*, 2016). For example, an RGD motif and fibronectin derived peptide, respectively, were fused to 4RepCT to promote cell adhesion of different human primary cells (Widhe *et al.*, 2016, 2013). Similarly, films composed of an hydroxyapatite binding domain fused to a recombinant spidroin were used to culture hMSCs that showed enhanced osteoinductive properties (Dinjaski *et al.*, 2017). Florczak *et al.* functionalized spheres composed of a mix of spidroins based on MaSp1 and MaSp2 with a human epidermal growth factor receptor 2 binding peptide to target cancer cells. When the spheres were loaded with cytostatic drugs, they effectively killed the targeted cells *in vitro* (Florczak *et al.*, 2017).

Hydrogels are an interesting type of material as they contain large amounts of water and can mimic the structure of the extracellular matrix (ECM), which makes them suitable for applications as cell culture scaffolds in tissue engineering. Their polymeric network makes them also an interesting material for the development as drug carrier and release systems (Geckil *et al.*, 2010; Guo *et al.*, 2019; Guvendiren and Burdick, 2013).

1.10.3 Recombinant spidroin hydrogels

Hydrogel formation of proteins is commonly associated with a structural transition that leads to increased intermolecular interactions (van der Linden and Foegeding, 2009; Ziegler and Foegeding, 1990). Therefore, most research on spider silk hydrogels has focused on the repetitive domain and CT due to their intrinsic ability to undergo major structural changes (Table 3), (DeSimone *et al.*, 2016, 2017; Heinritz *et al.*, 2021; Humenik *et al.*, 2020; Kumari, Bargel, *et al.*, 2020; Kumari, Lang, *et al.*, 2020; Laomeephol *et al.*, 2021; Lechner *et al.*, 2022; Luo *et al.*, 2018; Neubauer *et al.*, 2021; Qian *et al.*, 2015; Rammensee *et al.*, 2006; Schacht *et al.*, 2015; Schacht and Scheibel, 2011; Song *et al.*, 2021; Thamm *et al.*, 2017; Trossmann *et al.*, 2022). However, the underlying mechanism of hydrogel formation of the repetitive region and CT are poorly understood.

Gelation of the repetitive region can be induced by ammonium persulfate (APS) (Rammensee *et al.*, 2006; Schacht and Scheibel, 2011) or by incubation of the soluble precursors at 37°C (DeSimone *et al.*, 2017; Kumari, Lang, *et al.*, 2020; Schacht *et al.*, 2015). Gelation times of the repetitive region range from 5 hours (Lechner *et al.*, 2022) to several weeks (Rammensee *et al.*, 2006).

Qian and colleagues found that several CTs in isolation gel at low (< 2°C) and high (> 65°C) temperatures (Qian *et al.*, 2015). If fused to repeats from elastin, the CT-elastin fusion protein can gel at 37°C within 40 minutes if phosphate ions are added, however, the mechanical properties are very poor (Song *et al.*, 2021). Virtually all hydrogels formed under benign conditions i.e., at 37°C, show unsatisfactory mechanical properties. The hydrogel with the highest elastic modulus was produced by Thamm *et al.,* in 2017, reaching up to 18 kPa but the gelation occurred after 60 hours of incubation at 37°C and resulted in opaque gels, features which make this gel unsuitable for many applications (Thamm *et al.*, 2017). Hence, all the recombinant spider silk hydrogels developed thus far have one or more drawback, for example the use of harsh cross-linkers, long gelation times, low elastic modulus and/or lack of transparency (Table 3).

Table 3: Studies on recombinant spider silk hydrogels. APS: ammonium persulfate, DMEM: Dulbecco's Modified Eagle's Medium, O.N.: overnight, n.s.: not stated, KPi: Potassium phosphate, DMSO: Dimethyl sulfoxide, eADF4(C16): engineered spidroin with 16 repeats from *A. diadematus* fibroin 4 (MaSp2), eADF4(κ16): positively charged variant of eADF4(C16), eADF4(Ω16) uncharged variant of eADF4(C16), NcCT: MaSp1 CT from *T. clavipes* (former *Nephila clavipes*), MaSpIC: four repeats based on major ampullate spidroin 1 with CT from *T. clavipes*, AdCT: CT from *A. diadematus* fibroin 3, EaCT: CT from *E. australis* MaSp1.

Reference	Composition	Method of gelation	Gelation time	Concentration (%)	Elastic modulus (kPa)	Transparency	Application
Rammensee et al., 2006	ADF–4(C16)	APS and Rubpy	days – week	0.5–3	≈1	n.s.	no experimental data
Schacht & Scheibel., 2011	eADF4(C16)	cross–linking with APS	80 h	3–7	110	mostly opaque	no experimental data
Schacht et al., 2015	eADF4(C16), eADF4(C16)–RGD	37°C	O.N.	3	0.2	opaque	bioink for cell–loaded constructs
Qian et al., 2015	NcCT, AdCT, EaCT,MaSpI4C	2°C and 65°C	10 min	15	0.5 and 0.001	opaque	no experimental data
DeSimone et al., 2016	eADF4(C16)	ionic (by adding DMEM)	10–15 h	3	n.s.	slightly opaque	no experimental data
Thamm et al., 2017	eMaSp1s	37°C	60 h	3, 5, 7	5 – 18	opaque	bioink
DeSimone et al., 2017	eADF4(C16), eADF4(C16)–RGD +gelatin	37°C	O.N.	3–7	5	opaque	bioink
Luo et al., 2018	resilin–CT	37°C	7 h	15	0.4	transparent at low temp, slightly opaque at high temp	drug release
Kumari, Lang et al., 2020	eADF4(C16), eADF–RGD, eADF4(Ω16)	37°C	O.N.	2–3	n.s.	n.s.	antimicrobial materials
Kumari, Bargel et al., 2020	eADF4(C16) + silika–NP	37°C	n.s.	4	n.s.	n.s.	antibacterial, drug release, cell culture scaffold
Humenik et al., 2020	eADF4(C16)	100 mM KPi	24 h	n.s.	n.s.	n.s.	nanohydrogel for protein binding
Heinritz et al., 2021	eADF4(C16)	100 mM KPi	24 h	n.s.	n.s.	n.s.	nanohydrogel for cell attachment
Lechner et al., 2021	eADF4(C16) and eADF–RGD	37°C	5 –8 h	3	1	slightly opaque	bioink
Song et al., 2021	elastin–CT	22°C and 57°C	10 min	15	1 and 0.001	transparent at low, temp, a bit opaque at high temp	no experimental data
		37°C	40 min	15	n.s.	n.s.	
Neubauer et al., 2021	eADF4(C16), eADF4(κ16) and eADF(Ω16)	DMSO	"fast"	1–3	0.1	transparent	no experimental data
Laomeephol et al., 2021	eADF4(C16) + regenerated silkworm silk	37°C	>6 h	3	n.s.	n.s.	cell culture scaffold
Trossmann et al., 2022	eADF4(C16) and eADF–RGD	n.s.	n.s.	3.5	n.s.	opaque	continuous protein release from encapsulated cells
Paper III	NT	37°C	10 min – 2 h	1–50	1–100	transparent	enzyme immobilization

The potential applicability of recombinant spidroin hydrogels has been widely explored and includes their use as a bioink (DeSimone *et al.*, 2017; Schacht *et al.*, 2015; Thamm *et al.*, 2017), a drug delivery device (Luo *et al.*, 2018; Trossmann *et al.*, 2022), an antimicrobial material (Kumari, Bargel, *et al.*, 2020; Kumari, Lang, *et al.*, 2020) or as a cell culture scaffold (Laomeephol *et al.*, 2021; Song *et al.*, 2021).

2 RESEARCH AIMS

The overall aim of this thesis was to engineer and characterize spidroins and use them to produce biomimetic spider silk fibers and novel hydrogels.

More specific aims were to:

- Analyze flow properties and the degree of biomimicry of the artificial spider silk dope (**Paper I**).
- Engineer mini-spidroins to improve the mechanical properties of artificial spider silk fibers that are spun biomimetically (**Paper II**)
- Investigate the phenomena of hydrogel formation in mini-spidroins and their constituent domains (**Paper III**).
- Explore properties and potential application of mini-spidroin hydrogels (**Paper IV**).

3 METHODOLOGY

3.1 RHEOLOGY

Rheology is the experimental characterization of how materials flow or deform under a force. Ideally, two ways of deformation exist: an elastic and a viscous deformation. An ideal solid deforms when a force is applied and returns to its original shape once the force is removed. In contrast, an ideal liquid material remains deformed after the force is removed. However, most materials exhibit both elastic and viscous responses, thus they have viscoelastic behavior. The purpose of using rheology is to quantify the viscoelastic behavior of materials over different time and deformation scales. The results can give indirect information regarding the molecular structure of the material (Janmey *et al.*, 2007; Meyers and Chawla, 1999; Tschoegl, 2012).

The viscosity is a measure of a fluid's resistance to flow and is calculated by dividing the stress by the shear rate. A Newtonian liquid can be fully described by the viscosity as the viscosity is independent of the shear rate (Figure 12 A). However, many materials display shear rate dependent viscosity, i.e. are non-Newtonian. When the viscosity is increasing with an increasing shear rate, materials are considered shear-thickening (Figure 12 A), for example cornstarch suspensions are shear-thickening. Spider silk dope is a shear-thinning material which means that it shows a decrease in viscosity with increasing shear rates (Figure 12 A).

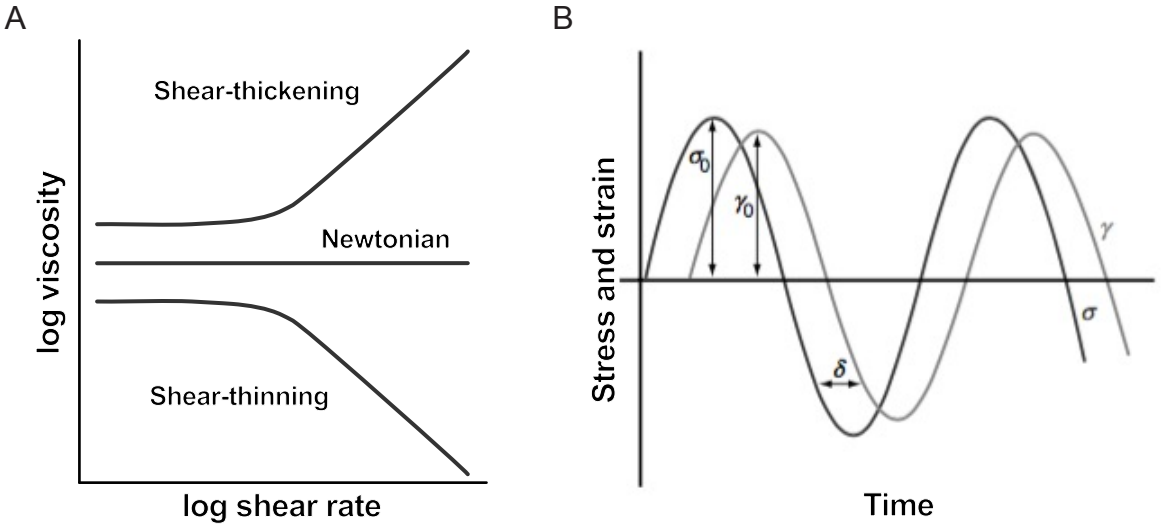

Figure 12: Exemplary graphs of shear and oscillatory measurements. A) Shear rate dependent viscosity of Newtonian and non-Newtonian materials. B) Stress (σ) and strain (γ) against time in oscillatory measurements of a viscoelastic material. σ_0 and γ_0 are the stress and strain amplitudes respectively. Adapted with permission from (Janmey *et al.*, 2007).

Commonly, the viscosity is not sufficient to describe the complex viscoelastic properties of a material. To quantify the elastic and the viscous portions of a material, oscillatory shear measurements are frequently performed. In frequency sweep experiments, the applied stress (σ) and the measured strain (γ) will oscillate phase shifted (δ), (Figure 12 B). This shif is quantified in the phase angle which can vary between 0° and 90°. An ideal elastic material has a phase angle of 0° and an ideal viscous material displays a phase angle of 90°. The stress amplitude (σ_0), strain amplitude (γ_0) and phase angle obtained from the oscillatory shear measurements can also be used to calculate the elastic (G') and the viscous (G'') modulus:

$$G' = \left(\frac{\sigma_0}{\gamma_0}\right)\cos\delta$$

$$G'' = \left(\frac{\sigma_0}{\gamma_0}\right)\sin\delta$$

The elastic modulus is a measure of the energy stored in the elastic portion while the viscous modulus describes the energy that is lost due to the viscous portion of the material (Janmey *et al.*, 2007; Meyers and Chawla, 1999; Tschoegl, 2012).

3.2 SPECTROSCOPIC METHODS

3.2.1 NMR spectroscopy

NMR spectroscopy is commonly used to study the structure and dynamics of proteins and is described in reference (Cavanagh *et al.*, 1996). Nuclear spins are oriented randomly but when placed in a strong magnetic field, they align and start to precess. Generally, nuclei have different spins. Nuclei with spins of ½ can exist in two different spin states and examples of spin 1/2 nuclei are ^{1}H, ^{13}C, ^{15}N, ^{19}F and ^{31}P. Protons are present in all organic compounds and are frequently analyzed by NMR spectroscopy. The resonance frequency of the spinning nuclei is dependent on the strength of the magnetic field and the gyromagnetic ratio which is a constant specific for each isotope.

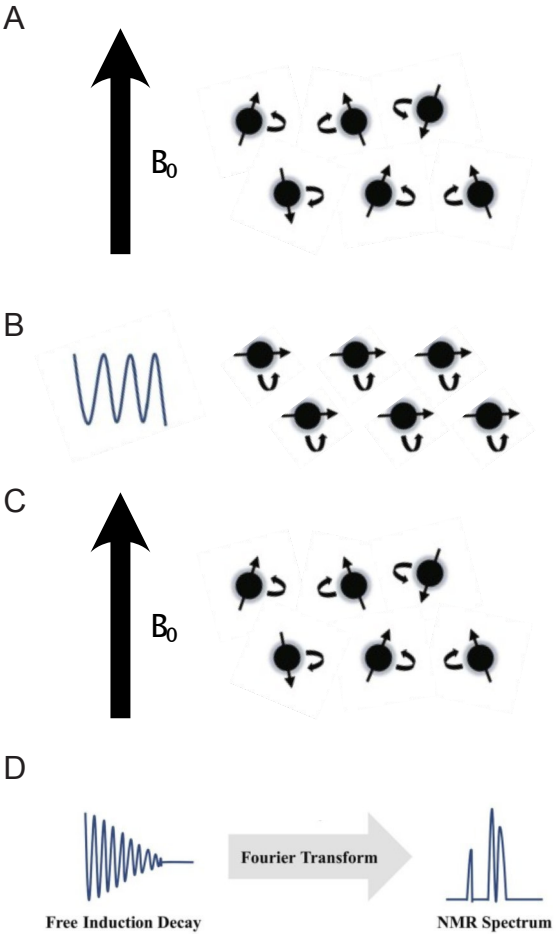

Figure 13: Basic principle of NMR spectroscopy. A) Nuclear spins are aligned along a strong magnetic field (B_0). B) A radio frequency applied perpendicular to the magnetic field causes the nuclear spins to align in the same direction. C) By re-aligning with the magnetic field, the nuclei create a magnetic moment which is D)

represented in the free induced decay wave that can be converted to an NMR spectrum by Fourier transform. Adapted with permission from (Cao *et al.*, 2021)

At equilibrium, the average magnetic moment will be aligned along the magnetic field (B_0). If a short radiofrequency (RF) pulse is applied at a right angle to B_0, the nuclei will align with the pulse, i.e. perpendicular to B_0. After the pulse, the nuclei will re-align again with B_0 while continuing to precess. This causes a magnetic moment which induces a current in a receiver coil that can be detected as a sine wave with decreasing magnitude over time as the nucleus re-aligns with B_0. This wave is called the free-induction decay (FID).

Each proton is in a unique local electromagnetic environment. A proton with a high local electron density is shielded from the external magnetic field. If an RF pulse is applied to a shielded nucleus, the FID will have a lower resonance frequency compared to de-shielded protons in a low electron density environment. The difference in resonance frequencies due to shielding are also called chemical shifts. By Fourier transformation, the FID can be converted to a spectrum to allow easier visual representation. Each proton will give a peak in that spectrum and the chemical environment around each proton can thus be deduced.

Due to the high number of protons in proteins, spectra in 1D-experiments (based on protons only) often overlap which prevents determination of unique structural features. Therefore, 2D experiments using ^{1}H, ^{13}C and ^{15}N nuclei are performed to resolve overlapping signals. In heteronuclear single quantum coherence (HSQC) experiments, magnetization from protons is transferred to ^{13}C and ^{15}N nuclei. HSQC spectra show a peak for every proton bound to a heteronucleus, i.e. each peak represents an amino acid residue, which needs to be assigned for structure determination. The unique conformation of a stably folded protein results in sharp and well dispersed peaks that allow residue-specific assignments, while the sampling of different conformations characteristic of unfolded proteins give overlapping peaks in a narrow spectral range, that often precludes further structural analyses.

3.2.2 CD spectroscopy

CD spectroscopy is used to determine the overall secondary structure content of proteins. Circularly polarized light is absorbed by the amide group of the peptide bonds. Absorption of left and right circularly polarized light is not equal as proteins are chiral molecules and the difference in absorbance at wavenlegths between 180-250 nm is characteristic for different types of secondary structures (Figure 14).

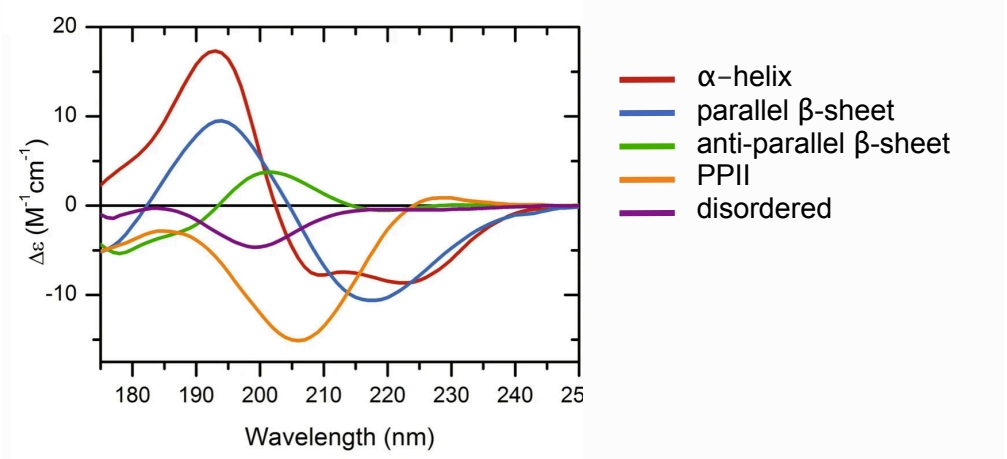

Figure 14: Typical CD spectra for different secondary structures. Adapted with permission from (Micsonai *et al.*, 2021).

4 RESULTS AND DISCUSSION

4.1 PAPER I

The properties of spider silk dope are crucial for the natural spinning process (Matsumoto *et al.*, 2008; Vollrath and Knight, 2001) which is likely also true for artificial spinning dope. Natural spinning dope has unique rheological behaviors including high viscosity, crossover of the loss and storage modulus and shear-thinning (Laity *et al.*, 2015). A previously developed mini-spidroin (NT2RepCT) has already been shown to be as soluble as native spidroins (Andersson *et al.*, 2017) and to recapitulate molecular behaviors important for the natural spinning process (Otikovs *et al.*, 2017). In paper I, we analyzed to which extend NT2RepCT dope recapitulates other dope properties related to flow behavior, structure and phase transition in response to decreased pH.

We showed that NT2RepCT dope had a rather low viscosity likely due to the relatively small size of NT2RepCT compared to native spidroins (66 kDa vs around 600 kDa (Babb *et al.*, 2017)). Even though we found evidence that protein chains interact with each other at concentrations above 300 mg/ml they were most likely fewer than in their longer natural counterparts which explained the lower viscosity. Park and Um showed that higher viscosity in reconstituted dope leads to fibers with increased mechanical properties (Park and Um, 2018). Increasing the length of the repetitive domain might enable us to improve the mechanical properties of the artificial fibers by increasing the viscosity and importantly also increase intermolecular interactions in the fiber.

Importantly, we found that NT2RepCT dope exhibits shear-thinning behavior (Figure 15 A) which likely is the reason why concentrated NT2RepCT solutions can be pumped through thin glass capillaries by a low-pressure syringe pump. Similarly, shear-thinning of natural spinning dopes are also crucial for energy efficient spinning *in vivo* (Holland *et al.*, 2006; Sparkes and Holland, 2017). However, the decrease in viscosity in the artificial dope was lower than what has been observed for natural spinning dope (Holland *et al.*, 2006) likely because the initial viscosity of NT2RepCT dope was lower to begin with.

Oscillatory measurements showed that the dope exhibits frequency dependent-viscoelastic properties (Figure 15 B) similar to natural dope with a dominant storage modulus at higher frequencies and a crossover, i.e. the loss modulus dominating at lower frequencies (Holland *et al.*, 2006). However, the shape of the curves was different for the NT2RepCT solutions compared to natural spinning dope.

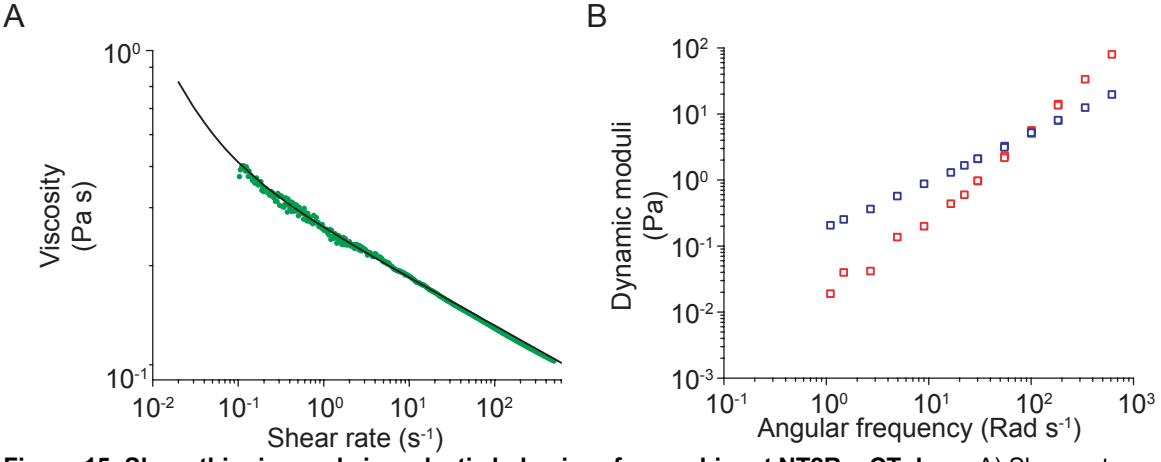

Figure 15: Shear-thinning and viscoelastic behavior of recombinant NT2RepCT dope. A) Shear-rate ramp of NT2RepCT (500 mg/ml), solid line represents the fitted Herschel-Bulkley model. B) Oscillatory measurements

for NT2RepCT at 300 mg/ml. Red: G' storage modulus; Blue: G'' loss modulus. Modified with permission from Paper I.

In the gland, decreased pH causes protein structural changes and phase transition from a solution into a solid fiber. We showed with CD spectroscopy that a lower pH decreased the thermal stability of NT2RepCT (Figure 16 A). By exposing NT2RepCT to acidic vapor during oscillatory measurements we showed that NT2RepCT undergoes pH-induced liquid-to-solid phase transition (Figure 16 B) which is an important part of the natural spinning process.

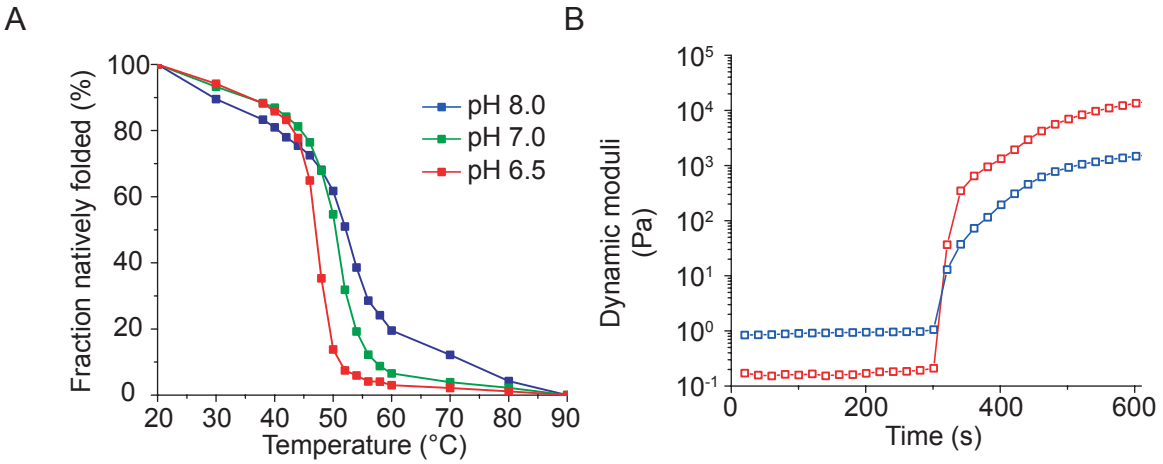

Figure 16: Effect of pH on recombinant NT2RepCT dope. A) Thermal unfolding curves obtained by CD spectroscopy at different pH. B) Oscillatory measurements of NT2RepCT spinning dope. Sample was exposed to acetic acid vapor at 300 s. Modified with permission from Paper I.

4.2 PAPER II

NT2RepCT (here A_{15}-A_{14}) can be expressed recombinantly at high yields which allows purification of pure protein in the gram per liter range (in bioreactor) using non-denaturing conditions (Schmuck *et al.*, 2021) which paves the road for economic large-scale production (Edlund *et al.*, 2018). However, the mechanical properties of biomimetic fibers are still inferior to some of the non-biomimetic and native counterparts (Andersson *et al.*, 2017; Bowen *et al.*, 2018; Gosline *et al.*, 1999; Heidebrecht *et al.*, 2015). One reason for that could be that the poly-Ala blocks in the repetitive region of NT2RepCT/ A_{15}-A_{14} transition back to an α-helical conformation in the dried fiber (Otikovs *et al.*, 2017). Alas have a low β-strand propensity but are the most hydrophobic residues that still promote passage through the translocon, a requisite for protein secretion (Johansson et al., 2010; Johansson & Rising, 2021). It seems that the repeat region is evolutionary optimized to be as hydrophobic as possible while still warranting secretion. Recombinant expression systems such as *E. coli* can express target proteins intracellularly. Thus, mini-spidroins expressed intracellularly in *E. coli* do not have to obey to the constraints spidroins have to adhere to in the silk gland and can contain more hydrophobic residues.

In this study, we used protein engineering to rationally design 15 proteins (Figure 17) with predicted increased β-strand propensity and increased inter-β-sheet interactions in the artificial silk fibers. Thirteen of those proteins could be overexpressed in *E. coli* and 9 yielded sufficient soluble protein for purification. Using non-denaturing conditions, protein purification yielded between 4 and 243 mg of pure protein from shake-flask cultures. Eight proteins could be concentrated to at least 200 mg/ml and 7 could be spun into fibers (Figure 18 A). Tensile tests of the fibers revealed that 5 engineered fibers had increased strength

compared to the non-engineered NT2RepCT/ A_{15}-A_{14} fibers (Figure 18 B). The strength of one fiber type, $(A_3I)_3$-A_{14} which has 3 isoleucines in the first poly-Ala repeat, increased 3-fold compared to NT2RepCT/ A_{15}-A_{14}. The mutations also had an effect on the extensibility of the fibers. We speculate that the load was solely carried by the amorphous region in A_{15}-A_{14} fibers and that the intermolecular interactions were too weak for the amorphous region to fully extend. Having increased the intermolecular interaction in the $(A_3I)_3$-A_{14} fibers, the amorphous region was likely able to fully which would increase the extensibility of the silk.

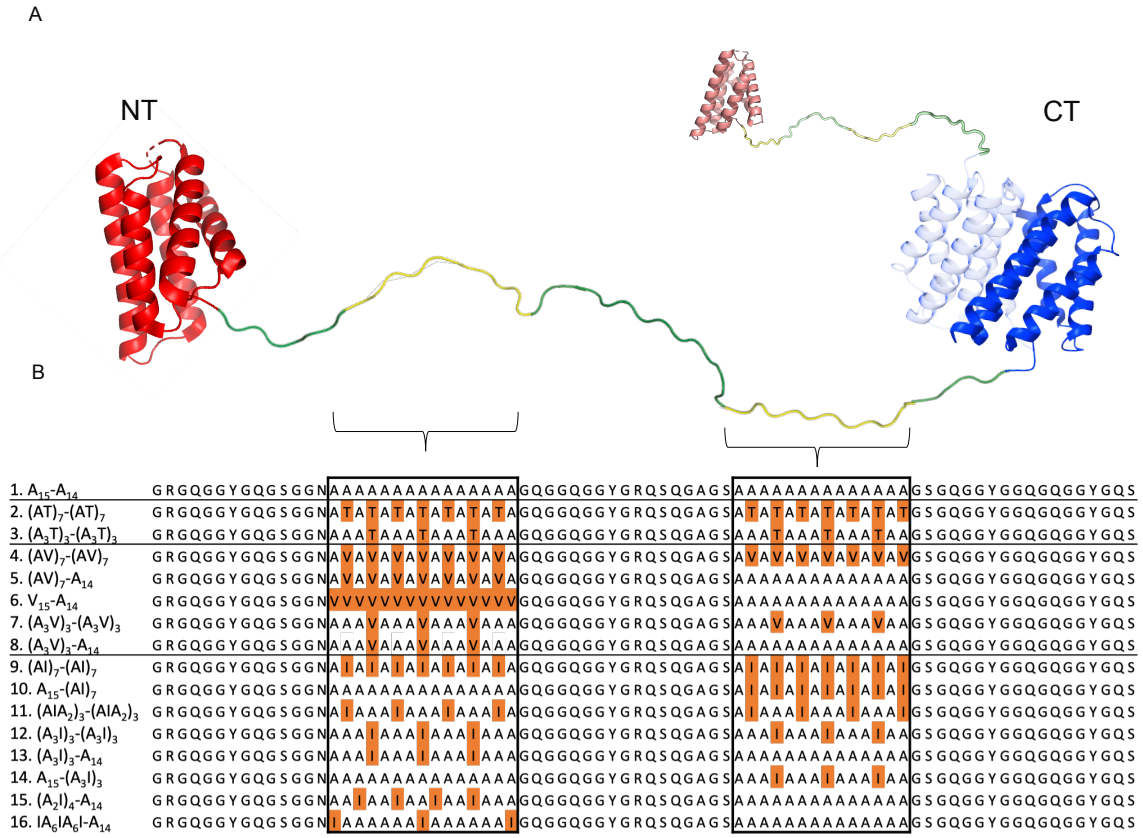

Figure 17: NT2RepCT/ A_{15}-A_{14} and its designed constructs. A) Schematic representation of NT2RepCT dimer and B) protein sequence of the engineered repetitive regions with substitutions shown in orange (all constructs contain NT and CT). Reprinted with permission from Paper II.

Having both increased strength and extensibility, $(A_3I)_3$-A_{14} reaches toughness moduli comparable to natural major ampullate silk fibers (Figure 18 C), (Blackledge and Hayashi, 2006). However, native major ampullate silk typically has higher tensile strength (1217 MPa vs 132 MPa) and lower extensibility (23 % vs 160%). Nevertheless, we showed that the mechanical properties can be altered by rational design and protein engineering, and we reported for the first time on a biomimetic spider silk fiber that can reach similar toughness moduli as native major ampullate silk.

We further showed that $(A_3I)_3$-A_{14} is expressed at very high yields (8.9 g/l) in a bioreactor, which is the second highest yield reported (second only to A_{15}-A_{14}) which vouches for economically feasible bulk production (Edlund *et al.*, 2018; Schmuck *et al.*, 2021).

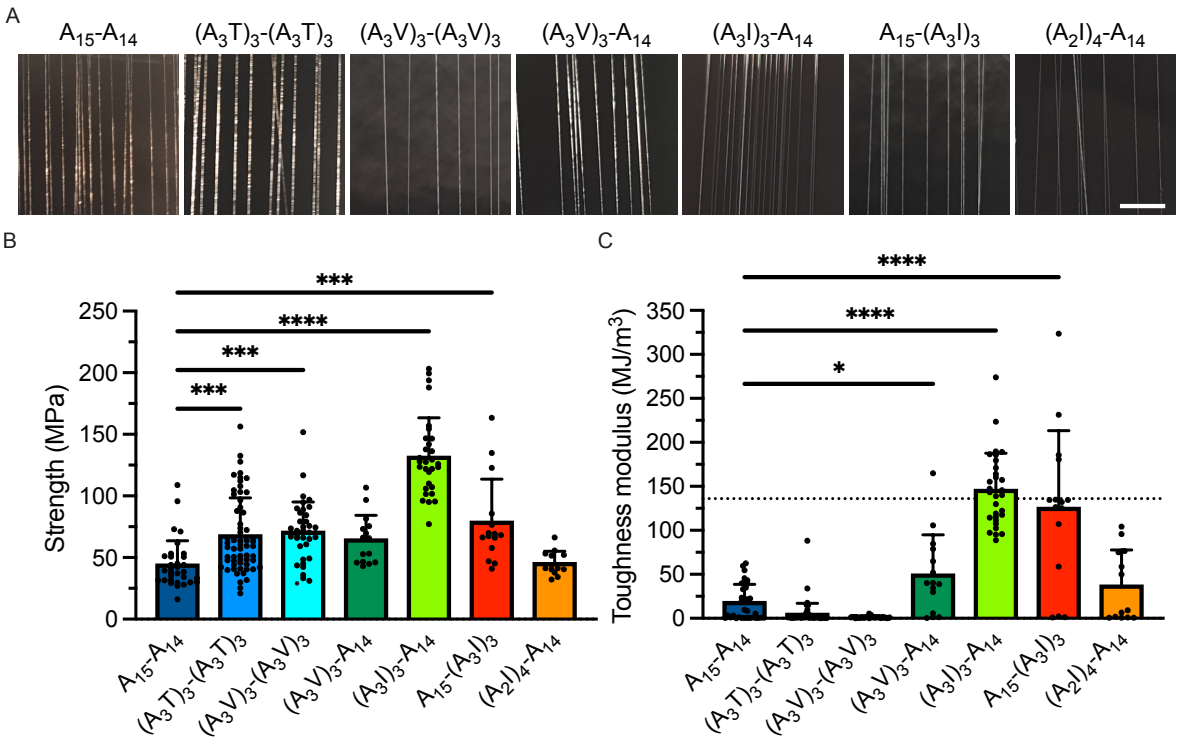

Figure 18: Fibers and their mechanical properties. Photographs of fibers made from spinnable proteins and the B) strength and C) toughness modulus of the respective fibers. Dashed line indicates toughness modulus of native major ampullate silk (Blackledge and Hayashi, 2006). Whiskers show standard deviation. *p < 0.05; **p < 0.01; ***p < 0.001; ****p < 0.0001. Scale bar is 2.5 mm. Modified with permission from Paper II.

4.3 PAPER III

Mini-spidroins cannot only form fibers but also other structures such as films, foams, spheres and hydrogels (Hansson *et al.*, 2021; Numata and Kaplan, 2010; Qian *et al.*, 2015; Schacht *et al.*, 2016; Schacht and Scheibel, 2011; Thamm *et al.*, 2017). Hydrogels are especially interesting as a biomaterial due to their fibrillar structure and high water content. In paper III, we analyzed hydrogel formation of NT2RepCT and its domains. We found that NT2RepCT forms hydrogels at 37°C at concentration between 50 and 500 mg/ml (Figure 19 A, B). Gelation times were short, ranging from 25 to 120 minutes. Curious as to which domain of this tripartite protein is responsible for hydrogel formation, we produced each domain separately and in combination with each other and tested for their potential to form hydrogels. Previous reports have focused on hydrogels made from the repeat region and CT due to their structural features during silk formation (DeSimone *et al.*, 2016; Neubauer *et al.*, 2021; Qian *et al.*, 2015; Rammensee *et al.*, 2006; Schacht and Scheibel, 2011; Song *et al.*, 2021). We could confirm hydrogel formation of CT but not for the repetitive region. Surprisingly, NT, which has been described as super-soluble and highly stable (Askarieh *et al.*, 2010; Hedhammar *et al.*, 2008; Kaldmäe *et al.*, 2020; Kronqvist *et al.*, 2014) formed hydrogels even faster than NT2RepCT at the same concentration range (50-500 mg/ml; 120-10 min gelation time), (Figure 19 A, B). Intrigued by the observations, we performed structural studies including FTIR and NMR spectroscopy and found that both NT2RepCT and NT hydrogels formed β-sheets during gelation (Figure 19 C). TEM showed that hydrogels contain nanofibrils (Figure 19 D) which also bound to ThT. Thus, we concluded that amyloid-like fibrils are formed during hydrogel formation.

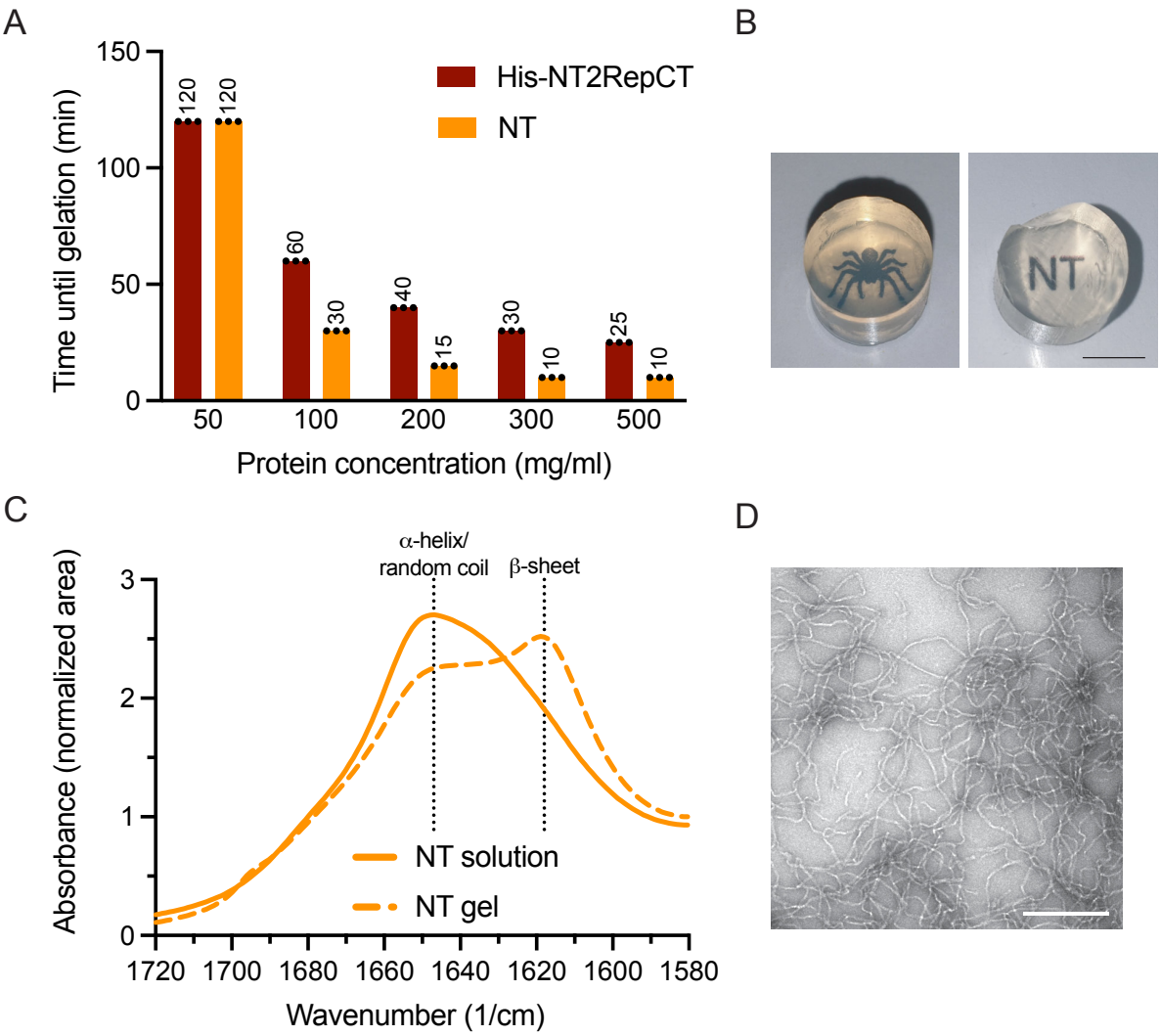

Figure 19: Hydrogel formation of NT2RepCT and NT. A) Time until gelation of His-NT2RepCT and NT at protein concentrations between 50 and 500 mg/ml at 37°C. B) Photographs of hydrogels made from NT2RepCT and NT with a spider and "NT" underneath. Scalebar is 5 mm). C) FTIR absorption spectra of NT before and after gelation at 37°C. D) TEM image of a resuspended NT gel (50 mg/ml) scale bar is 200 nm. Reprinted with permission from paper III.

NT has been studied extensively in the past but has never been found to be able to form amyloid-like structures (Andersson *et al.*, 2014; Hedhammar *et al.*, 2008; Heiby *et al.*, 2019; Kronqvist *et al.*, 2014; Landreh *et al.*, 2010; Otikovs *et al.*, 2015; Sarr *et al.*, 2022; Schwarze *et al.*, 2013). On the contrary, NT has been used to develop a solubility tag for proteins that are prone to form amyloid fibrils (Abelein *et al.*, 2020; Kronqvist *et al.*, 2017; Sarr *et al.*, 2018).

Next, we aimed to understand the mechanism of NT fibril formation. It has been shown previously that low pH and salt stabilize NT (Hagn *et al.*, 2011; Kronqvist *et al.*, 2014) and we found that under both conditions, gelation is inhibited. Two mutants that stay monomeric at low pH but differ in their stability, NT* (higher thermostability than NT) and NT^{A72R} (similar thermostability as NT) were found to differ in their ability to form hydrogels. NT* was not able to gel at 37°C while NT^{A72R} did (Figure 20). This led us to hypothesize that the meta stability of NT is responsible for gelation. The high methionine content in NT has previously been shown to fluidize NT fold and that substitutions of six Met for Leu (His-NT-L6) greatly stabilized the fold (Heiby *et al.*, 2019). We found that the His-NT-L6 mutant indeed was not able to gel (Figure 20), further supporting the hypothesis that high thermodynamic stability

of NT prevents gelation. In line with this, when NT* and His-NT-L6 were heated to 60°C, gelation was observed (Figure 20).

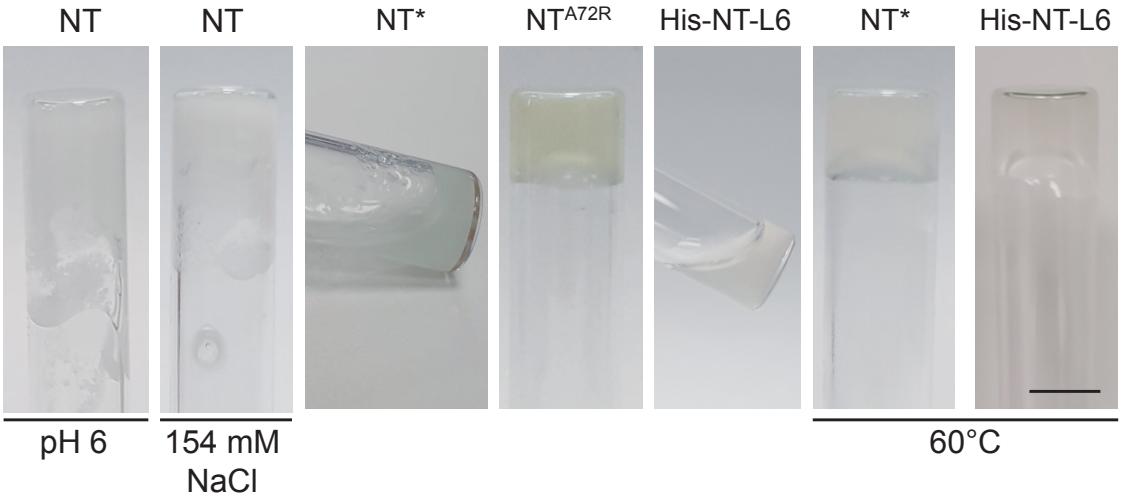

Figure 20: Vial inversion tests of different NTs. Gelation conditions are 37°C and no salt if not indicated otherwise. Scale bar is 5 mm.

Finally, we showed that NT can be fused to other proteins such as GFP and purine nucleoside phosphorylase (PNP) and the ability to form hydrogels is retained. Importantly, the fused moieties also retain their function to a large extend (70% for NT-GFP and 65% for His-NT-PNP).

4.4 PAPER IV

Intrigued by the benign gelation methods observed in paper III, we now explored the possibility to use spider silk protein hydrogels as a drug release system and as a tool in regenerative medicine to serve as a cell culture scaffold. We first determined the diffusion properties of NT2RepCT hydrogels by FRAP and by encapsulating GFP in the hydrogels. FRAP showed that diffusion can be tuned by changing the protein concentration of the hydrogel and by changing the size of the diffusing molecule (Figure 21 A). The diffusion is relatively slow due to the dense fibrillar network observed by SEM (Figure 21 B). GFP was encapsulated during formation of hydrogels at different final concentrations of 1-50 mg/ml, and we observed GFP release from hydrogels submerged in buffer until reaching equilibrium within 24 hours (Figure 21 C). Reaching equilibrium is especially favorable for costly compounds which would be waisted if retained in the hydrogel.

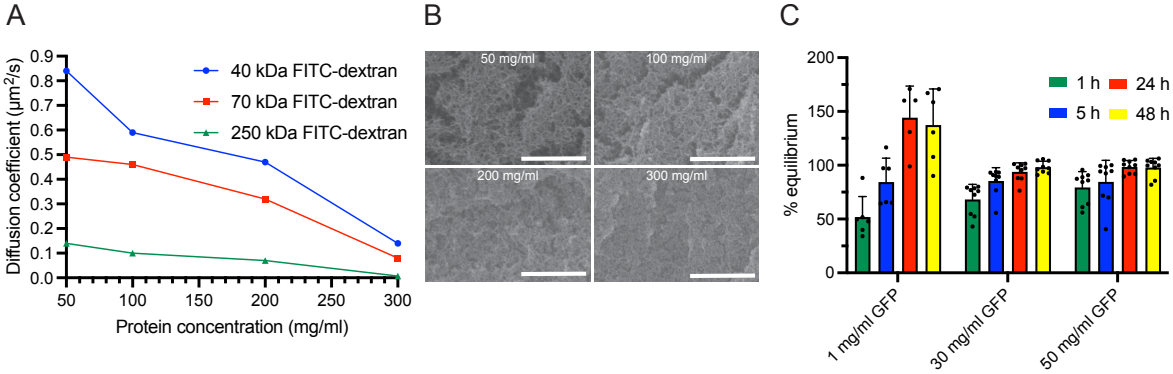

Figure 21: Diffusion properties and morphology of NT2RepCT hydrogels. A) Diffusion coefficients versus protein concentration of NT2RepCT hydrogels. FITC-dextrans of different sizes were encapsulated in NT2RepCT hydrogels and diffusion was determined by FRAP. B) SEM pictures of NT2RepCT hydrogels. C) Release profiles of GFP encapsulated at different concentrations in NT2RepCT hydrogels (50 mg/ml).

Next, we aimed to encapsulate human fetal mesenchymal stem cells in the hydrogels and analyze their survival and viability. Survival was determined with the Alamar blue assay and it was found that cells survived to a large extend over the 21 day culture period but were unable to proliferate likely due to the dense fibrillar network as observed with SEM. The number of live and dead cells (stained with Calcein AM and DRAQ7, respectively) were determined after 7 days in culture using a laser scanning confocal microscope. Cell viability was 53-67% depending on the cell seeding density and 3D projections showed that cells were distributed throughout the gels (Figure 22).

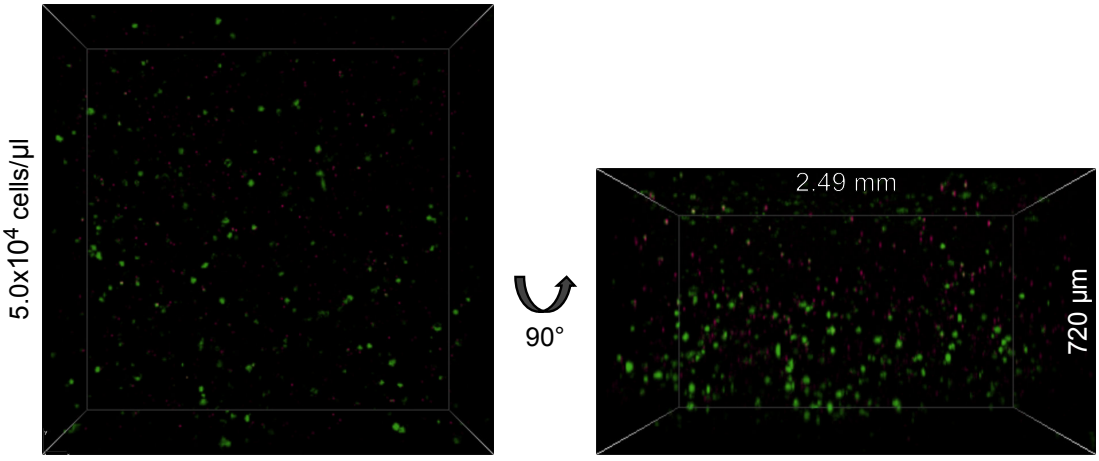

Figure 22: 3D projections of h(f)MSC encapsulated in NT2RepCT hydrogels. Cells were stained with Calcein AM (green, live) and DRAQ7(magenta, dead) after 7 days in culture.

Next, we encapsulated human progranulin secreting ARPE-19 cells which have several potential therapeutic applications (Abella *et al.*, 2017) in NT2RepCT hydrogels (50mg/ml). Using ELISA, we measured the level of secreted progranulin in the cell culture medium within 4 hours. The progranulin concentration in the cell culture medium increased over the 31-day study period and was similar to control cells grown under standard conditions (in 2D), (Figure 23). We hypothesize that the gels may be able to retain cells to a specific location for example at an injection site.

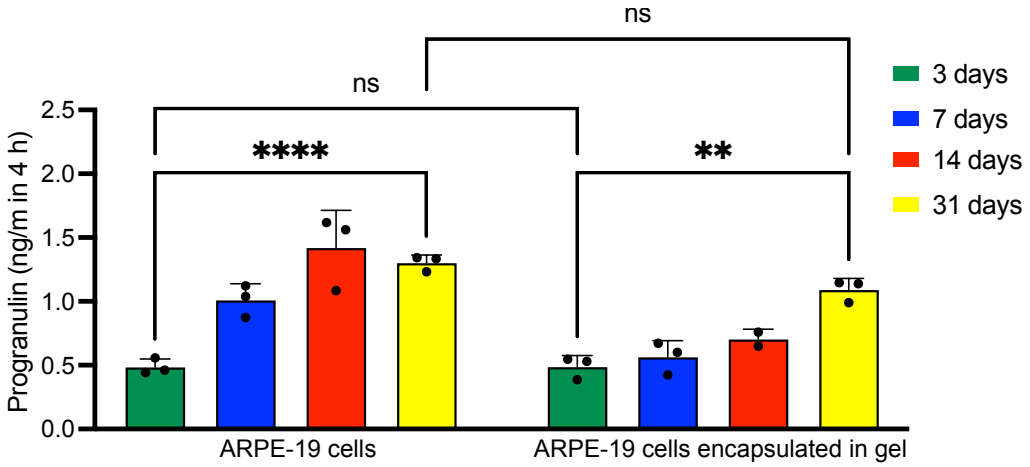

Figure 23: Progranulin release of ARPE-19 cells. Pulse experiment, comparison with cells cultured under standard conditions, Whiskers show standard deviation. ** $p < 0.01$; **** $p < 0.0001$; ns - not significant.

Cells can sense the stiffness of their substrate which affects morphology (Chaudhuri *et al.*, 2016; Engler *et al.*, 2006; Lou *et al.*, 2018; Tse and Engler, 2011). We analyzed the

mechanical properties of NT2RepCT hydrogels using unconfined compression test and found that different stiffnesses can be achieved by adjusting the protein concertation and that they matched different tissues (Figure 24).

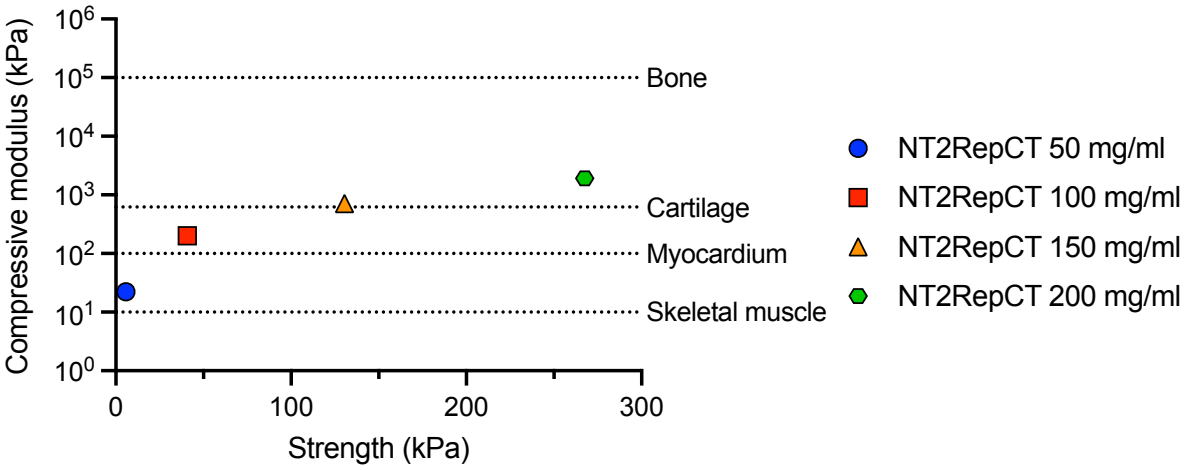

Figure 24: Compression modulus and strength of NT2RepCT hydrogels (50, 100, 150 and 200 mg/ml) in comparison to the compression modulus of different tissues (Mathur *et al.*, 2001; Mimar *et al.*, 2008; Ogneva *et al.*, 2010; Thurner *et al.*, 2009).

5 CONCLUSIONS

- NT2RepCT dope has biomimetic characteristics as it is shear-thinning, shows a cross-over of the viscoelastic moduli at increased frequency and undergoes structural and phase changes in response to low pH similarly to natural spider silk dope.
- Rationally engineered mini-spidroins designed to have increased β-sheet propensities and inter-β-sheet binding strength can be spun into fibers with increased tensile strength. Notably, those mini-spidroins are highly soluble, can be produced at very high yields, are spun biomimetically and two fiber types reach the same toughness as natural spider silk.
- NT forms amyloid-like fibrils at high concentrations and elevated temperature due to its fluid fold. Those fibrils form a hydrogel which can be used as a protein immobilization platform.
- Spider silk protein hydrogels made from NT2RepCT work as a macromolecule release system and are non-toxic to primary human cells. Diffusion rates and stiffness can be tuned, simply by adjusting the protein concentration.

6 POINTS OF PERSPECTIVE

We showed that NT2RepCT dope recapitulates important characteristics of native spinning dope. However, to increase the degree of biomimicry, the overall composition of artificial dopes should match that of native dope more closely, for example in terms of the ion composition, presence of other spidroins, non-spidroins and non-proteinaceous molecules. Incorporating those and analyzing their effect on flow-behavior, silk formation and silk properties will increase our understanding of the natural spinning process in general.

Spinning of biomimetic fibers with toughness reaching that of natural major ampullate silk along with the high-yield protein production described herein represents a breakthrough in the field of artificial spider silk production. Those fibers may already be suitable for biomedical applications such as nerve grafts or in an industrial setting for example in the textile industry.

To match the tensile strength and extensibility of natural silk future efforts should aim to reproduce those. Silk spinning in spiders is a complex process that current systems are not yet able to fully mimic. The following approaches could increase the degree of biomimicry and likely improve the mechanical properties:

- Mimic the overall dope composition
- Further promote β-sheet formation e.g. by post-spin stretching
- Microfluidic devices could be used to mimic the shear forces in the gland and introduce stepwise microenvironmental changes, e.g. decrease in pH and ion exchange.
- Mimic the overall silk fiber architecture including coatings

However, the approaches listed above require further studies on dope composition and storage conditions, shear and pulling forces involved in the spinning process and their effect on the proteins and the overall silk architecture to elucidate different layers of the silk.

The novel properties of NT described in paper III represent a paradigm shift in the spider silk field where NT was viewed as a highly stable and solubility-enhancing domain. Future efforts should focus on any possible implications of the phenomena during dope storage and silk fiber spinning. In a broader context, structural flexibility of proteins and amyloid-like fibril formation may also have implications in diseases involving amyloid formation.

The hydrogels described in paper III and IV are a versatile tool and we showed that it has great potential to be develop as a protein immobilization platform, a scaffold for tissue engineering and a drug release system. The proof-of principles presented herein can be used as a basis for future efforts in the development of those. For example, NT-PNP may be used to synthesize purine nucleoside analogues that can be used as antiviral or anticancer drugs. Potentially, precursors could be loaded on an NT-PNP column which then catalyzes enzymatic reactions of the desired product. This is not only limited to PNP but NT can likely be fused to a whole range of other enzymes.

The mechanical properties of the hydrogels, (especially 150 and 200 mg/ml NT2RepCT hydrogels) make them suitable to be used as scaffolds for cartilage or possibly even bone regeneration. Future efforts should focus on differentiating MSC into chondrocytes and osteoblasts. Similarly, fibroblast growth factor 18 (FGF-18) or bone morphogenetic protein

2 (BMP-2) could be encapsulated in the hydrogels to induce chondrogenic or osteogenic differentiation *in vitro* or *in vivo*.

7 ACKNOWLEDGEMENTS

First of all, I would like to thank **Anna** for being such a great supervisor. Not just have I learned so much from you on a scientific level, you're also a role model. Your passion and dedication are truly inspiring. I loved working with you and I'm so grateful for all the trust you put in me and freedom you gave me to explore my ideas. I couldn't have asked for a better supervisor than you. I am grateful that you always took the time to discuss things with me, read my texts or to just check in on how things are going, even on weekends and holydays. Thank you for your guidance and support.

Janne, I am so grateful to have had you as a supervisor. Your knowledge, positivity and calmness seem infinite. When times were bleak, you found the right words to encourage me. And when I was confident with my results, you asked the right questions to make me critically re-examine them.

Thank you both, Anna and Janne, for letting me work in your amazing groups so that I can follow my passion. This has been the best possible experience one could ask for.

My dear **Urmi**, I've really enjoyed working with you and we have worked together a LOT. I think at some point we could pretty much read each other's minds. We were such a great team and I will really miss you. But you're not just a dear colleague, you have also become a true friend. I wish you and your amazing family all the best. **Olga**, you have helped me so much during my PhD. If it wasn't for you, I'm sure I'd still be at my bench struggling with cloning and clogged columns. Thank you, thank you, thank you for everything! Oh **Gabriele**, I'm so grateful that you came to dark, cold Sweden to help us. You really saved my life :D Your passion for spiders (and food) is contagious and we love you for that. **Juanita**, you were not just the sunshine of the lab but also a biiiig help. Thank you for all the laughs and purified proteins :D I wish you all the best with your PhD. You'll be a great scientist. **Kerstin**, I'm still a bit mad that you left, and we still miss you. Thank you for all your help, keeping the lab together and your general positivity. **Benjamin,** you've had a big impact on the development of the group which means you made our lives in the lab a lot easier. Thanks for your input and dedication. **Nina**, you're the most organized person I've ever met (in a good and inspiring way). Your knowledge has saved me and my projects multiple times. Thank you! **Médoune**, you were my supervisor when I joined as a master student, you showed me all the important things and I thank you for that. I do not thank you for giving me the "project that must not be named" ;) **Gefei**, your knowledge is astonishing, and I really enjoyed our spider silk discussion and later also baby related conversations :D Thank you **Lorena** for the nice conversations we had. **Axel L.**, my fellow German lab mate. Thanks for your help and all the laugh in the lab. **Henrik**, thank you for all your unconventional lab and IT advice which have saved me multiple times. **Fredrik, Axel A., Laurén, Shaffi, Sameer, Helen, Rakesh, Sumalata** and **Cecilia** thank you for all the shared moments in the lab and office.

I would also like to thank the "old SLU gang" **Nathalie, Mike** and **Lotta** who made it bearable to travel to Uppsala. Thank you for all the conversations and laughs.

An immense thank you to all my co-authors and collaborators. Especially **Pete** and **Chris** who took me in to teach me about rheology and **Kristaps** who also hosted me to learn about NMR spectroscopy. Those were some intense study visits and I am grateful that you introduced me to your worlds and for being so patient with me.

While talking about patience, **Andreas**, thank you so much for being so patient with me and my FTIR analysis. Es war eine lange Geburt as we say but I'm happy we did such a thorough job and I learned a lot.

I would also like to thank the administration of NVS and BioNut, especially **Eva Kallestenius**, **Maria Roos** and **Monica Ahlberg**. Thank you for answering all my questions and taking care of me.

A special thanks goes to **Veronika**, you were the first friend I made when I first came to Sweden almost 7 years ago. We had some pretty crazy times together and I'm happy that we're still friends even though our life's are a little less crazy now. **Josefin,** thank you for being such an amazing friend. You were a real support during my PhD. **Oihana**, you made it to the friends section because that's what you are to me. Thank you for all the cat, dog and baby conversations. **Olivia**, I don't know what I would have done without you during my PhD. You are such an amazing friend and I loved our "meet you in the middle" fikas as well as dinner parties. I really miss those times.

Oma Hanni und **Opa Dietmar**, ich denke oft an euch und bin euch dankbar, dass ihr mich immer unterstützt habt. Einer eurer Wünsche war es mitzuerleben wie ich meinen Doktor abschließe, es tut mir leid dass es dazu nicht gekommen ist und ich denke heute extra doll an euch. Ich vermisse euch.

Oma Inge und **Opa Bernd**, ich bin so froh, dass es euch gibt und dass ihr immer für mich da seid. Ein großes Dankeschön für eure Unterstützung, ohne euch hätte ich es nie so weit geschafft.

Danke **Papa** für dein Interesse an meiner Arbeit, ich fand unsere Gespräche über meine Arbeit immer sehr interessant. Danke auch für all deine Hilfe auf meinem Weg hierhin und dass ich immer auf dich zählen kann.

Mutti, du warst und bist mir eine enorme Stütze. Du glaubst immer an mich und bist immer für mich da. Ich danke dir sehr dafür. Ich habe dir das schon oft gesagt und ich meine es wirklich mit vollem Herzen: du bist die beste Mutti, die man sich wünschen kann. DANKE!!

Victor, I don't believe that there are words that can describe how thankful I am for having you by my side. Thank you for your love, support and sacrifices. I'll never be able to pay you back for all the things you did for me. You're a great partner, father and hooman. **Bobby**, I know you can't read and you don't care about all this but I still thank you for showing me that there is more in life than work and always brightening up my day. **Sophie**, I didn't know one could love someone that much until you came into our lives. I am proud of what I have accomplished during my PhD but I am a hundered times prouder of you and every new skill you learn.

8 REFERENCES

Abdelkader, E.H. and Otting, G. 2021. NT*-HRV3CP: An optimized construct of human rhinovirus 14 3C protease for high-yield expression and fast affinity-tag cleavage. *J Biotechnol*, **325**: 145–151.

Abelein, A., Chen, G., Kitoka, K., Aleksis, R., Oleskovs, F., Sarr, M., Landreh, M., Pahnke, J., Nordling, K., Kronqvist, N., Jaudzems, K., Rising, A., Johansson, J. and Biverstål, H. 2020. High-yield Production of Amyloid-β Peptide Enabled by a Customized Spider Silk Domain. *Sci Rep*, **10**: 235.

Abella, V., Pino, J., Scotece, M., Conde, J., Lago, F., Gonzalez-Gay, M.A., Mera, A., Gómez, R., Mobasheri, A. and Gualillo, O. 2017. Progranulin as a biomarker and potential therapeutic agent. *Drug Discov Today*, **22**: 1557–1564.

Adzhubei, A.A., Sternberg, M.J.E. and Makarov, A.A. 2013. Polyproline-II helix in proteins: Structure and function. *J Mol Biol*, **425**: 2100–2132.

Agnarsson, I., Kuntner, M. and Blackledge, T.A. 2010. Bioprospecting finds the toughest biological material: Extraordinary silk from a giant riverine orb spider. *PLoS One*, **5**: 1–8.

Aigner, T.B., DeSimone, E. and Scheibel, T. 2018. Biomedical Applications of Recombinant Silk-Based Materials. *Advanced Materials*, **30**: e1704636.

Albertson, A.E., Teulé, F., Weber, W., Yarger, J.L. and Lewis, R. v. 2014. Effects of different post-spin stretching conditions on the mechanical properties of synthetic spider silk fibers. *J Mech Behav Biomed Mater*, **29**: 225–234.

Allmeling, C. 2006. Use of spider silk fibres as an innovative material in a biocompatible artificial nerve conduit. *J Cell Mol Med*, **10**.

Allmeling, C., Jokuszies, A., Reimers, K., Kall, S., Choi, C.Y., Brandes, G., Kasper, C., Scheper, T., Guggenheim, M. and Vogt, P.M. 2008. Spider silk fibres in artificial nerve constructs promote peripheral nerve regeneration. *Cell Prolif*, **41**: 408–420.

An, B., Hinman, M.B., Holland, G.P., Yarger, J.L. and Lewis, R. v. 2011. Inducing β-sheets formation in synthetic spider silk fibers by aqueous post-spin stretching. *Biomacromolecules*, **12**: 2375–2381.

An, B., Jenkins, J.E., Sampath, S., Holland, G.P., Hinman, M., Yarger, J.L. and Lewis, R. 2012. Reproducing natural spider silks' copolymer behavior in synthetic silk mimics. *Biomacromolecules*, **13**: 3938–3948.

An, B., Tang-Schomer, M.D., Huang, W., He, J., Jones, J.A., Lewis, R. v. and Kaplan, D.L. 2015. Physical and biological regulation of neuron regenerative growth andnetwork formation on recombinant dragline silks. *Biomaterials*, **48**: 137–146.

Andersson, M., Chen, G., Otikovs, M., Landreh, M., Nordling, K., Kronqvist, N., Westermark, P., Jörnvall, H., Knight, S., Ridderstråle, Y., Holm, L., Meng, Q., Jaudzems, K., Chesler, M., Johansson, J. and Rising, A. 2014. Carbonic Anhydrase Generates CO2 and H+ That Drive Spider Silk Formation Via Opposite Effects on the Terminal Domains. *PLoS Biol*, **12**: e1001921.

Andersson, M., Holm, L., Ridderstraìšle, Y., Johansson, J. and Rising, A. 2013. Morphology and composition of the spider major ampullate gland and dragline silk. *Biomacromolecules*, **14**: 2945–2952.

Andersson, M., Jia, Q., Abella, A., Lee, X.Y., Landreh, M., Purhonen, P., Hebert, H., Tenje, M., Robinson, C. v., Meng, Q., Plaza, G.R., Johansson, J. and Rising, A. 2017. Biomimetic spinning of artificial spider silk from a chimeric minispidroin. *Nat Chem Biol*, **13**: 262–264.

Arakawa, K., Kono, N., Malay, A.D., Tateishi, A., Ifuku, N., Masunaga, H., Sato, R., Tsuchiya, K., Ohtoshi, R., Pedrazzoli, D., Shinohara, A., Ito, Y., Nakamura, H., Tanikawa, A., Suzuki, Y., Ichikawa, T., Fujita, S., Fujiwara, M., Tomita, M., *et al.* 2022. 1000 spider silkomes: Linking sequences to silk physical properties. *Sci Adv*, **8**: 1–14.

Asakura, T., Matsuda, H., Naito, A. and Abe, Y. 2022. Formylation of Recombinant Spider Silk in Formic Acid and Wet Spinning Studied Using Nuclear Magnetic Resonance and Infrared Spectroscopies. *ACS Biomater Sci Eng*, **8**: 2390–2402.

Askarieh, G., Hedhammar, M., Nordling, K., Saenz, A., Casals, C., Rising, A., Johansson, J. and Knight, S.D. 2010. Self-assembly of spider silk proteins is controlled by a pH-sensitive relay. *Nature*, **465**: 236–238.
Åstrand, C., Chotteau, V., Falk, A. and Hedhammar, M. 2020. Assembly of FN-silk with laminin-521 to integrate hPSCs into a three-dimensional culture for neural differentiation. *Biomater Sci*, **8**: 2514–2525.
Augsten, K., Mühlig, P. and Herrmann, C. 2000. Glycoproteins and skin-core structure in Nephila clavipes spider silk observed by light and electron microscopy. *Scanning*, **22**: 12–15.
Ayoub, N.A., Garb, J.E., Tinghitella, R.M., Collin, M.A. and Hayashi, C.Y. 2007. Blueprint for a High-Performance Biomaterial: Full-Length Spider Dragline Silk Genes. *PLoS One*, **2**: e514.
Babb, P.L., Gregorič, M., Lahens, N.F., Nicholson, D.N., Hayashi, C.Y., Higgins, L., Kuntner, M., Agnarsson, I. and Voight, B.F. 2022. Characterization of the genome and silk-gland transcriptomes of Darwin's bark spider (Caerostris darwini). *PLoS One*, **17**: e0268660.
Babb, P.L., Lahens, N.F., Correa-Garhwal, S.M., Nicholson, D.N., Kim, E.J., Hogenesch, J.B., Kuntner, M., Higgins, L., Hayashi, C.Y., Agnarsson, I. and Voight, B.F. 2017. The Nephila clavipes genome highlights the diversity of spider silk genes and their complex expression. *Nat Genet*, **49**: 895–903.
Bauer, J. and Scheibel, T. 2017a. Conformational Stability and Interplay of Helical N- and C-Terminal Domains with Implications on Major Ampullate Spidroin Assembly. *Biomacromolecules*, **18**: 835–845.
Bauer, J. and Scheibel, T. 2017b. Dimerization of the Conserved N-Terminal Domain of a Spider Silk Protein Controls the Self-Assembly of the Repetitive Core Domain. *Biomacromolecules*, **18**: 2521–2528.
Bell, A.L. and Peakall, D.B. 1969. Changes in fine structure during silk protein production in the ampullate gland of the spider Araneus sericatus. *J Cell Biol*, **42**: 284–295.
Bini, E., Foo, C.W.P., Huang, J., Karageorgiou, V., Kitchel, B. and Kaplan, D.L. 2006. RGD-functionalized bioengineered spider dragline silk biomaterial. *Biomacromolecules*, **7**: 3139–3145.
Blackledge, T.A., Cardullo, R.A. and Hayashi, C.Y. 2005. Polarized light microscopy, variability in spider silk diameters, and the mechanical characterization of spider silk. *Invertebrate Biology*, **124**: 165–173.
Blackledge, T.A. and Hayashi, C.Y. 2006. Silken toolkits: Biomechanics of silk fibers spun by the orb web spider Argiope argentata (Fabricius 1775). *Journal of Experimental Biology*, **209**: 2452–2461.
Blamires, S.J., Blackledge, T.A. and Tso, I.M. 2017. Physicochemical Property Variation in Spider Silk: Ecology, Evolution, and Synthetic Production. *Annu Rev Entomol*, **62**: 443–460.
Blamires, S.J., Nobbs, M., Wolff, J.O. and Heu, C. 2022. Nutritionally induced nanoscale variations in spider silk structural and mechanical properties. *J Mech Behav Biomed Mater*, **125**: 104873.
Blobel, G. 1980. Intracellular protein topogenesis. *Proc Natl Acad Sci U S A*, **77**: 1496–1500.
Blobel, G. and Dobberstein, B. 1975. Transfer of proteins across membranes: I. Presence of proteolytically processed and unprocessed nascent immunoglobulin light chains on membrane-bound ribosomes of murine myeloma. *Journal of Cell Biology*, **67**: 835–851.
Boehler, R.M., Graham, J.G. and Shea, L.D. 2011. Tissue engineering tools for modulation of the immune response. *Biotechniques*, **51**: 239–254.
Borkner, C.B., Elsner, M.B. and Scheibel, T. 2014. Coatings and films made of silk proteins. *ACS Appl Mater Interfaces*, **6**: 15611–15625.
Boulet-Audet, M., Holland, C., Gheysens, T. and Vollrath, F. 2016. Dry-Spun Silk Produces Native-Like Fibroin Solutions. *Biomacromolecules*, **17**: 3198–3204.
Bowen, C.H., Dai, B., Sargent, C.J., Bai, W., Ladiwala, P., Feng, H., Huang, W., Kaplan, D.L., Galazka, J.M. and Zhang, F. 2018. Recombinant Spidroins Fully Replicate

Primary Mechanical Properties of Natural Spider Silk. *Biomacromolecules*, **19**: 3853–3860.
Bratzel, G. and Buehler, M.J. 2012. Sequence-structure correlations in silk: Poly-Ala repeat of N. clavipes MaSp1 is naturally optimized at a critical length scale. *J Mech Behav Biomed Mater*, **7**: 30–40.
Breslauer, D.N., Lee, L.P. and Muller, S.J. 2009. Simulation of flow in the silk gland. *Biomacromolecules*, **10**: 49–57.
Burgess, T.L. and Kelly, R.B. 1987. Constitutive and regulated secretion of proteins.
Candelas, G.C. and Cintron, J. 1981. A spider fibroin and its synthesis. *Journal of Experimental Zoology*, **216**: 1–6.
Cao, H., Parveen, S., Ding, D., Xu, H., Tan, T. and Liu, L. 2017. Metabolic engineering for recombinant major ampullate spidroin 2 (MaSp2) synthesis in Escherichia coli. *Sci Rep*, **7**: 11365.
Cao, R., Liu, X., Liu, Y., Zhai, X., Cao, T., Wang, A. and Qiu, J. 2021. Applications of nuclear magnetic resonance spectroscopy to the evaluation of complex food constituents. *Food Chem*, **342**: 128258.
Casem, M.L., Tran, L.P.P. and Moore, A.M.F. 2002. Ultrastructure of the major ampullate gland of the black widow spider, Latrodectus hesperus. *Tissue Cell*, **34**: 427–436.
Cavanagh, J., Fairbrother, W.J., Palmer III, A.G. and Skelton, N.J. 1996. *Protein NMR spectroscopy: principles and practice*.
Chaudhuri, O., Gu, L., Klumpers, D., Darnell, M., Sidi, A., Weaver, J.C., Huebsch, N., Lee, H., Lippens, E., Duda, G.N. and Mooney, D.J. 2016. Hydrogels with tunable stress relaxation regulate stem cell fate and activity. *Nat Mater*, **15**: 326–334.
Chaw, R.C., Correa-Garhwal, S.M., Clarke, T.H., Ayoub, N.A. and Hayashi, C.Y. 2015. Proteomic Evidence for Components of Spider Silk Synthesis from Black Widow Silk Glands and Fibers. *J Proteome Res*, **14**: 4223–4231.
Chen, G., Liu, X., Zhang, Y., Lin, S., Yang, Z., Johansson, J., Rising, A. and Meng, Q. 2012. Full-Length Minor Ampullate Spidroin Gene Sequence. *PLoS One*, **7**: e52293.
Chen, X., Knight, D.P. and Vollrath, F. 2002. Rheological characterization of nephila spidroin solution. *Biomacromolecules*, **3**: 644–648.
Cheng, J., Hu, C.F., Gan, C.Y., Xia, X.X. and Qian, Z.G. 2022. Functionalization and Reinforcement of Recombinant Spider Dragline Silk Fibers by Confined Nanoparticle Formation. *ACS Biomater Sci Eng*, **8**: 3299–3309.
Chouhan, D., Thatikonda, N., Nilebäck, L., Widhe, M., Hedhammar, M. and Mandal, B.B. 2018. Recombinant Spider Silk Functionalized Silkworm Silk Matrices as Potential Bioactive Wound Dressings and Skin Grafts. *ACS Appl Mater Interfaces*, **10**: 23560–23572.
Colgin, M.A. and Lewis, R. v. 1998. Spider minor ampullate silk proteins contain new repetitive sequences and highly conserved non-silk-like “spacer regions.” *Protein Science*, **7**: 667–672.
Collin, M.A., Clarke, T.H., Ayoub, N.A. and Hayashi, C.Y. 2018. Genomic perspectives of spider silk genes through target capture sequencing: Conservation of stabilization mechanisms and homology-based structural models of spidroin terminal regions. *Int J Biol Macromol*, **113**: 829–840.
Cookson, S.T., Nora, J.J., Kithas, J.A., Arduino, M.J., Bond, W.W., Miller, P.H., Monahan, J., Hoffman, R.E., Curiel, T., Kaufman, D., Groves, B.M. and Jarvis, W.R. 1997. Pyrogenic reactions in patients undergoing cardiac catheterization associated with contaminated glass medicine cups. *Cathet Cardiovasc Diagn*, **42**: 12–18.
Copeland, C.G., Bell, B.E., Christensen, C.D. and Lewis, R. v. 2015. Development of a Process for the Spinning of Synthetic Spider Silk. *ACS Biomater Sci Eng*, **1**: 577–584.
Craig, H.C., Blamires, S.J., Sani, M.A., Kasumovic, M.M., Rawal, A. and Hook, J.M. 2019. DNP NMR spectroscopy reveals new structures, residues and interactions in wild spider silks. *Chemical Communications*, **55**: 4687–4690.
Craig, H.C., Piorkowski, D., Nakagawa, S., Kasumovic, M.M. and Blamires, S.J. 2020. Meta-analysis reveals materiomic relationships in major ampullate silk across the spider phylogeny. *J R Soc Interface*, **17**.

Cranford, S.W., Pugno, N.M., Buehler, M.J. 2014. *Silk and Web Synergy: The Merging of Material and Structural Performance* (T. Asakura and T. Miller, eds).
Cranford, S.W., Tarakanova, A., Pugno, N.M. and Buehler, M.J. 2012. Nonlinear material behaviour of spider silk yields robust webs. *Nature*, **482**: 72–76.
Dams-Kozlowska, H., Majer, A., Tomasiewicz, P., Lozinska, J., Kaplan, D.L. and Mackiewicz, A. 2013. Purification and cytotoxicity of tag-free bioengineered spider silk proteins. *J Biomed Mater Res A*, **101 A**: 456–464.
Davies, G.J.G., Knight, D.P. and Vollrath, F. 2013. Structure and function of the major ampullate spinning duct of the golden orb weaver, Nephila edulis. *Tissue Cell*, **45**: 306–311.
Deptuch, T., Florczak, A., Lewandowska, A., Leporowska, E., Penderecka, K., Marszalek, A., Mackiewicz, A. and Dams-Kozlowska, H. 2021. MS1-type bioengineered spider silk nanoparticles do not exhibit toxicity in an in vivo mouse model. *Nanomedicine*, **16**: 1553–1565.
Deptuch, T., Penderecka, K., Kaczmarek, M., Molenda, S. and Dams-Kozlowska, H. 2022. In vivo study of the immune response to bioengineered spider silk spheres. *Sci Rep*, **12**: 1–14.
DeSimone, E., Schacht, K., Pellert, A. and Scheibel, T. 2017. Recombinant spider silk-based bioinks. *Biofabrication*, **9**: 44104.
DeSimone, E., Schacht, K. and Scheibel, T. 2016. Cations influence the cross-linking of hydrogels made of recombinant, polyanionic spider silk proteins. *Mater Lett*, **183**: 101–104.
Dicko, C., Knight, D., Kenney, J.M. and Vollrath, F. 2004. Secondary structures and conformational changes in flagelliform, cylindrical, major, and minor ampullate silk proteins. Temperature and concentration effects. *Biomacromolecules*, **5**: 2105–2115.
Dicko, C., Vollrath, F. and Kenney, J.M. 2004. Spider silk protein refolding is controlled by changing pH. *Biomacromolecules*, **5**: 704–710.
Dinjaski, N., Plowright, R., Zhou, S., Belton, D.J., Perry, C.C. and Kaplan, D.L. 2017. Osteoinductive recombinant silk fusion proteins for bone regeneration. *Acta Biomater*, **49**: 127–139.
dos Santos-Pinto, J.R.A., Arcuri, H.A., Esteves, F.G., Palma, M.S. and Lubec, G. 2018. Spider silk proteome provides insight into the structural characterization of Nephila clavipes flagelliform spidroin. *Sci Rep*, **8**: 14674.
dos Santos-Pinto, J.R.A., Arcuri, H.A., Lubec, G. and Palma, M.S. 2016. Structural characterization of the major ampullate silk spidroin-2 protein produced by the spider Nephila clavipes. *Biochimica et Biophysica Acta (BBA) - Proteins and Proteomics*, **1864**: 1444–1454.
dos Santos-Pinto, J.R.A., Arcuri, H.A., Priewalder, H., Salles, H.C., Palma, M.S. and Lubec, G. 2015. Structural model for the spider silk protein spidroin-1. *J Proteome Res*, **14**: 3859–3870.
dos Santos-Pinto, J.R.A., Esteves, F.G., Sialana, F.J., Ferro, M., Smidak, R., Rares, L.C., Nussbaumer, T., Rattei, T., Bilban, M., Bacci Júnior, M., Palma, M.S. and Lübec, G. 2019. A proteotranscriptomic study of silk-producing glands from the orb-weaving spiders. *Mol Omics*, **15**: 256–270.
dos Santos-Pinto, J.R.A., Lamprecht, G., Chen, W.Q., Heo, S., Hardy, J.G., Priewalder, H., Scheibel, T.R., Palma, M.S. and Lubec, G. 2014. Structure and post-translational modifications of the web silk protein spidroin-1 from Nephila spiders. *J Proteomics*, **105**: 174–185.
Du, N., Xiang, Y.L., Narayanan, J., Li, L., Lim, M.L.M. and Li, D. 2006. Design of superior spider silk: From nanostructure to mechanical properties. *Biophys J*, **91**: 4528–4535.
Eanes, E.D. and Glenner, G.G. 1968. X-ray diffraction studies on amyloid filaments. *J Histochem Cytochem*, **16**: 673–677.
Edlund, A.M., Jones, J., Lewis, R. and Quinn, J.C. 2018. Economic feasibility and environmental impact of synthetic spider silk production from escherichia coli. *N Biotechnol*, **42**: 12–18.
Eisenberg, D. and Jucker, M. 2012. The amyloid state of proteins in human diseases. *Cell*, **148**: 1188–1203.

Eisoldt, L., Hardy, J.G., Heim, M. and Scheibel, T.R. 2010. The role of salt and shear on the storage and assembly of spider silk proteins. *J Struct Biol*, **170**: 413–419.
Eisoldt, L., Thamm, C. and Scheibel, T. 2012. Review: The role of terminal domains during storage and assembly of spider silk proteins. *Biopolymers*, **97**: 355–361.
Engler, A.J., Sen, S., Sweeney, H.L. and Discher, D.E. 2006. Matrix Elasticity Directs Stem Cell Lineage Specification. *Cell*, **126**: 677–689.
Erbil, H.Y., Demirel, A.L., Avci, Y. and Mert, O. 2003. Transformation of a simple plastic into a superhydrophobic surface. *Science (1979)*, **299**: 1377–1380.
Esser, T.U., Trossmann, V.T., Lentz, S., Engel, F.B. and Scheibel, T. 2021. Designing of spider silk proteins for human induced pluripotent stem cell-based cardiac tissue engineering. *Mater Today Bio*, **11**: 100114.
Exler, J.H., Hümmerich, D. and Scheibel, T. 2007. The amphiphilic properties of spider silks are important for spinning. *Angewandte Chemie - International Edition*, **46**: 3559–3562.
Finnigan, W., Roberts, A.D., Ligorio, C., Scrutton, N.S., Breitling, R., Blaker, J.J. and Takano, E. 2020. The effect of terminal globular domains on the response of recombinant mini-spidroins to fiber spinning triggers. *Sci Rep*, **10**: 10671.
Florczak, A., Jastrzebska, K., Mackiewicz, A. and Dams-Kozlowska, H. 2017. Blending two bioengineered spider silks to develop cancer targeting spheres. *J Mater Chem B*, **5**: 3000–3011.
Franz, S., Rammelt, S., Scharnweber, D. and Simon, J.C. 2011. Immune responses to implants - A review of the implications for the design of immunomodulatory biomaterials. *Biomaterials*, **32**: 6692–6709.
Fraser, R.D.B., MacRae, T.P. and Suzuki, E. 1979. Chain conformation in the collagen molecule. *J Mol Biol*, **129**: 463–481.
Fredriksson, C., Hedhammar, M., Feinstein, R., Nordling, K., Kratz, G., Johansson, J., Huss, F. and Rising, A. 2009. Tissue response to subcutaneously implanted recombinant spider silk: An in vivo study. *Materials*, **2**: 1908–1922.
Frische, S., Maunsbach, A.B. and Vollrath, F. 1998. Elongate cavities and skin-core structure in Nephila spider silk observed by electron microscopy. *J Microsc*, **189**: 64–70.
Gao, Z., Lin, Z., Huang, W., Lai, C.C., Fan, J.S. and Yang, D. 2013. Structural Characterization of Minor Ampullate Spidroin Domains and Their Distinct Roles in Fibroin Solubility and Fiber Formation. *PLoS One*, **8**: e56142.
Garb, J.E., Ayoub, N.A. and Hayashi, C.Y. 2010. Untangling spider silk evolution with spidroin terminal domains. *BMC Evol Biol*, **10**: 1–16.
Garb, J.E., Haney, R.A., Schwager, E.E., Gregorič, M., Kuntner, M., Agnarsson, I. and Blackledge, T.A. 2019. The transcriptome of Darwin's bark spider silk glands predicts proteins contributing to dragline silk toughness. *Commun Biol*, **2**: 275.
Geckil, H., Xu, F., Zhang, X., Moon, S. and Demirci, U. 2010. Engineering hydrogels as extracellular matrix mimics. *Nanomedicine*, **5**: 469–484.
Gellynck, K., Verdonk, P., Almqvist, F., van Nimmen, E., de Bakker, D., van Langenhove, L., Mertens, J., Verbruggen, G. and Kiekens, P. 2005. A Spider Silk Supportive Matrix Used for Cartilage Regeneration. *Medical Textiles and Biomaterials for Healthcare: Incorporating Proceedings of MEDTEX03 International Conference and Exhibition on Healthcare and Medical Textiles*, 350–354.
Gellynck, K., Verdonk, P., Forsyth, R., Almqvist, K.F., van Nimmen, E., Gheysens, T., Mertens, J., van Langenhove, L., Kiekens, P. and Verbruggen, G. 2008. Biocompatibility and biodegradability of spider egg sac silk. *J Mater Sci Mater Med*, **19**: 2963–2970.
Giesa, T., Perry, C.C. and Buehler, M.J. 2016. Secondary Structure Transition and Critical Stress for a Model of Spider Silk Assembly. *Biomacromolecules*, **17**: 427–436.
Gnesa, E., Hsia, Y., Yarger, J.L., Weber, W., Lin-Cereghino, J., Lin-Cereghino, G., Tang, S., Agari, K. and Vierra, C. 2012. Conserved C-terminal domain of spider tubuliform spidroin 1 contributes to extensibility in synthetic fibers. *Biomacromolecules*, **13**: 304–312.

Gomes, S., Numata, K., Leonor, I.B., Mano, J.F., Reis, R.L. and Kaplan, D.L. 2011. AFM study of morphology and mechanical properties of a chimeric spider silk and bone sialoprotein protein for bone regeneration. *Biomacromolecules*, **12**: 1675–1685.

Gonska, N., López, P.A., Lozano-Picazo, P., Thorpe, M., Guinea, G. v., Johansson, J., Barth, A., Pérez-Rigueiro, J. and Rising, A. 2020. Structure-Function Relationship of Artificial Spider Silk Fibers Produced by Straining Flow Spinning. *Biomacromolecules*, **21**: 2116–2124.

Gosline, J.M., Guerette, P.A., Ortlepp, C.S. and Savage, K.N. 1999. The mechanical design of spider silks: from fibroin sequence to mechanical function. *Journal of Experimental Biology*, **202**: 3295–3303.

Gray, G.M., van der Vaart, A., Guo, C., Jones, J., Onofrei, D., Cherry, B.R., Lewis, R. v., Yarger, J.L. and Holland, G.P. 2016. Secondary structure adopted by the Gly-Gly-X repetitive regions of dragline spider silk. *Int J Mol Sci*, **17**.

Greco, G., Francis, J., Arndt, T., Schmuck, B., Bäcklund, F.G., Barth, A., Johansson, J., Pugno, N.M. and Rising, A. 2020. Properties of biomimetic artificial spider silk fibers tuned by PostSpin bath incubation. *Molecules*, **25**: 3248.

Greco, G., Mirbaha, H., Schmuck, B., Rising, A. and Pugno, N.M. 2022. Artificial and natural silk materials have high mechanical property variability regardless of sample size. *Sci Rep*, **12**: 1–9.

Greving, I., Terry, A.E., Holland, C., Boulet-Audet, M., Grillo, I., Vollrath, F., Dicko, C., Greving, I., Terry, A.E. and Dicko, C. 2020. Structural Diversity of Native Major Ampullate, Minor Ampullate, Cylindriform, and Flagelliform Silk Proteins in Solution. *Biomacromolecules*, **21**: 3387–3393.

Griffiths, G. and Simons, K. 1986. The trans Golgi network: Sorting at the exit site of the Golgi complex. *Science (1979)*, **234**: 438–443.

Grip, S., Johansson, J. and Hedhammar, M. 2009. Engineered disulfides improve mechanical properties of recombinant spider silk. *Protein Sci*, **18**: 1012–1022.

Guinea, G. v., Elices, M., Plaza, G.R., Perea, G.B., Daza, R., Riekel, C., Agulló-Rueda, F., Hayashi, C., Zhao, Y. and Pérez-Rigueiro, J. 2012. Minor ampullate silks from Nephila and Argiope spiders: Tensile properties and microstructural characterization. *Biomacromolecules*, **13**: 2087–2098.

Guo, J.L., Kim, Y.S. and Mikos, A.G. 2019. Biomacromolecules for Tissue Engineering: Emerging Biomimetic Strategies. *Biomacromolecules*, **20**: 2904–2912.

Guvendiren, M. and Burdick, J.A. 2013. Engineering synthetic hydrogel microenvironments to instruct stem cells. *Curr Opin Biotechnol*, **24**: 841–846.

Hagn, F., Eisoldt, L., Hardy, J.G., Vendrely, C., Coles, M., Scheibel, T. and Kessler, H. 2010. A conserved spider silk domain acts as a molecular switch that controls fibre assembly. *Nature*, **465**: 239–242.

Hagn, F., Thamm, C., Scheibel, T. and Kessler, H. 2011. PH-dependent dimerization and salt-dependent stabilization of the N-terminal domain of spider dragline silk - Implications for fiber formation. *Angewandte Chemie - International Edition*, **50**: 310–313.

Han, L., Zhang, L., Zhao, T., Wang, Y. and Nakagaki, M. 2013. Analysis of a new type of major ampullate spider silk gene, MaSp1s. *Int J Biol Macromol*, **56**: 156–161.

Hansson, M.L., Chatterjee, U., Francis, J., Arndt, T., Broman, C., Johansson, J., Sköld, M.K. and Rising, A. 2021. Artificial spider silk supports and guides neurite extension in vitro. *FASEB Journal*, **35**: 1–14.

Harvey, D., Bray, G., Zamberlan, F., Amer, M., Goodacre, S.L. and Thomas, N.R. 2020. Cyclo(RGDfK) Functionalized Spider Silk Cell Scaffolds: Significantly Improved Performance in Just One Click. *Macromol Biosci*, **20**: e2000255.

Hayashi, C.Y., Blackledge, T.A. and Lewis, R. v. 2004. Molecular and mechanical characterization of aciniform silk: Uniformity of iterated sequence modules in a novel member of the spider silk fibroin gene family. *Mol Biol Evol*, **21**: 1950–1959.

Hayashi, C.Y., Shipley, N.H. and Lewis, R. v. 1999. Hypotheses that correlate the sequence, structure, and mechanical properties of spider silk proteins. *Int J Biol Macromol*, **24**: 271–275.

Hedhammar, M., Rising, A., Grip, S., Martinez, A.S., Nordling, K., Casals, C., Stark, M. and Johansson, J. 2008. Structural properties of recombinant nonrepetitive and repetitive parts of major ampullate spidroin 1 from Euprosthenops australis: Implications for fiber formation. *Biochemistry*, **47**: 3407–3417.
Heiby, J.C., Goretzki, B., Johnson, C.M., Hellmich, U.A. and Neuweiler, H. 2019. Methionine in a protein hydrophobic core drives tight interactions required for assembly of spider silk. *Nat Commun*, **10**: 4378.
Heidebrecht, A., Eisoldt, L., Diehl, J., Schmidt, A., Geffers, M., Lang, G. and Scheibel, T. 2015. Biomimetic Fibers Made of Recombinant Spidroins with the Same Toughness as Natural Spider Silk. *Advanced Materials*, **27**: 2189–2194.
Heinritz, C., Lamberger, Z., Kocourková, K., Minařík, A. and Humenik, M. 2021. DNA Functionalized Spider Silk Nanohydrogels for Specific Cell Attachment and Patterning. *ACS Nano*, **16**: 7626–7635.
Hennecke, K., Redeker, J., Kuhbier, J.W., Strauss, S., Allmeling, C., Kasper, C., Reimers, K. and Vogt, P.M. 2013. Bundles of Spider Silk, Braided into Sutures, Resist Basic Cyclic Tests: Potential Use for Flexor Tendon Repair. *PLoS One*, **8**: e61100.
Heppner, R., Weichert, N., Schierhorn, A., Conrad, U. and Pietzsch, M. 2016. Low-tech, pilot scale purification of a recombinant spider silk protein analog from tobacco leaves. *Int J Mol Sci*, **17**.
Hermanson, K.D., Huemmerich, D., Scheibel, T. and Bausch, A.R. 2007. Engineered microcapsules fabricated from reconstituted spider silk. *Advanced Materials*, **19**: 1810–1815.
Herold, H.M., Döbl, A., Wohlrab, S., Humenik, M. and Scheibel, T. 2020. Designed Spider Silk-Based Drug Carrier for Redox- or pH-Triggered Drug Release. *Biomacromolecules*, **21**: 4904–4912.
Hessa, T., Kim, H., Bihlmaier, K., Lundin, C., Boekel, J., Andersson, H., Nilsson, I.M., White, S.H. and von Heijne, G. 2005. Recognition of transmembrane helices by the endoplasmic reticulum translocon. *Nature*, **433**: 377–381.
Hessa, T., Meindl-Beinker, N.M., Bernsel, A., Kim, H., Sato, Y., Lerch-Bader, M., Nilsson, I., White, S.H. and von Heijne, G. 2007. Molecular code for transmembrane-helix recognition by the Sec61 translocon. *Nature*, **450**: 1026–1030.
Hijirida, D.H., Do, K.G., Michal, C., Wong, S., Zax, D. and Jelinski, L.W. 1996. 13C NMR of Nephila clavipes major ampullate silk gland. *Biophys J*, **71**: 3442–3447.
Holland, C., Terry, A.E., Porter, D. and Vollrath, F. 2006. Comparing the rheology of native spider and silkworm spinning dope. *Nat Mater*, **5**: 870–874.
Holland, C., Terry, A.E., Porter, D. and Vollrath, F. 2007. Natural and unnatural silks. *Polymer (Guildf)*, **48**: 3388–3392.
Holland, G.P., Creager, M.S., Jenkins, J.E., Lewis, R. v. and Yarger, J.L. 2008. Determining secondary structure in spider dragline silk by carbon-carbon correlation solid-state NMR spectroscopy. *J Am Chem Soc*, **130**: 9871–9877.
Hronska, M., van Beek, J.D., Williamson, P.T.F., Vollrath, F. and Meier, B.H. 2004. NMR characterization of native liquid spider dragline silk from Nephila edulis. *Biomacromolecules*, **5**: 834–839.
Hu, C.F., Qian, Z.G., Peng, Q., Zhang, Y. and Xia, X.X. 2021. Unconventional Spidroin Assemblies in Aqueous Dope for Spinning into Tough Synthetic Fibers. *ACS Biomater Sci Eng*, **7**: 3608–3617.
Huang, T., Kumari, S., Herold, H., Bargel, H., Aigner, T.B., Heath, D.E., O'brien-Simpson, N.M., O'connor, A.J. and Scheibel, T. 2020. Enhanced antibacterial activity of se nanoparticles upon coating with recombinant spider silk protein eadf4(κ16). *Int J Nanomedicine*, **15**: 4275–4288.
Humenik, M., Preiß, T., Gödrich, S., Papastavrou, G. and Scheibel, T. 2020. Functionalized DNA-spider silk nanohydrogels for controlled protein binding and release. *Mater Today Bio*, **6**: 100045.
Ittah, S., Cohen, S., Garty, S., Cohn, D. and Gat, U. 2006. An essential role for the C-terminal domain of a dragline spider silk protein in directing fiber formation. *Biomacromolecules*, **7**: 1790–1795.

Ittah, S., Michaeli, A., Goldblum, A. and Gat, U. 2007. A model for the structure of the C-terminal domain of dragline spider silk and the role of its conserved cysteine. *Biomacromolecules*, **8**: 2768–2773.
Jahn, T.R., Makin, O.S., Morris, K.L., Marshall, K.E., Tian, P., Sikorski, P. and Serpell, L.C. 2010. The Common Architecture of Cross-β Amyloid. *J Mol Biol*, **395**: 717–727.
Janmey, P.A., Georges, P.C. and Hvidt, S. 2007. Basic Rheology for Biologists. *Methods Cell Biol*, **83**: 1–27.
Jansson, R., Lau, C.H., Ishida, T., Ramström, M., Sandgren, M. and Hedhammar, M. 2016. Functionalized silk assembled from a recombinant spider silk fusion protein (Z-4RepCT) produced in the methylotrophic yeast Pichia pastoris. *Biotechnol J*, **11**: 687–699.
Jaudzems, K., Askarieh, G., Landreh, M., Nordling, K., Hedhammar, M., Jörnvall, H., Rising, A., Knight, S.D. and Johansson, J. 2012. PH-dependent dimerization of spider silk N-terminal domain requires relocation of a wedged tryptophan side chain. *J Mol Biol*, **422**: 477–487.
Jenkins, J.E., Creager, M.S., Butler, E.B., Lewis, R. v., Yarger, J.L. and Holland, G.P. 2010. Solid-state NMR evidence for elastin-like β-turn structure in spider dragline silk. *Chemical Communications*, **46**: 6714–6716.
Jenkins, J.E., Sampath, S., Butler, E., Kim, J., Henning, R.W., Holland, G.P. and Yarger, J.L. 2013. Characterizing the secondary protein structure of black widow dragline silk using solid-state NMR and X-ray diffraction. *Biomacromolecules*, **14**: 3472–3483.
Jin, Q., Pan, F., Hu, C.-F., Lee, S.Y., Xia, X.-X. and Qian, Z.-G. 2022. Secretory production of spider silk proteins in metabolically engineered Corynebacterium glutamicum for spinning into tough fibers. *Metab Eng*, **70**: 102–114.
Johansson, J., Nerelius, C., Willander, H. and Presto, J. 2010. Conformational preferences of non-polar amino acid residues: An additional factor in amyloid formation. *Biochem Biophys Res Commun*, **402**: 515–518.
Johansson, J. and Rising, A. 2021. Doing what spiders cannot-a road map to supreme artificial silk fibers. *ACS Nano*, **15**: 1952–1959.
Johansson, U., Shalaly, N.D., Hjelm, L.C., Ria, M., Berggren, P.O. and Hedhammar, M. 2020. Integration of Primary Endocrine Cells and Supportive Cells Using Functionalized Silk Promotes the Formation of Prevascularized Islet-like Clusters. *ACS Biomater Sci Eng*, **6**: 1186–1195.
Johansson, U., Widhe, M., Shalaly, N.D., Arregui, I.L., Nilebäck, L., Tasiopoulos, C.P., Åstrand, C., Berggren, P.O., Gasser, C. and Hedhammar, M. 2019. Assembly of functionalized silk together with cells to obtain proliferative 3D cultures integrated in a network of ECM-like microfibers. *Sci Rep*, **9**.
Johnson, A.E. and van Waes, M.A. 1999. The translocon: A dynamic gateway at the ER membrane. *Annu Rev Cell Dev Biol*, **15**: 799–842.
Jones, J.A., Harris, T.I., Tucker, C.L., Berg, K.R., Christy, S.Y., Day, B.A., Gaztambide, D.A., Needham, N.J.C., Ruben, A.L., Oliveira, P.F., Decker, R.E. and Lewis, R. v. 2015. More Than Just Fibers: An Aqueous Method for the Production of Innovative Recombinant Spider Silk Protein Materials. *Biomacromolecules*, **16**: 1418–1425.
Kaldmäe, M., Leppert, A., Chen, G., Sarr, M., Sahin, C., Nordling, K., Kronqvist, N., Gonzalvo-Ulla, M., Fritz, N., Abelein, A., Laín, S., Biverstål, H., Jörnvall, H., Lane, D.P., Rising, A., Johansson, J. and Landreh, M. 2020. High intracellular stability of the spidroin N-terminal domain in spite of abundant amyloidogenic segments revealed by in-cell hydrogen/deuterium exchange mass spectrometry. *FEBS Journal*, **287**: 2823–2833.
Kehoe, S., Zhang, X.F. and Boyd, D. 2012. FDA approved guidance conduits and wraps for peripheral nerve injury: A review of materials and efficacy. *Injury*, **43**: 553–572.
Kenney, J.M., Knight, D., Wise, M.J. and Vollrath, F. 2002. Amyloidogenic nature of spider silk. *Eur J Biochem*, **269**: 4159–4163.
Kerkam, K., Viney, C., Kaplan, D. and Lombardi, S. 1991. Liquid crystallinity of natural silk secretions. *Nature*, **349**: 596–598.
Keten, S. and Buehler, M.J. 2010. Nanostructure and molecular mechanics of spider dragline silk protein assemblies. *J R Soc Interface*, **7**: 1709–1721.

Keten, S., Xu, Z., Ihle, B. and Buehler, M.J. 2010. Nanoconfinement controls stiffness, strength and mechanical toughness of B-sheet crystals in silk. *Nat Mater*, **9**: 359–367.
Kienzle, C. and von Blume, J. 2014. Secretory cargo sorting at the trans-Golgi network. *Trends Cell Biol*, **24**: 584–593.
Knight, D.P., Knight, M.M. and Vollrath, F. 2000. Beta transition and stress-induced phase separation in the spinning of spider dragline silk. *Int J Biol Macromol*, **27**: 205–210.
Knight, D.P. and Vollrath, F. 2001. Changes in element composition along the spinning duct in a Nephila spider. *Naturwissenschaften*, **88**: 179–182.
Knight, D.P. and Vollrath, F. 1999. Liquid crystals and flow elongation in a spider's silk production line. *Proceedings of the Royal Society B: Biological Sciences*, **266**: 519–523.
Koeppel, A. and Holland, C. 2017. Progress and Trends in Artificial Silk Spinning: A Systematic Review. *ACS Biomater Sci Eng*, **3**: 226–237.
Kojić, N., Bico, J., Glasen, C. and McKinley, G.H. 2006. Ex vivo rheology of spider silk. *Journal of Experimental Biology*, **209**: 4355–4362.
Kono, N., Nakamura, H., Mori, M., Yoshida, Y., Ohtoshi, R., Malay, A.D., Pedrazzoli Moran, D.A., Tomita, M., Numata, K. and Arakawa, K. 2021. Multicomponent nature underlies the extraordinary mechanical properties of spider dragline silk. *Proceedings of the National Academy of Sciences*, **118**: e2107065118.
Kono, N., Nakamura, H., Ohtoshi, R., Moran, D.A.P., Shinohara, A., Yoshida, Y., Fujiwara, M., Mori, M., Tomita, M. and Arakawa, K. 2019. Orb-weaving spider Araneus ventricosus genome elucidates the spidroin gene catalogue. *Sci Rep*, **9**: 8380.
Kono, N., Ohtoshi, R., Malay, A.D., Mori, M., Masunaga, H., Yoshida, Y., Nakamura, H., Numata, K. and Arakawa, K. 2021. Darwin's bark spider shares a spidroin repertoire with Caerostris extrusa but achieves extraordinary silk toughness through gene expression. *Open Biol*, **11**: 210242
Koop, F., Strauß, S., Peck, C.-T., Aper, T., Wilhelmi, M., Hartmann, C., Hegermann, J., Schipke, J., Vogt, P.M. and Bucan, V. 2022. Preliminary application of native Nephila edulis spider silk and fibrin implant causes granulomatous foreign body reaction in vivo in rat's spinal cord. *PLoS One*, **17**: e0264486.
Kornfeld, T., Nessler, J., Helmer, C., Hannemann, R., Waldmann, K.H., Peck, C.T., Hoffmann, P., Brandes, G., Vogt, P.M. and Radtke, C. 2021. Spider silk nerve graft promotes axonal regeneration on long distance nerve defect in a sheep model. *Biomaterials*, **271**: 120692.
Kornfeld, T., Vogt, P., Bucan, V., Peck, C.-T., Reimers, K. and Radtke, C. 2016. Characterization and Schwann Cell Seeding of up to 15.0 cm Long Spider Silk Nerve Conduits for Reconstruction of Peripheral Nerve Defects. *J Funct Biomater*, **7**: 30.
Kozlowska, A.K., Florczak, A., Smialek, M., Dondajewska, E., Mackiewicz, A., Kortylewski, M. and Dams-Kozlowska, H. 2017. Functionalized bioengineered spider silk spheres improve nuclease resistance and activity of oligonucleotide therapeutics providing a strategy for cancer treatment. *Acta Biomater*, **59**: 221–233.
Kronqvist, N., Otikovs, M., Chmyrov, V., Chen, G., Andersson, M., Nordling, K., Landreh, M., Sarr, M., Jörnvall, H., Wennmalm, S., Widengren, J., Meng, Q., Rising, A., Otzen, D., Knight, S.D., Jaudzems, K. and Johansson, J. 2014. Sequential pH-driven dimerization and stabilization of the N-terminal domain enables rapid spider silk formation. *Nat Commun*, **5**: 3254.
Kronqvist, N., Sarr, M., Lindqvist, A., Nordling, K., Otikovs, M., Venturi, L., Pioselli, B., Purhonen, P., Landreh, M., Biverstål, H., Toleikis, Z., Sjöberg, L., Robinson, C. v., Pelizzi, N., Jörnvall, H., Hebert, H., Jaudzems, K., Curstedt, T., Rising, A., *et al.* 2017. Efficient protein production inspired by how spiders make silk. *Nat Commun*, **8**: 15504.
Kuhbier, J.W., Coger, V., Mueller, J., Liebsch, C., Schlottmann, F., Bucan, V., Vogt, P.M. and Strauss, S. 2017. Influence of direct or indirect contact for the cytotoxicity and blood compatibility of spider silk. *J Mater Sci Mater Med*, **28**: 127.
Kumari, S., Bargel, H. and Scheibel, T. 2020. Recombinant Spider Silk–Silica Hybrid Scaffolds with Drug-Releasing Properties for Tissue Engineering Applications. *Macromol Rapid Commun*, **41**.

Kumari, S., Lang, G., DeSimone, E., Spengler, C., Trossmann, V.T., Lücker, S., Hudel, M., Jacobs, K., Krämer, N. and Scheibel, T. 2020. Engineered spider silk-based 2D and 3D materials prevent microbial infestation. *Materials Today*, **41**: 21–33.
Kümmerlen, J., van Beek, J.D., Vollrath, F. and Meier, B.H. 1996. Local structure in spider dragline silk investigated by two-dimensional spin-diffusion nuclear magnetic resonance. *Macromolecules*, **29**: 2920–2928.
Kvick, M., Tasiopoulos, C.P., Barth, A., Söderberg, L.D., Lundell, F. and Hedhammar, M. 2021. Cyclic Expansion/Compression of the Air–Liquid Interface as a Simple Method to Produce Silk Fibers. *Macromol Biosci*, **21**: 1–9.
Lacava, M., Camargo, A., Garcia, L.F., Benamú, M.A., Santana, M., Fang, J., Wang, X. and Blamires, S.J. 2018. Web building and silk properties functionally covary among species of wolf spider. *J Evol Biol*, **31**: 968–978.
Laity, P.R., Gilks, S.E. and Holland, C. 2015. Rheological behaviour of native silk feedstocks. *Polymer (Guildf)*, **67**: 28–39.
Lammel, A., Schwab, M., Slotta, U., Winter, G. and Scheibel, T. 2008. Processing conditions for the formation of spider silk microspheres. *ChemSusChem*, **1**: 413–416.
Landreh, M., Askarieh, G., Nordling, K., Hedhammar, M., Rising, A., Casals, C., Astorga-Wells, J., Alvelius, G., Knight, S.D., Johansson, J., Jörnvall, H. and Bergman, T. 2010. A pH-Dependent Dimer Lock in Spider Silk Protein. *J Mol Biol*, **404**: 328–336.
Lane, A.K., Hayashi, C.Y., Whitworth, G.B. and Ayoub, N.A. 2013. Complex gene expression in the dragline silk producing glands of the Western black widow (Latrodectus hesperus). *BMC Genomics*, **14**: 846.
Lang, G., Grill, C. and Scheibel, T. 2022. Site-Specific Functionalization of Recombinant Spider Silk Janus Fibers. *Angewandte Chemie - International Edition*, **61**.
Laomeephol, C., Vasuratna, A., Ratanavaraporn, J., Kanokpanont, S., Luckanagul, J.A., Humenik, M., Scheibel, T. and Damrongsakkul, S. 2021. Impacts of blended bombyx mori silk fibroin and recombinant spider silk fibroin hydrogels on cell growth. *Polymers (Basel)*, **13**: 1–14.
Larracas, C., Hekman, R., Dyrness, S., Arata, A., Williams, C., Crawford, T. and Vierra, C.A. 2016. Comprehensive proteomic analysis of spider dragline silk from blackwidows: A recipe to build synthetic silk fibers. *Int J Mol Sci*, **17**: 1–16.
Laurent, P., Jolivel, V., Manicki, P., Chiu, L., Contin-Bordes, C., Truchetet, M.-E. and Pradeu, T. 2017. Immune-Mediated Repair: A Matter of Plasticity. *Front Immunol*, **8**: 1–8.
Lawrence, B.A., Vierra, C.A. and Moore, A.M.F. 2004. Molecular and mechanical properties of major ampullate silk of the black widow spider, Latrodectus hesperus. *Biomacromolecules*, **5**: 689–695.
Lazaris, A., Arcidiacono, S., Huang, Y., Zhou, J.F., Duguay, F., Chretien, N., Welsh, E.A., Soares, J.W. and Karatzas, C.N. 2002. Spider silk fibers spun from soluble recombinant silk produced in mammalian cells. *Science (1979)*, **295**: 472–476.
Lechner, A., Trossmann, V.T. and Scheibel, T. 2022. Impact of Cell Loading of Recombinant Spider Silk Based Bioinks on Gelation and Printability. *Macromol Biosci*, **22**: 2100390.
Leclerc, J., Lefèvre, T., Gauthier, M., Gagné, S.M. and Auger, M. 2013. Hydrodynamical properties of recombinant spider silk proteins: Effects of pH, salts and shear, and implications for the spinning process. *Biopolymers*, **99**: 582–593.
Lefèvre, T., Boudreault, S., Cloutier, C. and Pézolet, M. 2008. Conformational and orientational transformation of silk proteins in the major ampullate gland of Nephila clavipes spiders. *Biomacromolecules*, **9**: 2399–2407.
Lefèvre, T., Boudreault, S., Cloutier, C. and Pézolet, M. 2011. Diversity of molecular transformations involved in the formation of spider silks. *J Mol Biol*, **405**: 238–253.
Lefèvre, T., Leclerc, J., Rioux-Dubé, J.F., Buffeteau, T., Paquin, M.C., Rousseau, M.E., Cloutier, I., Auger, M., Gagné, S.M., Boudreault, S., Cloutier, C. and Pézelot, M. 2007. In situ conformation of spider silk proteins in the intact major ampullate gland and in solution. *Biomacromolecules*, **8**: 2342–2344.

Li, H., Chen, S., Piao, S., An, T. and Wang, C. 2020. Production of artificial synthetic spidroin gene 4S-transgenic cloned sheep embryos using somatic cell nuclear transfer. *Anim Biotechnol*, **32**: 616–626
Li, S.F., McGhie, A.J. and Tang, S.L. 1994. New internal structure of spider dragline silk revealed by atomic force microscopy. *Biophys J*, **66**: 1209–1212.
Liebsch, C., Bucan, V., Menger, B., Köhne, F., Waldmann, K.H., Vaslaitis, D., Vogt, P.M., Strauss, S. and Kuhbier, J.W. 2018. Preliminary investigations of spider silk in wounds in vivo — Implications for an innovative wound dressing. *Burns*, **44**: 1829–1838.
Lin, C., Ekblad-Nordberg, Å., Michaëlsson, J., Götherström, C., Hsu, C.-C., Ye, H., Johansson, J., Rising, A., Sundström, E. and Åkesson, E. 2021. In Vitro Study of Human Immune Responses to Hyaluronic Acid Hydrogels, Recombinant Spidroins and Human Neural Progenitor Cells of Relevance to Spinal Cord Injury Repair. *Cells*, **10**: 1713.
Lin, S., Chen, G., Liu, X. and Meng, Q. 2016. Chimeric spider silk proteins mediated by intein result in artificial hybrid silks. *Biopolymers*, **105**: 385–392.
Lin, T.Y., Masunaga, H., Sato, R., Malay, A.D., Toyooka, K., Hikima, T. and Numata, K. 2017. Liquid Crystalline Granules Align in a Hierarchical Structure To Produce Spider Dragline Microfibrils. *Biomacromolecules*, **18**: 1350–1355.
Lomakin, A., Chung, D.S., Benedek, G.B., Kirschner, D.A. and Teplow, D.B. 1996. On the nucleation and growth of amyloid β-protein fibrils: Detection of nuclei and quantitation of rate constants. *Proc Natl Acad Sci U S A*, **93**: 1125–1129.
Lopes, J.L.S., Miles, A.J., Whitmore, L. and Wallace, B.A. 2014. Distinct circular dichroism spectroscopic signatures of polyproline II and unordered secondary structures: Applications in secondary structure analyses. *Protein Science*, **23**: 1765–1772.
Lou, J., Stowers, R., Nam, S., Xia, Y. and Chaudhuri, O. 2018. Stress relaxing hyaluronic acid-collagen hydrogels promote cell spreading, fiber remodeling, and focal adhesion formation in 3D cell culture. *Biomaterials*, **154**: 213–222.
Luo, F., Qian, Z.G. and Xia, X.X. 2018. Responsive protein hydrogels assembled from spider silk carboxyl-terminal domain and resilin copolymers. *Polymers (Basel)*, **10**.
Lyda, T.A., Wagner, E.L., Bourg, A.X., Peng, C., Tomaraei, G.N., Dean, D., Kennedy, M.S. and Marcotte, W.R. 2017. A Leishmania secretion system for the expression of major ampullate spidroin mimics. *PLoS One*, **12**: 1–15.
Madsen, B., Shao, Z.Z. and Vollrath, F. 1999. Variability in the mechanical properties of spider silks on three levels: Interspecific, intraspecific and intraindividual. *Int J Biol Macromol*, **24**: 301–306.
Malay, A.D., Craig, H.C., Chen, J., Oktaviani, N.A. and Numata, K. 2022. Complexity of Spider Dragline Silk. *Biomacromolecules*, **23**: 1827–1840.
Malay, A.D., Suzuki, T., Katashima, T., Kono, N., Arakawa, K. and Numata, K. 2020. Spider silk self-assembly via modular liquid-liquid phase separation and nanofibrillation. *Sci Adv*, **6**.
Mamat, U., Wilke, K., Bramhill, D., Schromm, A.B., Lindner, B., Kohl, T.A., Corchero, J.L., Villaverde, A., Schaffer, L., Head, S.R., Souvignier, C., Meredith, T.C. and Woodard, R.W. 2015. Detoxifying Escherichia coli for endotoxin-free production of recombinant proteins. *Microb Cell Fact*, **14**: 1–15.
Mathur, A.B., Collinsworth, A.M., Reichert, W.M., Kraus, W.E. and Truskey, G.A. 2001. Endothelial, cardiac muscle and skeletal muscle exhibit different viscous and elastic properties as determined by atomic force microscopy. *J Biomech*, **34**: 1545–1553.
Matsumoto, A., Lindsay, A., Abedian, B. and Kaplan, D.L. 2008. Silk fibroin solution properties related to assembly and structure. *Macromol Biosci*, **8**: 1006–1018.
Maurer-Stroh, S., Debulpaep, M., Kuemmerer, N., de La Paz, M.L., Martins, I.C., Reumers, J., Morris, K.L., Copland, A., Serpell, L., Serrano, L., Schymkowitz, J.W.H. and Rousseau, F. 2010. Exploring the sequence determinants of amyloid structure using position-specific scoring matrices. *Nat Methods*, **7**: 237–242.
Meyers, M.A. and Chawla, K.A. 1999. Viscoelasticity.

Micsonai, A., Bulyáki, É. and Kardos, J. 2021. BeStSel: From Secondary Structure Analysis to Protein Fold Prediction by Circular Dichroism Spectroscopy. *Methods in Molecular Biology*, **2199**: 175–189.
Mimar, R., Limb, D. and Hall, R.M. 2008. Evaluation of the mechanical and architectural properties of glenoid bone. *J Shoulder Elbow Surg*, **17**: 336–341.
Mohammadi, P., Jonkergouw, C., Beaune, G., Engelhardt, P., Kamada, A., Timonen, J.V.I., Knowles, T.P.J., Penttila, M. and Linder, M.B. 2019. Controllable coacervation of recombinantly produced spider silk protein using kosmotropic salts. *J Colloid Interface Sci*, **560**: 149–160.
Mulinti, P., Diekjürgen, D., Kurtzeborn, K., Balasubramanian, N., Stafslien, S.J., Grainger, D.W. and Brooks, A.E. 2022. Anti-Coagulant and Antimicrobial Recombinant Heparin-Binding Major Ampullate Spidroin 2 (MaSp2) Silk Protein. *Bioengineering*, **9**.
Müller, M.M. 2018. Post-Translational Modifications of Protein Backbones: Unique Functions, Mechanisms, and Challenges. *Biochemistry*, **57**: 177–185.
Müller, U.C., Deller, T. and Korte, M. 2017. Not just amyloid: Physiological functions of the amyloid precursor protein family. *Nat Rev Neurosci*, **18**: 281–298.
Naik, R.R. and Singamaneni, S. 2017. Introduction: Bioinspired and Biomimetic Materials. *Chem Rev*, **117**: 12581–12583.
Nelson, R., Sawaya, M.R., Balbirnie, M., Madsen, A., Riekel, C., Grothe, R. and Eisenberg, D. 2005. Structure of the cross-β spine of amyloid-like fibrils. *Nature*, **435**: 773–778.
Neubauer, V.J., Trossmann, V.T., Jacobi, S., Döbl, A. and Scheibel, T. 2021. Recombinant Spider Silk Gels Derived from Aqueous–Organic Solvents as Depots for Drugs. *Angewandte Chemie - International Edition*, **60**: 11847–11851.
Nilebäck, L., Hedin, J., Widhe, M., Floderus, L.S., Krona, A., Bysell, H. and Hedhammar, M. 2017. Self-Assembly of Recombinant Silk as a Strategy for Chemical-Free Formation of Bioactive Coatings: A Real-Time Study. *Biomacromolecules*, **18**: 846–854.
Nova, A., Keten, S., Pugno, N.M., Redaelli, A. and Buehler, M.J. 2010. Molecular and nanostructural mechanisms of deformation, strength and toughness of spider silk fibrils. *Nano Lett*, **10**: 2626–2634.
Numata, K. and Kaplan, D.L. 2011. Differences in Cytotoxicity of β-Sheet Peptides Originated from Silk and Amyloid β. *Macromol Biosci*, **11**: 60–64.
Numata, K. and Kaplan, D.L. 2010. Silk-based delivery systems of bioactive molecules. *Adv Drug Deliv Rev*, **62**: 1497–1508.
Numata, K., Mieszawska-Czajkowska, A.J., Kvenvold, L.A. and Kaplan, D.L. 2012. Silk-based nanocomplexes with tumor-homing peptides for tumor-specific gene delivery. *Macromol Biosci*, **12**: 75–82.
Ogneva, I. v., Lebedev, D. v. and Shenkman, B.S. 2010. Transversal stiffness and young's modulus of single fibers from rat soleus muscle probed by atomic force microscopy. *Biophys J*, **98**: 418–424.
Ohgo, K., Kawase, T., Ashida, J. and Asakura, T. 2006. Solid-state NMR analysis of a peptide (Gly-Pro-Gly-Gly-Ala)6-Gly derived from a flagelliform silk sequence of Nephila clavipes. *Biomacromolecules*, **7**: 1210–1214.
Ohtomo, Y., Kakegawa, T., Ishida, A., Nagase, T. and Rosing, M.T. 2014. Evidence for biogenic graphite in early Archaean Isua metasedimentary rocks. *Nat Geosci*, **7**: 25–28.
Oktaviani, N.A., Matsugami, A., Hayashi, F. and Numata, K. 2019. Ion effects on the conformation and dynamics of repetitive domains of a spider silk protein: Implications for solubility and β-sheet formation. *Chemical Communications*, **55**: 9761–9764.
Oktaviani, N.A., Matsugami, A., Malay, A.D., Hayashi, F., Kaplan, D.L. and Numata, K. 2018. Conformation and dynamics of soluble repetitive domain elucidates the initial beta-sheet formation of spider silk. *Nat Commun*, **9**: 2121.
Otikovs, M., Andersson, M., Jia, Q., Nordling, K., Meng, Q., Andreas, L.B., Pintacuda, G., Johansson, J., Rising, A. and Jaudzems, K. 2017. Degree of Biomimicry of Artificial Spider Silk Spinning Assessed by NMR Spectroscopy. *Angew Chem Int Ed Engl*, **56**: 12571–12575.

Otikovs, M., Chen, G., Nordling, K., Landreh, M., Meng, Q., Jornvall, H., Kronqvist, N., Rising, A., Johansson, J. and Jaudzems, K. 2015. Diversified Structural Basis of a Conserved Molecular Mechanism for pH-Dependent Dimerization in Spider Silk N-Terminal Domains. *Chembiochem*, **16**: 1720–1724.

Parent, L.R., Onofrei, D., Xu, D., Stengel, D., Roehling, J.D., Bennett Addison, J., Forman, C., Amin, S.A., Cherry, B.R., Yarger, J.L., Gianneschi, N.C. and Holland, G.P. 2018. Hierarchical spidroin micellar nanoparticles as the fundamental precursors of spider silks. *Proc Natl Acad Sci U S A*, **115**: 11507–11512.

Parida, P., Behera, A. and Chandra Mishra, S. 2012. Classification of Biomaterials used in Medicine. *International Journal of Advances in Applied Sciences*, **1**: 31–35.

Park, B.K. and Um, I.C. 2018. Effect of molecular weight on electro-spinning performance of regenerated silk. *Int J Biol Macromol*, **106**: 1166–1172.

Parkhe, A.D., Seeley, S.K., Gardner, K., Thompson, L. and Lewis, R. v. 1997. Structural studies of spider silk proteins in the fiber. *Journal of Molecular Recognition*, **10**: 1–6.

Peakall, D.B. 1969. Synthesis of silk, mechanism and location. *Integr Comp Biol*, **9**: 71–79.

Peng, Q., Zhang, Y., Lu, L., Shao, H., Qin, K., Hu, X. and Xia, X. 2016. Recombinant spider silk from aqueous solutions via a bio-inspired microfluidic chip. *Sci Rep*, **6**: 36473.

Perea, G.B., Riekel, C., Guinea, G. v., Madurga, R., Daza, R., Burghammer, M., Hayashi, C., Elices, M., Plaza, G.R. and Pérez-Rigueiro, J. 2013. Identification and dynamics of polyglycine II nanocrystals in Argiope trifasciata flagelliform silk. *Sci Rep*, **3**: 1–6.

Petkova, A.T., Ishii, Y., Balbach, J.J., Antzutkin, O.N., Leapman, R.D., Delaglio, F. and Tycko, R. 2002. A structural model for Alzheimer's β-amyloid fibrils based on experimental constraints from solid state NMR. *Proc Natl Acad Sci U S A*, **99**: 16742–16747.

Pignatello, R. 2013. *Advances in Biomaterials Science and Biomedical Applications*.

Price, R., Poursaid, A. and Ghandehari, H. 2014. Controlled release from recombinant polymers. *J Control Release*, **190**: 304–313.

Prince, J.T., McGrath, K.P., DiGirolamo, C.M. and Kaplan, D.L. 1995. Construction, cloning, and expression of synthetic genes encoding spider dragline silk. *Biochemistry*, **34**: 10879–10885.

Qian, Z.G., Zhou, M.L., Song, W.W. and Xia, X.X. 2015. Dual Thermosensitive Hydrogels Assembled from the Conserved C-Terminal Domain of Spider Dragline Silk. *Biomacromolecules*, **16**: 3704–3711.

Radtke, C., Allmeling, C., Waldmann, K.H., Reimers, K., Thies, K., Schenk, H.C., Hillmer, A., Guggenheim, M., Brandes, G. and Vogt, P.M. 2011. Spider silk constructs enhance axonal regeneration and remyelination in long nerve defects in sheep. *PLoS One*, **6**: e16990.

Ramachandran, G.N. and Gould, B.S. 1967. *Treatise on collagen*.

Rammensee, S., Huemmerich, D., Hermanson, K.D., Scheibel, T. and Bausch, A.R. 2006. Rheological characterization of hydrogels formed by recombinantly produced spider silk. *Appl Phys A Mater Sci Process*, **82**: 261–264.

Rammensee, S., Slotta, U., Scheibel, T. and Bausch, A.R. 2008. Assembly mechanism of recombinant spider silk proteins. *Proc Natl Acad Sci U S A*, **105**: 6590–6595.

Resch, A., Wolf, S., Mann, A., Weiss, T., Stetco, A.L. and Radtke, C. 2018. Co-Culturing Human Adipose Derived Stem Cells and Schwann Cells on Spider Silk-A New Approach as Prerequisite for Enhanced Nerve Regeneration. *Int J Mol Sci*, **20**.

Rice, J.J., Martino, M.M., de Laporte, L., Tortelli, F., Briquez, P.S. and Hubbell, J.A. 2013. Engineering the Regenerative Microenvironment with Biomaterials. *Adv Healthc Mater*, **2**: 57–71.

Riekel, C., Burghammer, M., Dane, T.G., Ferrero, C. and Rosenthal, M. 2017. Nanoscale Structural Features in Major Ampullate Spider Silk. *Biomacromolecules*, **18**: 231–241.

Rising, A. 2014. Controlled assembly: a prerequisite for the use of recombinant spider silk in regenerative medicine? *Acta Biomater*, **10**: 1627–1631.

Rising, A., Hjälm, G., Engström, W. and Johansson, J. 2006. N-terminal nonrepetitive domain common to dragline, flagelliform, and cylindriform spider silk proteins. *Biomacromolecules*, **7**: 3120–3124.

Rising, A. and Johansson, J. 2015. Toward spinning artificial spider silk. *Nat Chem Biol*, **11**: 309–315.
Rousseau, M.E., Lefevre, T. and Pezolet, M. 2009. Conformation and orientation of proteins in various types of silk fibers produced by Nephila clavipes spiders. *Biomacromolecules*, **10**: 2945–2953.
Rucker, A.L. and Creamer, T.P. 2002. Polyproline II helical structure in protein unfolded states: lysine peptides revisited. *Protein Sci*, **11**: 980–5.
Saitô, H., Tabeta, R., Asakura, T., Iwanaga, Y., Shoji, A., Ozaki, T. and Ando, I. 1984. High-Resolution 13C NMR Study of Silk Fibroin in the Solid State by the Cross-Polarization-Magic Angle Spinning Method. Conformational Characterization Of Silk I and Silk II Type Forms of Bombyx Mori Fibroin by the Conformation-Dependent 13C Chemical Shif. *Macromolecules*, **17**: 1405–1412.
Saitô, H., Tabeta, R., Shoji, A., Ozaki, T., Ando, I. and Miyata, T. 1984. A high-resolution 13C-NMR study of collagenlike polypeptides and collagen fibrils in solid state studied by the cross-polarization–magic angle-spinning method. Manifestation of conformation-dependent 13C chemical shifts and application to conformational c. *Biopolymers*, **23**: 2279–2297.
Samavedi, S., Poindexter, L.K., van Dyke, M. and Goldstein, A.S. 2014. *Synthetic biomaterials for regenerative medicine applications*.
Sampath, S., Isdebski, T., Jenkins, J.E., Ayon, J. v., Henning, R.W., Orgel, J.P.R.O., Antipoa, O. and Yarger, J.L. 2012. X-ray diffraction study of nanocrystalline and amorphous structure within major and minor ampullate dragline spider silks. *Soft Matter*, **8**: 6713–6722.
Sanggaard, K.W., Bechsgaard, J.S., Fang, X., Duan, J., Dyrlund, T.F., Gupta, V., Jiang, X., Cheng, L., Fan, D., Feng, Y., Han, L., Huang, Z., Wu, Z., Liao, L., Settepani, V., Thøgersen, I.B., Vanthournout, B., Wang, T., Zhu, Y., *et al.* 2014. Spider genomes provide insight into composition and evolution of venom and silk. *Nat Commun*, **5**: 3765.
Saric, M., Eisoldt, L., Döring, V. and Scheibel, T. 2021. Interplay of Different Major Ampullate Spidroins during Assembly and Implications for Fiber Mechanics. *Advanced Materials*, **33**: 2006499.
Sarr, M., Kitoka, K., Walsh-White, K.-A., Kaldmäe, M., Metlāns, R., Tārs, K., Mantese, A., Shah, D., Landreh, M., Rising, A., Johansson, J., Jaudzems, K. and Kronqvist, N. 2022. The dimerization mechanism of the N-terminal domain of spider silk proteins is conserved despite extensive sequence divergence. *Journal of Biological Chemistry*, **298**: 101913.
Sarr, M., Kronqvist, N., Chen, G., Aleksis, R., Purhonen, P., Hebert, H., Jaudzems, K., Rising, A. and Johansson, J. 2018. A spidroin-derived solubility tag enables controlled aggregation of a designed amyloid protein. *FEBS J*, **285**: 1873–1885.
Sawaya, M.R., Sambashivan, S., Nelson, R., Ivanova, M.I., Sievers, S.A., Apostol, M.I., Thompson, M.J., Balbirnie, M., Wiltzius, J.J.W., McFarlane, H.T., Madsen, A., Riekel, C. and Eisenberg, D. 2007. Atomic structures of amyloid cross-β spines reveal varied steric zippers. *Nature*, **447**: 453–457.
Schacht, K., Jungst, T., Schweinlin, M., Ewald, A., Groll, J. and Scheibel, T. 2015. Biofabrication of cell-loaded 3D spider silk constructs. *Angew Chem Int Ed Engl*, **54**: 2816–2820.
Schacht, K. and Scheibel, T. 2011. Controlled hydrogel formation of a recombinant spider silk protein. *Biomacromolecules*, **12**: 2488–2495.
Schacht, K., Vogt, J. and Scheibel, T. 2016. Foams Made of Engineered Recombinant Spider Silk Proteins as 3D Scaffolds for Cell Growth. *ACS Biomater Sci Eng*, **2**: 517–525.
Schäfer-Nolte, F., Hennecke, K., Reimers, K., Schnabel, R., Allmeling, C., Vogt, P.M., Kuhbier, J.W. and Mirastschijski, U. 2014. Biomechanics and biocompatibility of woven spider silk meshes during remodeling in a rodent fascia replacement model. *Ann Surg*, **259**: 781–792.

Schmuck, B., Greco, G., Barth, A., Pugno, N.M., Johansson, J. and Rising, A. 2021. High-yield production of a super-soluble miniature spidroin for biomimetic high-performance materials. *Materials Today*, **50**: 16–23.
Schwarze, S., Zwettler, F.U., Johnson, C.M. and Neuweiler, H. 2013. The N-terminal domains of spider silk proteins assemble ultrafast and protected from charge screening. *Nat Commun*, **4**: 2815.
Shi, Z., Anders Olson, C., Rose, G.D., Baldwin, R.L. and Kallenbach, N.R. 2002. Polyproline II structure in a sequence of seven alanine residues. *Proc Natl Acad Sci U S A*, **99**: 9190–9195.
Shi, Z., Chen, K., Liu, Z., Ng, A., Bracken, W.C. and Kallenbach, N.R. 2005. Polyproline II propensities from GGXGG peptides reveal an anticorrelation with β-sheet scales. *Proc Natl Acad Sci U S A*, **102**: 17964–17968.
Shoulders, M.D. and Raines, R.T. 2009. Collagen Structure and Stability. *Annu Rev Biochem*, **78**: 929–958.
Simmons, A.H., Michal, C.A. and Jelinski, L.W. 1996. Molecular orientation and two-component nature of the crystalline fraction of spider dragline silk. *Science (1979)*, **271**: 84–87.
Sipe, J.D., Benson, M.D., Buxbaum, J.N., Ikeda, S.I., Merlini, G., Saraiva, M.J.M. and Westermark, P. 2016. Amyloid fibril proteins and amyloidosis: chemical identification and clinical classification International Society of Amyloidosis 2016 Nomenclature Guidelines. *Amyloid*, **23**: 209–213.
Slotta, U., Hess, S., Spiess, K., Stromer, T., Serpell, L. and Scheibel, T. 2007. Spider silk and amyloid fibrils: a structural comparison. *Macromol Biosci*, **7**: 183–188.
Slotta, U.K., Rammensee, S., Gorb, S. and Scheibel, T. 2008. An Engineered Spider Silk Protein Forms Microspheres. *Angewandte Chemie International Edition*, **47**: 4592–4594.
Sogawa, H., Nakano, K., Tateishi, A., Tajima, K. and Numata, K. 2020. Surface Analysis of Native Spider Draglines by FE-SEM and XPS. *Front Bioeng Biotechnol*, **8**: 1–6.
Song, W.W., Qian, Z.G., Liu, H., Chen, H.F., Kaplan, D.L. and Xia, X.X. 2021. On-Demand Regulation of Dual Thermosensitive Protein Hydrogels. *ACS Macro Lett*, **10**: 395–400.
Sonnleitner, D., Sommer, C., Scheibel, T. and Lang, G. 2021. Approaches to inhibit biofilm formation applying natural and artificial silk-based materials. *Materials Science and Engineering C*, **131**: 112458.
Sparkes, J. and Holland, C. 2017. Analysis of the pressure requirements for silk spinning reveals a pultrusion dominated process. *Nat Commun*, **8**: 594.
Sponner, A, Schlott, B., Vollrath, F., Unger, E., Grosse, F. and Weisshart, K. 2005. Characterization of the protein components of Nephila clavipes dragline silk. *Biochemistry*, **44**: 4727–4736.
Sponner, A., Unger, E., Grosse, F. and Weisshart, K. 2004. Conserved C-termini of spidroins are secreted by the major ampullate glands and retained in the silk thread. *Biomacromolecules*, **5**: 840–845.
Sponner, A., Vater, W., Monajembashi, S., Unger, E., Grosse, F. and Weisshart, K. 2007. Composition and hierarchical organisation of a spider silk. *PLoS One*, **2**: e998.
Sponner, A., Vater, W., Rommerskirch, W., Vollrath, F., Unger, E., Grosse, F. and Weisshart, K. 2005. The conserved C-termini contribute to the properties of spider silk fibroins. *Biochem Biophys Res Commun*, **338**: 897–902.
Stark, M., Grip, S., Rising, A., Hedhammar, M., Engstrom, W., Hjalm, G. and Johansson, J. 2007. Macroscopic fibers self-assembled from recombinant miniature spider silk proteins. *Biomacromolecules*, **8**: 1695–1701.
Stern-Tal, D., Ittah, S. and Sklan, E. 2021. A new cell-sized support for 3D cell cultures based on recombinant spider silk fibers. *J Biomater Appl*, **36**: 1748–1757.
Strickland, M., Tudorica, V., Řezáč, M., Thomas, N.R. and Goodacre, S.L. 2018. Conservation of a pH-sensitive structure in the C-terminal region of spider silk extends across the entire silk gene family. *Heredity (Edinb)*, **120**: 574–580.
Sunde, M. and Blake, C. 1997. The structure of amyloid fibrils by electron microscopy and x-ray diffraction. *Adv Protein Chem*, **50**: 123–159.

Teule, F., Addison, B., Cooper, A.R., Ayon, J., Henning, R.W., Benmore, C.J., Holland, G.P., Yarger, J.L. and Lewis, R. v. 2012. Combining flagelliform and dragline spider silk motifs to produce tunable synthetic biopolymer fibers. *Biopolymers*, **97**: 418–431.
Teulé, F., Furin, W.A., Cooper, A.R., Duncan, J.R. and Lewis, R. v. 2007. Modifications of spider silk sequences in an attempt to control the mechanical properties of the synthetic fibers. *J Mater Sci*, **42**: 8974–8985.
Teulé, F., Miao, Y.G., Sohn, B.H., Kim, Y.S., Hull, J.J., Fraser, M.J., Lewis, R. v. and Jarvis, D.L. 2012. Silkworms transformed with chimeric silkworm/spider silk genes spin composite silk fibers with improved mechanical properties. *Proc Natl Acad Sci U S A*, **109**: 923–928.
Thamm, C., DeSimone, E. and Scheibel, T. 2017. Characterization of Hydrogels Made of a Novel Spider Silk Protein eMaSp1s and Evaluation for 3D Printing. *Macromol Biosci*, **17**.
Thamm, C. and Scheibel, T. 2017. Recombinant Production, Characterization, and Fiber Spinning of an Engineered Short Major Ampullate Spidroin (MaSp1s). *Biomacromolecules*, **18**: 1365–1372.
Thurber, A.E., Omenetto, F.G. and Kaplan, D.L. 2015. In vivo bioresponses to silk proteins. *Biomaterials*, **71**: 145–157.
Thurner, P.J., Erickson, B., Turner, P., Jungmann, R., Lelujian, J., Proctor, A., Weaver, J.C., Schitter, G., Morse, D.E. and Hansma, P.K. 2009. The effect of NaF in vitro on the mechanical and material properties of trabecular and cortical bone. *Advanced Materials*, **21**: 451–457.
Tian, M. and Lewis, R. v. 2005. Tubuliform silk protein: A protein with unique molecular characteristics and mechanical properties in the spider silk fibroin family. *Applied Physics A*, **82**: 265–273.
Tiwari, A., Nordin, A.N. and Nordin, A.N. 2014. *Advanced Biomaterials and Biodevices*.
Trossmann, V.T., Heltmann-Meyer, S., Amouei, H., Wajant, H., Horch, R.E., Steiner, D. and Scheibel, T. 2022. Recombinant Spider Silk Bioinks for Continuous Protein Release by Encapsulated Producer Cells. *Biomacromolecules*, **23**: 4427–4437.
Tschoegl, N.W. 2012. *The phenomenological theory of linear viscoelastic behavior: an introduction*.
Tse, J.R. and Engler, A.J. 2011. Stiffness gradients mimicking in vivo tissue variation regulate mesenchymal stem cell fate. *PLoS One*, **6**.
Ullah, S. and Chen, X. 2020. Fabrication, applications and challenges of natural biomaterials in tissue engineering. *Appl Mater Today*, **20**.
van Beek, J.D., Hess, S., Vollrath, F. and Meier, B.H. 2002. The molecular structure of spider dragline silk: Folding and orientation of the protein backbone. *Proceedings of the National Academy of Sciences*, **99**: 10266–10271.
van der Linden, E. and Foegeding, E.A. 2009. Gelation: Principles, Models and Applications to Proteins. In: *Modern Biopolymer Science: Bridging the Divide between Fundamental Treatise and Industrial Application* (S. Kasapis, I. T. Norton, and J. B. B. T.-M. B. S. Ubbink, eds), pp. 29–91.
Vezy, C., Hermanson, K.D., Scheibel, T. and Bausch, A.R. 2009. Interfacial rheological properties of recombinant spider-silk proteins. *Biointerphases*, **4**: 43–46.
Viotti, C. 2016. ER to golgi-dependent protein secretion: The conventional pathway. In: *Methods in Molecular Biology* (A. Pompa and F. de Marchis, eds), pp. 3–29.
Vollrath, F., Barth, P., Basedow, A., Engstrom, W. and List, H. 2002. Local tolerance to spider silks and protein polymers in vivo. *In Vivo (Brooklyn)*, **16**: 229–234.
Vollrath, F., Holtet, T., Thøgersen, H.C. and Frische, S. 1997. Structural organization of spider silk. *Proc R Soc Lond B Biol Sci*, **263**: 147–151.
Vollrath, F. and Knight, D.P. 2001. Liquid crystalline spinning of spider silk, Review. *Nature*, **410**: 541–548.
Vollrath, F. and Knight, D.P. 1999. Structure and function of the silk production pathway in the Spider Nephila edulis. *Int J Biol Macromol*, **24**: 243–249.
Vollrath, F., Knight, D.P. and Hu, X.W. 1998. Silk production in a spider involves acid bath treatment. *Proc R Soc Lond B Biol Sci*, **265**: 817–820.

Vollrath, F., Madsen, B. and Shao, Z. 2001. The effect of spinning conditions on the mechanics of a spider's dragline silk. *Proc Biol Sci*, **268**: 2339–2346.
von Heijne, G. 1990. The signal peptide. *J Membr Biol*, **115**: 195–201.
Wallace, J.A. and Shen, J.K. 2012. Unraveling A Trap-and-Trigger Mechanism in the pH-Sensitive Self-Assembly of Spider Silk Proteins. *J Phys Chem Lett*, **3**: 658–662.
Warkentin, E., Weidenweber, S., Schühle, K., Demmer, U., Heider, J. and Ermler, U. 2017. A rare polyglycine type II-like helix motif in naturally occurring proteins. *Proteins: Structure, Function and Bioinformatics*, **85**: 2017–2023.
White, S.H. and von Heijne, G. 2005. Transmembrane helices before, during, and after insertion. *Curr Opin Struct Biol*, **15**: 378–386.
Widhe, M., Bysell, H., Nystedt, S., Schenning, I., Malmsten, M., Johansson, J., Rising, A. and Hedhammar, M. 2010. Recombinant spider silk as matrices for cell culture. *Biomaterials*, **31**: 9575–9585.
Widhe, M., Johansson, U., Hillerdahl, C.O. and Hedhammar, M. 2013. Recombinant spider silk with cell binding motifs for specific adherence of cells. *Biomaterials*, **34**: 8223–8234.
Widhe, M., Shalaly, N.D. and Hedhammar, M. 2016. A fibronectin mimetic motif improves integrin mediated cell biding to recombinant spider silk matrices. *Biomaterials*, **74**: 256–266.
Williams, D.F. and European society for biomaterials. 1986. Definitions in biomaterials: proceedings of a consensus conference of the European Society for Biomaterials, Chester, England, March 3-5.
Wilson, R.S. 1969. Control of drag-line spinning in certain spiders. *Am Zool*, **9**: 103–111.
Wirth, M., Wolff, J.O., Appel, E. and Gorb, S.N. 2019. Ultrastructure of spider thread anchorages. *J Morphol*, **280**: 534–543.
Wolff, S.M. 1973. Biological Effects of Bacterial Endotoxins in Man. *J Infect Dis*, **128**: S259–S264.
Xia, X.X., Qian, Z.G., Ki, C.S., Park, Y.H., Kaplan, D.L. and Lee, S.Y. 2010. Native-sized recombinant spider silk protein produced in metabolically engineered Escherichia coli results in a strong fiber. *Proc Natl Acad Sci U S A*, **107**: 14059–14063.
Xu, D., Shi, X., Thompson, F., Weber, W.S., Mou, Q. and Yarger, J.L. 2015. Protein secondary structure of Green Lynx spider dragline silk investigated by solid-state NMR and X-ray diffraction. *Int J Biol Macromol*, **81**: 171–179.
Xu, D., Yarger, J.L. and Holland, G.P. 2014. Exploring the backbone dynamics of native spider silk proteins in Black Widow silk glands with solution-state NMR spectroscopy. *Polymer (Guildf)*, **55**: 3879–3885.
Xu, S., Li, X., Zhou, Y., Lin, Y. and Meng, Q. 2020. Structural characterization and mechanical properties of chimeric Masp1/Flag minispidroins. *Biochimie*, **168**: 251–258.
Yazawa, K., Malay, A.D., Masunaga, H. and Numata, K. 2018. Role of Skin Layers on Mechanical Properties and Supercontraction of Spider Dragline Silk Fiber. *Macromol Biosci*, **2:** e1800220.
Zeplin, P.H., Maksimovikj, N.C., Jordan, M.C., Nickel, J., Lang, G., Leimer, A.H., Römer, L. and Scheibel, T. 2014. Spider Silk Coatings as a Bioshield to Reduce Periprosthetic Fibrous Capsule Formation. *Adv Funct Mater*, **24**: 2658–2666.
Zhang, C., Mi, J., Qi, H., Huang, J., Liu, S., Zhang, L. and Fan, D. 2020. Engineered a novel pH-sensitive short major ampullate spidroin. *Int J Biol Macromol*, **154**: 698–705
Zhang, X., Xia, L., Day, B.A., Harris, T.I., Oliveira, P., Knittel, C., Licon, A.L., Gong, C., Dion, G., Lewis, R. v and Jones, J.A. 2019. CRISPR/Cas9 Initiated Transgenic Silkworms as a Natural Spinner of Spider Silk. *Biomacromolecules*, **20**: 2252–2264.
Zhou, Y., Rising, A., Johansson, J. and Meng, Q. 2018. Production and Properties of Triple Chimeric Spidroins. *Biomacromolecules*, **19**: 2825–2833.
Zhou, Y., Wu, S. and Conticello, V.P. 2001. Genetically Directed Synthesis and Spectroscopic Analysis of a Protein Polymer Derived from a Flagelliform Silk Sequence. *Biomacromolecules*, **2**: 111–125.

Zhu, B.F., Li, W., Lewis, R. v, Segre, C.U. and Wang, R. 2015. E-Spun Composite Fibers of Collagen and Drag line Silk Protein: Fiber Mechanics, Biocompatibility, and Application in Stem Cell Differentiation. *Biomacromolecules*, **16**: 202–213.

Zhu, H., Rising, A., Johansson, J., Zhang, X., Lin, Y., Zhang, L., Yi, T., Mi, J. and Meng, Q. 2020. Tensile properties of synthetic pyriform spider silk fibers depend on the number of repetitive units as well as the presence of N- and C-terminal domains. *Int J Biol Macromol*, **154**: 765–772.

Zhu, H., Sun, Y., Yi, T., Wang, S., Mi, J. and Meng, Q. 2020. Tough synthetic spider-silk fibers obtained by titanium dioxide incorporation and formaldehyde cross-linking in a simple wet-spinning process. *Biochimie*, **175**: 77–84

Ziegler, G.R. and Foegeding, E.A. 1990. The gelation of proteins. In: *Advances in Food and Nutrition Research* (J. E. B. T.-A. in F. and N. R. Kinsella, ed), pp. 203–298.